

Electromagnetic mass splittings of the low lying hadrons and quark masses from 2 + 1 flavor lattice QCD + QED

Tom Blum and Ran Zhou*

*Physics Department, University of Connecticut, Storrs, Connecticut 06269-3046, USA
and RIKEN-BNL Research Center, Brookhaven National Laboratory, Upton, New York 11973, USA*

Takumi Doi

*Graduate School of Pure and Applied Science, University of Tsukuba, Tennodai 1-1-1, Tsukuba, Ibaraki 305-8571, Japan
and RIKEN Nishina Center for Accelerator-Based Science, Wako, Saitama 351-0198, Japan*

Masashi Hayakawa

*Department of Physics, Nagoya University, Nagoya 464-8602, Japan
and Theoretical Physics Laboratory, Nishina Center, RIKEN, Wako, 351-0198, Japan*

Taku Izubuchi

*Brookhaven National Laboratory, Upton, New York 11973, USA
and RIKEN-BNL Research Center, Brookhaven National Laboratory, Upton, New York 11973, USA*

Shunpei Uno

*Department of Physics, Nagoya University, Nagoya 464-8602, Japan
and RIKEN-BNL Research Center, Brookhaven National Laboratory, Upton, New York 11973, USA*

Norikazu Yamada

*KEK Theory Center, Institute of Particle and Nuclear Studies, High Energy Accelerator Research Organization (KEK),
Tsukuba 305-0801, Japan
and School of High Energy Accelerator Science, The Graduate University for Advanced Studies (Sokendai),
Tsukuba 305-0801, Japan*

(Received 2 September 2010; published 24 November 2010)

Results computed in lattice QCD + QED are presented for the electromagnetic mass splittings of the low-lying hadrons. These are used to determine the renormalized, nondegenerate, light quark masses. It is found that $m_u^{\overline{\text{MS}}} = 2.24(10)(34)$, $m_d^{\overline{\text{MS}}} = 4.65(15)(32)$, and $m_s^{\overline{\text{MS}}} = 97.6(2.9)(5.5)$ MeV at the renormalization scale 2 GeV, where the first error is statistical and the second systematic. We find the lowest-order electromagnetic splitting $(m_{\pi^+} - m_{\pi^0})_{\text{QED}} = 3.38(23)$ MeV, the splittings including next-to-leading order, $(m_{\pi^+} - m_{\pi^0})_{\text{QED}} = 4.50(23)$ MeV, $(m_{K^+} - m_{K^0})_{\text{QED}} = 1.87(10)$ MeV, and the $m_u \neq m_d$ contribution to the kaon mass difference, $(m_{K^+} - m_{K^0})_{(m_u - m_d)} = -5.840(96)$ MeV. All errors are statistical only, and the next-to-leading-order pion splitting is only approximate in that it does not contain all next-to-leading-order contributions. We also computed the proton-neutron mass difference, including for the first time, QED interactions in a realistic 2 + 1 flavor calculation. We find $(m_p - m_n)_{\text{QED}} = 0.383(68)$ MeV, $(m_p - m_n)_{(m_u - m_d)} = -2.51(14)$ MeV (statistical errors only), and the total $m_p - m_n = -2.13(16) \times (70)$ MeV, where the first error is statistical, and the second, part of the systematic error. The calculations are carried out on QCD ensembles generated by the RBC and UKQCD collaborations, using domain wall fermions and the Iwasaki gauge action (gauge coupling $\beta = 2.13$ and lattice cutoff $a^{-1} \approx 1.78$ GeV). We use two lattice sizes, 16^3 and 24^3 $((1.8 \text{ fm})^3$ and $(2.7 \text{ fm})^3$), to address finite-volume effects. Noncompact QED is treated in the quenched approximation. The valence pseudoscalar meson masses in our study cover a range of about 250 to 700 MeV, though we use only those up to about 400 MeV to quote final results. We present new results for the electromagnetic low-energy constants in SU(3) and SU(2) partially quenched chiral perturbation theory to the next-to-leading order, obtained from fits to our data. Detailed analysis of systematic errors in our results and methods for improving them are discussed. Finally, new analytic results for SU(2)_L × SU(2)_R-plus-kaon chiral perturbation theory, including the one-loop logs proportional to $\alpha_{\text{em}} m$, are given.

DOI: 10.1103/PhysRevD.82.094508

PACS numbers: 11.15.Ha, 11.30.Rd, 12.38.Gc, 12.39.Fe

*Present Address: Department of Physics, Indiana University, Bloomington, IN 47405, USA

I. INTRODUCTION

The mass splitting in the meson and baryon systems is an interesting topic in hadron spectroscopy. It is related to the quark masses which are fundamental parameters of the standard model. The mass splitting in the pseudoscalar meson octet is a signature of the breaking of the strong isospin symmetry by the electromagnetic (EM) interaction and nondegenerate quark masses.

The hadron spectra are rich in diversity due to two origins: the nonperturbative quantum dynamics of the strong interaction and the presence of flavor symmetry breaking. In the standard model, the latter originates from nondegenerate quark masses as well as the difference between up-type quarks and down-type quarks. These sources of flavor symmetry breaking significantly affect hadron spectra less than $(1 \sim 2)$ GeV. In the baryon octet, for instance, the mass difference of the proton and neutron is crucial to the phenomenological model of nuclei because it plays an important role in neutron β decay, which is related to the stability of nuclei. If the up and down quark masses were degenerate, the proton would be heavier due to the EM interaction, and our Universe would not exist! Even though the mass differences in the baryon octet spectrum have already been measured in experiments to good accuracy, it is important to confirm that we can *predict* these splittings in the standard model from first-principles computation. Parameterizing the calculated splittings in terms of low-energy constants (LEC) is also useful for effective theories like chiral perturbation theory (ChPT).

The mass of a hadron is determined by both quantum chromodynamics (QCD) and quantum electrodynamics (QED), though the vast majority of the mass is due to QCD. For the QCD interaction, since the coupling constant is large in the low-energy regime ($E \lesssim 1$ GeV), perturbation theory is not applicable, and we must turn to the techniques of lattice gauge theory to solve QCD for the hadron spectrum. On the other hand, the EM contributions to the masses, which break degeneracies due to flavor SU(3) (and isospin) symmetry since the up quark has charge $+2/3e$ and the down and strange quarks have charge $-1/3e$, are expected to depend on the small QED coupling constant, $\alpha_{\text{em}} \equiv e^2/4\pi \approx 1/137$. However, since the hadrons are formed from bound states of the quarks, there is no systematic way to treat the contributions in weak-coupling perturbation theory. Thus, calculations are done nonperturbatively in a combined lattice QCD + QED theory (indeed, even if the strong coupling constant were small, one is forced to a nonperturbative solution for QCD because of confinement). The state of the art in lattice calculations is such that subpercent errors (statistical and systematic) on low-lying hadron masses and other observable quantities are becoming the norm (for a broad review, see [1] and references therein). As the precision of lattice calculations improve, the EM splittings become more and more relevant. Indeed, the splittings themselves can be

computed with subpercent precision, at least for the statistical errors [2].

It is well known that the lowest-order EM effect, the so-called Dashen term [3], which enters at $O(\alpha_{\text{em}})$, is the dominant contribution to the charged-neutral pion mass difference. In the chiral limit where the quarks are all massless, it is also true for the kaons. This theorem, known as Dashen's theorem, is broken by terms of order $O(\alpha_{\text{em}}m)$ away from the chiral limit. Using an effective theory of QCD known as chiral perturbation theory, these corrections can be identified in the lattice calculation, and the nondegenerate quark masses determined by matching to the experimentally measured mass splittings [4],

$$m_{\pi^\pm} - m_{\pi^0} = 4.5936(5) \text{ MeV}, \quad (1)$$

$$m_{K^\pm} - m_{K^0} = -3.937(28) \text{ MeV}, \quad (2)$$

$$m_n - m_p = 1.293\,332\,1(4) \text{ MeV}. \quad (3)$$

In fact, any three hadron masses are enough to determine the three light quark masses, and we choose m_{π^+} , m_{K^+} , and m_{K^0} for reasons explained later. The determination of the up quark mass, m_u , is particularly interesting since one can check the simplest solution to the strong CP problem, $m_u = 0$.

In the study presented here, we work with lattice domain wall fermions (DWF) [5,6] for the quarks and the Iwasaki gauge action for the gluons. We use an ensemble of gluon configurations with a single lattice spacing, generated by the RBC and UKQCD collaborations using $(2 + 1)$ flavors of dynamical quarks, a pair of degenerate quarks for the up and down, and a heavier strange quark [7]. The photons are simulated in noncompact, quenched QED, as was done in the pioneering quenched QCD + quenched QED calculations [8,9].

There are several differences between this work and our previous one [2]. The most obvious is that the dynamical strange sea quark has been included here. In Ref. [2] the QED gauge potential was fixed to the Coulomb gauge, and here we work in the Feynman gauge in QED on finite volume, as described in Ref. [10]. Next, we perform fits to full next-to-leading order (NLO) partially quenched chiral perturbation theory (PQ χ PT), including photons, for both $SU(3)_L \times SU(3)_R$ chiral symmetry [11] and $SU(2)_L \times SU(2)_R$ plus kaon [7,12,13], where the latter treats only the pion triplet as pseudo-Nambu-Goldstone bosons. The NLO PQ χ PT for $SU(2)_L \times SU(2)_R$ plus kaon, including photons, is new, and is presented here for the first time. Calculations by the RBC and UKQCD collaborations [7,14–17], and more recently PACS-CS [18,19], have shown that the physical strange quark mass is out of reach for NLO SU(3) chiral perturbation theory. Since we also wish to determine the strange quark mass in our calculation, we have developed the chiral perturbation theory for the $SU(2)_L \times SU(2)_R$ -plus-kaon system, including photons. In addition, since the photons are not

confined, finite-volume effects are expected to be large, so we work with two lattice sizes, 16^3 and 24^3 , with the same lattice spacing to investigate these effects. The leading EM finite-volume effects have been computed in PQ χ PT [10], which we also use in our analysis.

This paper is organized as follows. In Sec. II we summarize the chiral perturbation theories used to fit our lattice calculations (details are given in Appendix B). In Sec. III the basic framework and details of the lattice simulations are given. Section IV contains results and discussion of the calculation, including the fitted LEC's and the quark masses. Section V discusses systematic errors, and in Secs. VI and VII we give the final values for the quark masses and meson splittings, respectively. We examine the impact of $(m_u - m_d)$ on the decay constant ratio, f_K/f_π in Sec. VIII. The nucleon mass splitting is computed in Sec. IX. Finally, this work is summarized in Sec. X.

We reported the preliminary results from the SU(3) PQ χ PT study in this work in Refs. [20,21]. The MILC Collaboration also presented their first results on the EM splittings, using improved staggered fermions and non-compact, quenched QED configurations in Ref. [22].

II. CHIRAL PERTURBATION THEORY

We briefly review the framework and formulas of partially quenched chiral perturbation theory relevant for our $2 + 1$ flavor calculation. The EM corrections in SU(2) chiral perturbation theory coupled to kaons are new. Details are given in Appendix B.

Recently it has been shown that SU(3) chiral perturbation theory is poorly convergent for quark masses near the physical strange quark mass, and that a straightforward and effective solution is to treat the strange quark mass m_s as large compared to the light quark masses m_l in an expansion in m_l/m_s [7,12,18,19]. We carry out fits to the data using both SU(3) and SU(2) chiral perturbation theory. We find the poor convergence extends to the EM sector as well, and use SU(2) chiral perturbation theory to quote our central results.

Before proceeding, it is important to discuss the order in chiral perturbation theory to which we work. For the SU(3) case where the kaon is a Nambu-Goldstone boson, the LO

includes all terms that are $O(p^2)$ and $O(e^2)$, and the NLO includes all terms that are $O(p^4)$, $O(e^2 p^2)$, and $O(e^4)$, where the conventional power counting is $O(e) \sim O(p)$. This counting is the same for the square of the masses and the mass-squared splittings. $O(e^4)$ contributions have so far been ignored [2,11] since $O(e^4) \ll O(e^2 p^2)$ in practice, and we also follow this here.

In the SU(2) theory coupled to kaons the power counting becomes a bit more complicated for the kaon (for the pion it is the same as in the SU(3) case). Since the kaon is no longer a Nambu-Goldstone boson, LO for the mass squared is now $O(p^0)$, and NLO is $O(p^2)$ and $O(e^2)$. The mass-squared EM splitting, however, remains the same order of magnitude as in (partially quenched) SU(3) chiral perturbation theory. That is, to obtain the NLO contributions to the mass-squared splittings, we must work to next-to-next-to-leading order (NNLO) for the masses. Since the aim here is to include all effects up to and including $O(e^2 p^2)$ terms in the meson mass-squared splittings as well as $m_d - m_u$, we include all $O(e^2 p^2)$ contributions to the kaon mass. Because we compute $m_d - m_u$ from the neutral-charged kaon mass-squared difference, the pure QCD effects at $O(p^4)$, including the one-loop logarithms [12], cancel and are not included in our analysis.

Finally, to avoid confusion we emphasize that in this paper we only calculate correlation functions for ‘‘charged,’’ or ‘‘off-diagonal’’ mesons. However, since we are free to change the charges and masses of the valence quarks making up these mesons, the total charge of the (unphysical) meson may happen to be zero. Sometimes we refer to these as ‘‘neutral’’ mesons, but it must be kept in mind these never correspond to the π^0 meson which requires so-called disconnected quark diagrams in its correlation function as well as the full treatment of ‘‘diagonal’’ mesons in PQ χ PT.

A. SU(3)_L \times SU(3)_R

The partially quenched chiral perturbation theory has been worked out in Ref. [11], and we adopt their notation. For three nondegenerate sea quarks and two nondegenerate valence quarks, labeled by ‘‘1’’ and ‘‘3,’’ the meson mass squared at NLO is

$$\begin{aligned}
M^2 = & \chi_{13} + \frac{2Ce^2}{F_0^2} q_{13}^2 + \frac{48L_6^r - 24L_4^r}{F_0^2} \chi_{13} \bar{\chi}_1 + \frac{16L_8^r - 8L_5^r}{F_0^2} \chi_{13}^2 - 48e^2 \frac{C}{F_0^4} L_4^r q_{13}^2 \bar{\chi}_1 - 16e^2 \frac{C}{F_0^4} L_5^r q_{13}^2 \chi_{13} - e^2 [12K_1^{Er} \\
& + 12K_2^{Er} - 12K_7^{Er} - 12K_8^{Er}] \bar{q}^2 \chi_{13} - e^2 [4K_5^{Er} + 4K_6^{Er}] q_p^2 \chi_{13} + e^2 [4K_9^{Er} + 4K_{10}^{Er}] q_p^2 \chi_p + 12e^2 K_8^{Er} q_{13}^2 \bar{\chi}_1 \\
& + 8e^2 [K_{10}^{Er} + K_{11}^{Er}] q_{13}^2 \chi_{13} - e^2 [8K_{18}^{Er} + 4K_{19}^{Er}] q_1 q_3 \chi_{13} + \frac{1}{3} \frac{1}{16\pi^2 F_0^2} R_{n13}^m \chi_{13} \chi_m \log \frac{\chi_m}{\mu^2} + \frac{1}{3} \frac{1}{16\pi^2 F_0^2} \\
& \times R_{q\pi\eta}^p \chi_{13} \chi_p \log \frac{\chi_p}{\mu^2} - 2e^2 \frac{C}{F_0^4} \frac{1}{16\pi^2} \left(\chi_{14} \log \frac{\chi_{14}}{\mu^2} q_{14} + \chi_{15} \log \frac{\chi_{15}}{\mu^2} q_{15} + \chi_{16} \log \frac{\chi_{16}}{\mu^2} q_{16} \right) q_{13} + 2e^2 \frac{C}{F_0^4} \frac{1}{16\pi^2} \\
& \times \left(\chi_{34} \log \frac{\chi_{34}}{\mu^2} q_{34} + \chi_{35} \log \frac{\chi_{35}}{\mu^2} q_{35} + \chi_{36} \log \frac{\chi_{36}}{\mu^2} q_{36} \right) q_{13} - \frac{(q_{13}^2) e^2}{16\pi^2} \chi_{13} \left[3 \log \left(\frac{\chi_{13}}{\mu^2} \right) - 4 \right] + e^2 \delta_{m_{\text{res}}} (q_1^2 + q_3^2). \quad (4)
\end{aligned}$$

Indices 1–3 always refer to valence quarks, 4–6 to sea quarks. The coefficients R_{n13}^m and $R_{q\pi\eta}^p$ are the residue functions written in terms of quark masses and are defined in Ref. [11]. The index p implies summation over valence indices 1 and 3, and if q is also present, then the sum is over pairs (1,3) and (3,1). The indices (m, n) signify a sum over pairs (π, η) and (η, π) . $\chi_{ij} = B_0(m_i + m_j)$ is the LO mass squared for a meson made of quarks with masses m_i and m_j , $q_{ij} = q_i - q_j$ where q_i is the electric charge of the i th quark in units of the fundamental charge e . $\bar{\chi}_1 = 2B_0(m_4 + m_5 + m_6)/3$ and $\bar{q}^2 = (q_4^2 + q_5^2 + q_6^2)/3$. χ_π and χ_η are given by the solution of

$$\chi_\pi + \chi_\eta = 2\bar{\chi}_1, \quad (5)$$

$$\chi_\pi\chi_\eta = \frac{4}{3}B_0^2(m_4m_5 + m_5m_6 + m_4m_6). \quad (6)$$

The LO Dashen term is proportional to the LEC C and the fine structure constant α_{em} . B_0 and F_0^1 are the LO QCD LEC's, the L 's are the Gasser-Leutwyler LEC's at NLO, and the K 's are the EM LEC's at $O(\alpha_{\text{em}}m)$. $\delta_{m_{\text{res}}}$ is a pure lattice-artifact LEC associated with the finite size of the extra dimension for DWF.

We note from Eq. (4) that masses of mesons $\sim \bar{q}q'$ made from degenerate valence quarks q, q' with equal charges do not have logarithmic corrections at NLO. This happens for the SU(2) case as well.

Following Ref. [11], the EM LEC's can be written in terms of five independent linear combinations of the K 's, which is all that can be determined from lattice calculations,

$$Y_1 = K_1^{Er} + K_2^{Er} - K_7^{Er} - K_8^{Er}, \quad (7)$$

$$Y_2 = K_9^{Er} + K_{10}^{Er}, \quad (8)$$

$$Y_3 = -K_5^{Er} - K_6^{Er} + 2K_{10}^{Er} + 2K_{11}^{Er}, \quad (9)$$

$$Y_4 = 2K_5^{Er} + 2K_6^{Er} + 2K_{18}^{Er} + K_{19}^{Er}, \quad Y_5 = K_8^{Er}. \quad (10)$$

The EM mass-squared splitting of the pseudoscalar meson is defined as $\Delta M^2 = M^2(e \neq 0) - M^2(e = 0)$. In terms of the Y_i 's, it becomes

$$\begin{aligned} \Delta M^2 = & \frac{2Ce^2}{F_0^2}q_{13}^2 - 48e^2\frac{C}{F_0^4}L_4^r q_{13}^2\bar{\chi}_1 - 16e^2\frac{C}{F_0^4}L_5^r q_{13}^2\chi_{13} - 12e^2Y_1\bar{q}^2\chi_{13} + 4e^2Y_2q_p^2\chi_p + 4e^2Y_3q_{13}^2\chi_{13} \\ & - 4e^2Y_4q_1q_3\chi_{13} + 12e^2Y_5q_{13}^2\bar{\chi}_1 - 2e^2\frac{C}{F_0^4}\frac{1}{16\pi^2}\left(\chi_{14}\log\frac{\chi_{14}}{\mu^2}q_{14} + \chi_{15}\log\frac{\chi_{15}}{\mu^2}q_{15} + \chi_{16}\log\frac{\chi_{16}}{\mu^2}q_{16}\right)q_{13} \\ & + 2e^2\frac{C}{F_0^4}\frac{1}{16\pi^2}\left(\chi_{34}\log\frac{\chi_{34}}{\mu^2}q_{34} + \chi_{35}\log\frac{\chi_{35}}{\mu^2}q_{35} + \chi_{36}\log\frac{\chi_{36}}{\mu^2}q_{36}\right)q_{13} - \frac{(q_{13})^2e^2}{16\pi^2}\chi_{13}\left[3\log\left(\frac{\chi_{13}}{\mu^2}\right) - 4\right] \\ & + e^2\delta_{m_{\text{res}}}(q_1^2 + q_3^2). \end{aligned} \quad (11)$$

Note that Y_1 is proportional to the sea quark charges. Since we work with quenched QED, this LEC cannot be obtained from our calculation.

We carry out the fit in Sec. IV B 2 with the finite-volume correction to the chiral logarithms taken into account. The finite-volume correction to the leading-order chiral logarithms was computed in Ref. [10],

$$\begin{aligned} \delta M^2(L) \equiv & M^2(L) - M^2(\infty) \\ = & \frac{1}{3}\frac{1}{16\pi^2F_0^2}R_{n13}^m\chi_{13}\frac{\mathcal{M}(\sqrt{\chi_m}L)}{L^2} + \frac{1}{3}\frac{1}{16\pi^2F_0^2}R_{q\pi\eta}^p\chi_{13}\frac{\mathcal{M}(\sqrt{\chi_p}L)}{L^2} - 2e^2\frac{C}{F_0^4}\frac{1}{16\pi^2}q_{13}\left(q_{14}\frac{\mathcal{M}(\sqrt{\chi_{14}}L)}{L^2}\right. \\ & + q_{15}\frac{\mathcal{M}(\sqrt{\chi_{15}}L)}{L^2} + q_{16}\frac{\mathcal{M}(\sqrt{\chi_{16}}L)}{L^2}) + 2e^2\frac{C}{F_0^4}\frac{1}{16\pi^2}q_{13}\left(q_{34}\frac{\mathcal{M}(\sqrt{\chi_{34}}L)}{L^2} + q_{35}\frac{\mathcal{M}(\sqrt{\chi_{35}}L)}{L^2}\right. \\ & + q_{36}\frac{\mathcal{M}(\sqrt{\chi_{36}}L)}{L^2}) - 3\frac{(q_{13})^2e^2}{4\pi}\frac{\kappa}{L^2} + \frac{(q_{13})^2e^2}{(4\pi)^2}\left[\frac{\mathcal{K}(\sqrt{\chi_{13}}L)}{L^2} - 4\sqrt{\chi_{13}}\frac{\mathcal{H}(\sqrt{\chi}L)13}{L}\right]. \end{aligned} \quad (12)$$

$\mathcal{M}(x)$ is the function appearing in the finite-volume correction to the chiral logarithm induced by the tadpole diagram,

¹ F_0 is normalized such that the physical decay constant is roughly 92 MeV.

$$\mathcal{M}(x) \equiv 4\pi \int_0^\infty \frac{d\lambda}{\lambda^2} \exp\left(-\frac{x^2}{4\pi}\lambda\right) \mathcal{T}(\lambda),$$

$$\mathcal{T}(\lambda) \equiv \left(\vartheta_3\left(0, i\frac{1}{\lambda}\right)\right)^3 - 1, \quad (13)$$

where $\vartheta_3(v; \tau)$ is a Jacobi-theta function,

$$\vartheta_3(v, \tau) \equiv \sum_{n=-\infty}^{\infty} \exp(\pi\tau in^2 + 2\pi\tau in).$$

The other functions and a constant κ are given by [10]

$$\kappa \equiv \int_0^\infty \frac{d\lambda}{\lambda^2} \mathcal{S}(\lambda) = 2.837 \dots, \quad (14)$$

$$\mathcal{S}(\lambda) \equiv -\left[\left(\vartheta_3\left(0, i\frac{1}{\lambda}\right)\right)^3 - 1 - \lambda^{3/2}\right], \quad (15)$$

$$\mathcal{H}(x) \equiv \pi \int_0^\infty \frac{d\lambda}{\lambda^{3/2}} \operatorname{erf}\left(x\sqrt{\frac{\lambda}{4\pi}}\right) \mathcal{S}(\lambda), \quad (16)$$

$$\mathcal{K}(x) \equiv 4\pi \int_0^\infty \frac{d\lambda}{\lambda} \frac{1}{\lambda} (1 - e^{-(x^2/4\pi)\lambda}) \mathcal{S}(\lambda), \quad (17)$$

where $\operatorname{erf}(x)$ is the error function,

$$\operatorname{erf}(x) = \frac{2}{\sqrt{\pi}} \int_0^x ds e^{-s^2}.$$

B. $SU(2)_L \times SU(2)_R$ plus kaon

Some time ago Roesl [12] worked out the low-energy $SU(2)$ Lagrangian of pions coupled to a kaon. Recently, the RBC and UKQCD collaborations showed that $SU(3)$ chiral perturbation theory is poorly convergent for quark masses near the strange quark mass but that $SU(2)$ chiral perturbation theory coupled to a kaon worked well for pions with masses less than about 400 MeV at NLO [7]. In Ref. [7], the unitary Lagrangian was extended to the partially quenched case. Here, we extend both works to include the EM interactions to the order $\alpha_{\text{em}}m$ for the kaon mass, including the one-loop diagrams proportional to α_{em} . For the pion mass, we begin with the partially quenched $SU(3)$ Lagrangian in Ref. [11] and expand in m_l/m_s .

1. Pions

We derive the $SU(2)_L \times SU(2)_R$ result for the pion mass-squared splitting by expanding Eq. (11) in $(m_1, m_3, m_4, m_5)/m_6$, where m_6 is the strange sea quark mass, m_1 and m_3 are taken as nondegenerate light valence quark masses, and m_4 and m_5 the light sea quark masses,

$$\begin{aligned} \Delta M^2 = & \frac{2Ce^2}{F_0^2} q_{13}^2 - 48e^2 \frac{C}{F_0^4} L_4^r q_{13}^2 \frac{\chi_4 + \chi_5}{3} - 16e^2 \frac{C}{F_0^4} L_5^r q_{13}^2 \chi_{13} - 12e^2 Y_1 \bar{q}^2 \chi_{13} + 4e^2 Y_2 q_p^2 \chi_p + 4e^2 Y_3 q_{13}^2 \chi_{13} \\ & - 4e^2 Y_4 q_1 q_3 \chi_{13} + 12e^2 Y_5 q_{13}^2 \frac{\chi_4 + \chi_5}{3} - e^2 \frac{3}{16\pi^2} \chi_{13} \log \frac{\chi_{13}}{\mu^2} q_{13}^2 + e^2 \frac{1}{4\pi^2} \chi_{13} q_{13}^2 - e^2 \frac{C}{F_0^4} \\ & \times \frac{1}{8\pi^2} q_{13} \left(q_{14} \chi_{14} \log \frac{\chi_{14}}{\mu^2} + q_{15} \chi_{15} \log \frac{\chi_{15}}{\mu^2} - q_{34} \chi_{34} \log \frac{\chi_{34}}{\mu^2} - q_{35} \chi_{35} \log \frac{\chi_{35}}{\mu^2} \right) + e^2 \delta_{m_{\text{res}}} (q_1^2 + q_3^2). \end{aligned} \quad (18)$$

In Eq. (18) all of the low-energy constants now depend implicitly on the strange sea quark mass which is fixed (we rename them below to distinguish them from their $SU(3)$ counterparts). In addition the Dashen term has absorbed contributions from the NLO $SU(3)$ LEC's and the logs which do not depend on the charges or masses of the up and down quarks,

$$\begin{aligned} & \frac{2Ce^2}{F_0^2} q_{13}^2 + 12e^2 Y_5 q_{13}^2 \frac{\chi_6}{3} - \frac{2e^2}{16\pi^2} \frac{C}{F_0^4} q_{13}^2 \chi_6 \log \frac{\chi_6}{\mu^2} \\ & - 48e^2 \frac{C}{F_0^4} L_4^r q_{13}^2 \frac{\chi_6}{3}. \end{aligned} \quad (19)$$

Including the contributions in pure QCD [7], the pion mass squared to NLO becomes

$$\begin{aligned} M^2 = & \chi_{13} \left[1 + \frac{24}{F^2} (2L_6^{(2)} - L_4^{(2)}) \frac{\chi_4 + \chi_5}{3} + \frac{8}{F^2} (2L_8^{(2)} - L_5^{(2)}) \chi_{13} + \frac{1}{2} \frac{1}{16\pi^2 F^2} \left(R_{13}^\pi \chi_\pi \log \frac{\chi_\pi}{\mu^2} + R_{\pi 3}^1 \chi_1 \log \frac{\chi_1}{\mu^2} \right. \right. \\ & \left. \left. + R_{\pi 1}^3 \chi_3 \log \frac{\chi_3}{\mu^2} \right) \right] + \frac{2C^{(2)} e^2}{F^2} q_{13}^2 - 12e^2 Y_1^{(2)} \bar{q}^2 \chi_{13} + 4e^2 Y_2^{(2)} q_p^2 \chi_p + 4e^2 Y_3^{(2)} q_{13}^2 \chi_{13} - 4e^2 Y_4^{(2)} q_1 q_3 \chi_{13} \\ & + 12e^2 Y_5^{(2)} q_{13}^2 \frac{\chi_4 + \chi_5}{3} - e^2 \frac{3}{16\pi^2} \chi_{13} \log \frac{\chi_{13}}{\mu^2} q_{13}^2 + e^2 \frac{1}{4\pi^2} \chi_{13} q_{13}^2 - e^2 \frac{C^{(2)}}{F^4} \frac{1}{8\pi^2} q_{13} \left(q_{14} \chi_{14} \log \frac{\chi_{14}}{\mu^2} \right. \\ & \left. + q_{15} \chi_{15} \log \frac{\chi_{15}}{\mu^2} - q_{34} \chi_{34} \log \frac{\chi_{34}}{\mu^2} - q_{35} \chi_{35} \log \frac{\chi_{35}}{\mu^2} \right) + e^2 \delta_{m_{\text{res}}} (q_1^2 + q_3^2). \end{aligned} \quad (20)$$

The LO LEC's F and B are the counterparts of F_0 and B_0 from the SU(3) theory, and the other SU(2) LEC's are denoted by an explicit superscript "(2)." R_{jk}^i is given in SU(2) partially quenched case as

$$R_{jk}^i \equiv \frac{(\chi_i - \chi_4)(\chi_i - \chi_5)}{(\chi_i - \chi_j)(\chi_i - \chi_k)}. \quad (21)$$

The finite-volume correction to Eq. (20) is given by

$$\begin{aligned} \delta M^2(L) &\equiv M^2(L) - M^2(\infty) \\ &= \frac{1}{2} \frac{\chi_{13}}{16\pi^2 F^2} \left(R_{13}^\pi \frac{\mathcal{M}(\sqrt{\chi_\pi} L)}{L^2} + R_{\pi 3}^1 \frac{\mathcal{M}(\sqrt{\chi_1} L)}{L^2} \right. \\ &\quad \left. + R_{\pi 1}^3 \frac{\mathcal{M}(\sqrt{\chi_3} L)}{L^2} \right) - 2e^2 \frac{C^{(2)}}{F^4} \frac{1}{16\pi^2} q_{13} \\ &\quad \times \left(q_{14} \frac{\mathcal{M}(\sqrt{\chi_{14}} L)}{L^2} + q_{15} \frac{\mathcal{M}(\sqrt{\chi_{15}} L)}{L^2} \right. \\ &\quad \left. - q_{34} \frac{\mathcal{M}(\sqrt{\chi_{34}} L)}{L^2} - q_{35} \frac{\mathcal{M}(\sqrt{\chi_{35}} L)}{L^2} \right) \\ &\quad - 3 \frac{(q_{13})^2 e^2}{4\pi} \frac{\kappa}{L^2} + \frac{(q_{13})^2 e^2}{(4\pi)^2} \\ &\quad \times \left\{ \frac{\mathcal{K}(\sqrt{\chi_{13}} L)}{L^2} - 4\sqrt{\chi_{13}} \frac{\mathcal{H}(\sqrt{\chi_{13}} L)}{L} \right\}. \quad (22) \end{aligned}$$

The constant κ and various functions are defined in Eqs. (13), (14), (16), and (17).

2. Kaons

The kaon mass can be obtained from the tree-level Lagrangian, following Refs. [12,13], by constructing the kaon from one light and one "heavy" quark and writing down all operators with the desired symmetries in a nonrelativistic theory where the power counting is straightforward. The needed relativistic Lagrangian is then constructed such that in the limit that the kaon is heavy, the nonrelativistic theory is recovered. This has been done in the case of QCD to NNLO in Ref. [12] and to NLO in partially quenched QCD in Ref. [7]. Here we add the order $e^2 p^2$ terms induced by the EM interactions. Once the tree-level Lagrangian is known, the one-loop corrections can be computed. The $O(e^2)$ Lagrangian and details of the one-loop calculation are given in Appendix B.

The $O(e^2 p^2)$ Lagrangian is quite complicated, with many operators appearing. While we have listed all possible operators in Appendix B that contribute, we have not yet reduced them to a linearly independent set using relativistic invariance and the equations of motion. Still, this is enough to give the general quark mass and charge dependence. In the following, this is given by the generic LEC's $x_3^{(K)} \sim x_8^{(K)}$.

From Eqs. (B36), (B39), and (B42), the mass squared of the kaon is

$$\begin{aligned} M_K^2 &= M^2 - 4B(A_3 m_1 + A_4(m_4 + m_5)) \\ &\quad + e^2(2(A_K^{(1,1)} + A_K^{(2,1)})q_1^2 + A_K^{(s,1,1)}q_3^2 + 2A_K^{(s,2)}q_1 q_3) \\ &\quad - \frac{e^2}{(4\pi)^2 F^2} ((A_K^{(1,1)} + 3A_K^{(2,1)})q_1^2 + A_K^{(s,2)}q_1 q_3) \\ &\quad \times \sum_{s=4,5} \chi_{1s} \log \frac{\chi_{1s}}{\mu^2} + e^2 m_1 (x_3^{(K)}(q_1 + q_3)^2 \\ &\quad + x_4^{(K)}(q_1 - q_3)^2 + x_5^{(K)}(q_1^2 - q_3^2)) + e^2 \frac{m_4 + m_5}{2} \\ &\quad \times (x_6^{(K)}(q_1 + q_3)^2 + x_7^{(K)}(q_1 - q_3)^2 \\ &\quad + x_8^{(K)}(q_1^2 - q_3^2)) + e^2 \delta_{m_{\text{res}}} (q_1^2 + q_3^2), \quad (23) \end{aligned}$$

where we have included the explicit chiral symmetry breaking LEC $\delta_{m_{\text{res}}}$, the same as for the pion. Here the subscript "1" stands for a light valence quark, u or d , and "3" for the strange valence quark (charge). "4" and "5" refer to the u and d sea quarks, respectively. To avoid confusion we note that LEC's without superscripts denote the pure QCD LEC's of Refs. [7,12] while those with superscripts are EM LEC's defined in Appendix B. The finite-volume correction to Eq. (23) is given in Appendix B, Eqs. (B40) and (B41).

Notice that the LO "Dashen" term is different than for the pion: the latter is a single LEC proportional to q_{13}^2 while the former consists of three LEC's and depends on the u , d , and s charges separately. This is a consequence of the different chiral symmetries assumed in the two cases.

We remind the reader that we do not keep terms of order p^4 and e^4 .

III. LATTICE FRAMEWORK

Following Ref. [8], the lattice calculation employs combined QCD + QED gauge configurations. A combined gluon-photon gauge link is simply the product of two independent links, a SU(3) color matrix for the gluons and a U(1) phase for the photons.

$$U_{x,\mu} = U_{x,\mu}^{(3)} \times (U_{x,\mu}^{(1)})^{Q_i}, \quad (24)$$

where $Q_i = e q_i$ is the charge of the quark with flavor i . It is the combined link that appears in the lattice Dirac operator, in the usual gauge-invariant way. The gluon and photon links were generated independently in our calculation, so the sea quarks were not electrically charged. This quenched QED calculation suffers a systematic error that is expected to be $O(\alpha_{\text{em}} \alpha_s)$ from a simple vacuum polarization argument. In chiral perturbation theory, the charged sea quarks first contribute at $O(\alpha_{\text{em}} m_{\text{val}})$ for the valence quark mass m_{val} , as we have seen in Sec. II. This drawback can be eliminated with the technique of reweighting [23–25], which is becoming common in large scale dynamical calculations [15–17,26], and is under active investigation by us [27,28]. In a different context, combined dynamical simulations have also been performed for the

TABLE I. Ensembles of QCD gauge field configurations generated by the RBC and UKQCD collaborations [7,17,30] for $\beta = 2.13$ with the Iwasaki gauge action that were used in this work. Δ is the separation between measurements in molecular dynamics time units. N_{meas} denotes the total number of measurements, and t_{src} is the Euclidean time-slice location of the source.

Lat	m_{sea}	m_{val}	Trajectories	Δ	N_{meas}	t_{src}
16^3	0.01	0.01, 0.02, 0.03	500–4000	20	352	4,20
16^3	0.02	0.01, 0.02, 0.03	500–4000	20	352	4,20
16^3	0.02	0.01, 0.02, 0.03	500–4000	20	352	4,20
24^3	0.005	0.001, 0.005, 0.01, 0.02, 0.03	900–8660	40	195	0
24^3	0.01	0.001, 0.01, 0.02, 0.03	1460–5040	20	180	0
24^3	0.02	0.02	1800–3580	20	360	0, 16, 32, 48
24^3	0.03	0.03	1260–3040	20	360	0, 16, 32, 48

first time [29], where the sea quarks are charged from the beginning.

For the QCD configurations, we use the 2 + 1 flavor QCD configurations generated with DWF and the Iwasaki gauge action ($\beta = 2.13$) by the RBC and UKQCD collaborations [7,17,30]. The lattice sizes are $16^3 \times 32$ and $24^3 \times 64$. The lattice spacing² is $a^{-1} = 1.784(44)$ GeV, as determined from the Ω baryon mass on the larger lattice, and which yields physical volumes $(1.76 \text{ fm})^3$ and $(2.65 \text{ fm})^3$, respectively. The domain wall height M_5 and the size of the extra dimension L_5 are 1.8 and 16, respectively. The residual quark mass in the chiral limit for pure QCD is found to be $m_{\text{res}} = 0.003 148(46)$ and $0.003 203$ (15), for the 16^3 and 24^3 lattice sizes, respectively. The latter is slightly larger than the value $0.003 15(2)$ determined in Ref. [7] on a smaller ensemble of configurations.

The ensembles and number of measurements on each are summarized in Table I. The stopping criterion in the conjugate-gradient algorithm used to compute quark propagators was 10^{-8} , the same as in Ref. [7]. To increase our statistics on some of the ensembles, two or more different locations of the source are used on each configuration (see Table I). The QCD configurations are separated by 20 or 40 Monte Carlo time units to suppress the autocorrelations in them. Our calculation is for the pseudoscalar meson at the unitary point ($m_1 = m_3 = m_4 = m_5$) and the partially quenched point (arbitrary quark mass combination).

The quenched QED configurations were generated on the noncompact manifold [2,10]. Here we employ the Feynman gauge instead of the Coulomb gauge which was used previously [2] in our two-flavor calculation. Since the mass is a gauge-invariant quantity, the result should be consistent within the statistical error, up to the effects of zero modes. Further, removal of the modes also results in the satisfaction of Gauss' Law on the torus [10]. An advantage of the noncompact QED formalism is that the

$U(1)$ gauge potential A_μ can be chosen randomly with the correct Gaussian distribution in momentum space, then Fourier transformed to coordinate space, so there are no autocorrelations in the ensemble. Finally, yet another advantage is that there is no lattice-artifact photon self-interactions in the action. To couple A_μ to the fermions, the noncompact field is exponentiated to produce the photon link, $U_{x,\mu}^{(1)} = \exp(ieA_{x,\mu})$, where $e = \sqrt{4\pi\alpha_{\text{em}}} \approx 0.30286$.

Since the QED interaction does not confine, it is possible that the finite volume may induce a significant systematic error. We thus do our simulation on both 16^3 and 24^3 lattice configurations with the same lattice spacing. This allows direct investigation of the finite-volume effect in the mass spectrum.

IV. RESULTS

In this section we present our results, focusing on the 24^3 ensembles, for the electromagnetic pseudoscalar mass splittings (ΔM^2), EM LEC's in SU(3) and SU(2) chiral perturbation theory describing the pseudoscalar masses, and the quark masses. Results from the 16^3 ensemble are used for estimating finite-volume effects which are discussed extensively in Sec. V. Before turning to the results for ΔM^2 , we first describe lattice-artifact electromagnetic effects induced by the finite size of the fifth dimension of the DWF used to simulate the four dimensional u , d , and s quarks.

In the following the notation $u\bar{u}$ ($d\bar{d}$) denotes a meson whose two-point correlation function is made from just the connected quark diagram using degenerate light quarks with equal charges, $q = 2/3(-1/3)$. Such a meson is neutral, but should not be confused with the π^0 , which requires disconnected quark diagrams.

A. Electromagnetic effects in m_{res}

We first calculate the residual mass m_{res} [31–33] from the pure QCD configurations. Then we consider the residual mass from the combined QCD + QED configurations so that the QED contribution to m_{res} can be extracted. In the lattice DWF, m_{res} is determined from the ratio

²This result is slightly larger than the published one, 1.729 (28) GeV, in Ref. [7] because it was determined on a larger ensemble of lattices. It is also larger than the result of a combined fit, including new 32^3 , $\beta = 2.25$, ensembles [15–17]. Later, we use the slight difference as a systematic error.

$$R(t) = \frac{\langle \sum_x J_{5q}^a(\vec{x}, t) \pi^a(0) \rangle}{\langle \sum_x J_5^a(\vec{x}, t) \pi^a(0) \rangle}, \quad (25)$$

where t is the Euclidean time, J_{5q}^a is a pseudoscalar density evaluated at the midpoint of the extra dimension, π^a denotes the usual $4d$ pseudoscalar density, and the superscript a is a nonsinglet flavor index. The correlation functions in Eq. (25) are computed from wall source, point-sink, quark propagators.

The residual mass is an ultraviolet, additive shift of the input, bare quark mass. Because we are interested only in the EM meson mass-squared splittings, the leading-order dependence of m_{res} on the bare quark mass cancels, and we use a mass-independent residual mass in our later analysis that can be identified by extrapolating $R(t)$ for the unitary quark masses to $m_f = 0$ with a suitable t average.

Table II shows the numerical result of the residual mass computed from the QCD configurations alone. In each case, $R(t)$ was averaged over the range $9 \leq t \leq N_t/2$ for the size N_t of the lattice in the time direction, after folding the correlation function about $N_t/2$. Figure 1 shows the chiral extrapolation of m_{res} . The residual mass at the chiral limit is very close between the 16^3 and 24^3 lattices. m_{res} is around 0.003, which is comparable to the lightest input sea quark mass, $m_l = 0.005$, and larger than the smallest valence quark mass $m_f = 0.001$, so the effect of the explicit violation of chiral symmetry from finite L_s is not negligible in our calculation. Our measured values are roughly consistent with those found by the RBC and UKQCD collaborations [7,30].

Next we consider the QED contribution to the residual quark mass. The QED contribution from quark flavor i can be expressed as

$$m_{\text{res},i}(\text{QCD} + \text{QED}) - m_{\text{res}}(\text{QCD}) = e^2 C_2 q_i^2, \quad (26)$$

where $m_{\text{res},i}(\text{QCD} + \text{QED})$ means the residual mass computed on the combined QCD + QED configurations and $m_{\text{res}}(\text{QCD})$, the residual mass computed on the pure QCD configurations. Both are evaluated at $m_f = 0$ and the former with physical quark charge q_i . C_2 , which is of order $O(m_{\text{res}})$, parametrizes the QED contribution to the additive shift of the quark mass. Although we compute this

TABLE II. The QCD residual mass for 16^3 and 24^3 lattice sizes. The data correspond to unitary mass points. The fit range for $R(t)$ [defined in Eq. (25)] is $9 \leq t \leq N_t/2$.

m_{sea}	16^3 m_{res}	24^3 m_{res}
Chiral limit	0.0031 48(46)	0.003 203(15)
0.005	N/A	0.003 222(16)
0.01	0.003 177(31)	0.003 230(15)
0.02	0.003 262(29)	0.003 261(16)
0.03	0.003 267(28)	0.003 297(15)

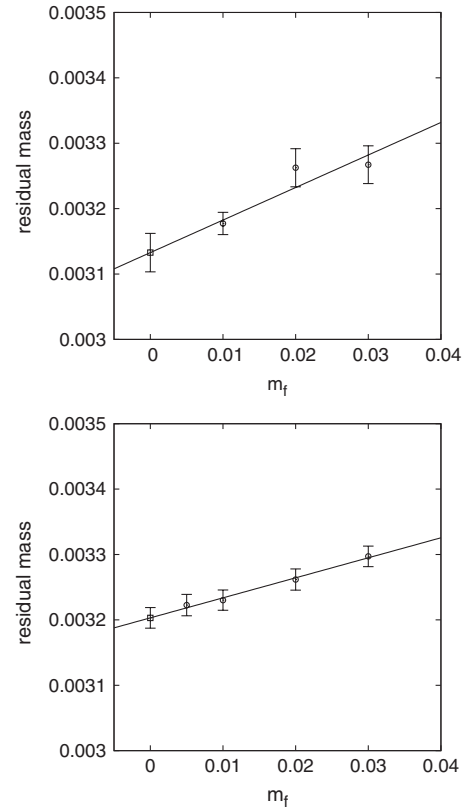


FIG. 1. The QCD residual mass for 16^3 (upper) and 24^3 (lower) lattice sizes. The data correspond to unitary mass points. The linear chiral extrapolation to the $m_f = 0$ limit is also shown on the plot.

correction via the Ward-Takahashi identity for DWF [31], using a neutral meson made with degenerate, equally charged quarks, the form of Eq. (26) is completely consistent with a calculation in weak-coupling perturbation theory, say from the one-loop self-energy Feynman diagram for a quark with charge q_i . In our chiral perturbation theory power counting, the QED contribution to the residual mass is $O(\alpha_{\text{em}} m_{\text{res}})$ and must therefore be included in our NLO analysis discussed in the next section.

To compute the residual mass and extract the EM contribution via Eq. (26), we use $u\bar{u}$ or $d\bar{d}$ correlation functions in Eq. (25).³ The total contribution to the meson mass squared due to explicit chiral symmetry breaking is, as in the case of pure DWF QCD, just the sum of contributions from each quark in the meson, modulo higher order than $O(\alpha_{\text{em}} m_{\text{res}})$ corrections. Table III shows the results for C_2 from $u\bar{u}$ and $d\bar{d}$ correlation functions. They agree well up to two digits, which implies that the $O(\alpha_{\text{em}}^2 m_{\text{res}})$ contribution is quite small. These differences are higher

³In an earlier paper [2] we mistakenly included an independent contribution, proportional to $q_i q_j$, to the residual mass for the charged mesons made of quarks with charges q_i and q_j . This is clearly inconsistent with flavor conservation and the definition of a renormalized quark mass defined in perturbation theory.

TABLE III. $C_2 (\times 10^3)$ in Eq. (26), representing the electromagnetic contribution to the residual mass. $u\bar{u}$ and $d\bar{d}$ denote the type of correlation function used to extract C_2 .

L_s	$u\bar{u}$	$d\bar{d}$
16 ³ lattice size		
16	2.597(23)	2.532(22)
32	0.309(16)	0.301(16)
24 ³ lattice size		
16	2.585(7)	2.519(7)

order in chiral perturbation theory relative to the one we work to in this paper, so we neglect them. We note that $C_2 e^2 q_i^2$ is the expected size, $O(\alpha_{\text{em}} m_{\text{res}})$. The attained statistical precision on C_2 , which is impressive, of course stems from the fact that $m_{\text{res},i}(\text{QCD} + \text{QED})$ and $m_{\text{res}}(\text{QCD})$ are computed on *exactly* the same set of gluon configurations, so they are highly correlated, and the QCD fluctuations cancel between them. In addition, C_2 appears to be insensitive to the volume (see Table III), presumably because the residual mass arises from the UV, short distance, regime.

B. Meson mass splittings

The electromagnetic mass splittings are determined from the pseudoscalar masses computed with $e \neq 0$ and $e = 0$, using the same gluon configurations. We use the additional trick of averaging correlation functions over $\pm e$, configuration by configuration [2,34].

In Fig. 2, the improvement due to the $\pm e$ averaging is demonstrated for the meson mass-squared splitting. The vertical axis shows the ratio of the statistical error *without* the trick to that with the trick, so that larger values indicate smaller statistical error for the $\pm e$ averaging trick. In most cases there is a large decrease ($\sim 1/10$) in the error over the naive factor of $\sqrt{2}$ that would result simply from doubling of the measurements (dashed line), while the few points with ratio exactly equal to one correspond to combinations that are trivially invariant under the change $e \rightarrow -e$. This procedure corresponds to including the QED configuration $-A_{x,\mu}$ for each $A_{x,\mu}$ in the path integral and can exactly cancel unphysical $O(e)$ noise with finite statistics which would have obscured the physical $O(e^2)$ signal of interest, only the latter of which survives in the infinite statistics limit. Together, the complete procedure yields mass-squared splittings with subpercent statistical precision.

The pseudoscalar meson masses are obtained from single state fits to wall source, point-sink correlation functions with periodic boundary conditions in time with use of the fit function

$$C_{\text{fit}}(t - t_{\text{src}}) = A[e^{-M(t-t_{\text{src}}+N_t)\%N_t} + e^{-M(N_t-t+t_{\text{src}})\%N_t}], \quad (27)$$

where M is the ground state meson mass, and t_{src} is the time slice where the source is placed. To improve statistics in

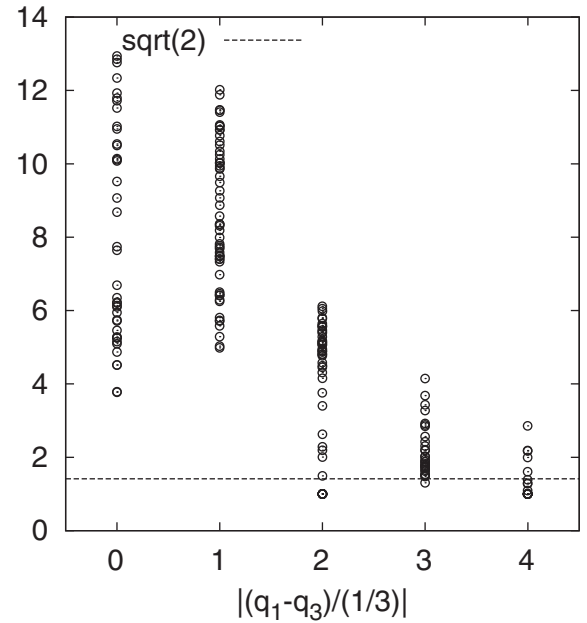


FIG. 2. A comparison of the statistical errors for the meson mass-squared splitting with and without the $\pm e$ averaging trick [2,34]. The vertical axis shows the ratio of the error *without* the average to that with the average, so that larger values indicate smaller statistical error from the $\pm e$ averaging trick. In most cases there is a large decrease ($\sim 1/10$) in the error over the naive factor of $\sqrt{2}$ that would result simply from doubling of the measurements (dashed line). The few points with ratio exactly equal to one correspond to combinations that are trivially invariant under the change $e \rightarrow -e$, i.e., $m_1 = m_3$ and $q_1 = -q_3$.

some cases, we average results from two sources (see Table I). The fitting procedure is done with the standard χ^2 minimization (maximum likelihood), and the error on the mass is obtained by the standard jackknife method. Since the meson correlation function is symmetric about the midpoint (from the source) in the time direction, we fold the data about this point and fit with a time range smaller than $N_t/2$. Based on the obtained effective masses (a representative example is shown in Fig. 3), for all correlation functions we chose a fit range of $9 \leq t - t_s \leq N_t/2$.

The pseudoscalar meson masses are tabulated in Tables XIII and XIV. We have extracted the masses in two ways, one being from the fits to the correlation functions using the full covariance matrix and the other being uncorrelated fits following [7,17]. The values of χ^2/dof for the covariant fits are roughly one for the 24³ ensembles, but somewhat higher in some cases for the 16³ ones and for the heavier quark masses on both ensembles. Such behavior for the 16³ ensembles was seen in the earlier, pure QCD, analysis using these configurations, and was attributed to an inferior gauge field evolution algorithm [30]. An improved algorithm was used to generate the 24³ ensemble. From Tables XIII and XIV the masses and errors determined with either fit method agree quite well. Our final analysis is based on the masses from the uncorrelated fits in

order to be consistent with the analysis in Refs. [7,17] from which we take the pure QCD LEC's. The typical statistical error on the mass is at the half of a percent level and smaller.

The meson mass-squared splittings are given by $\Delta M^2 = M^2(e \neq 0) - M^2(e = 0)$, and the errors are again computed using a jackknife procedure. As an example, in Figs. 4 and 5, ΔM^2 for the $d\bar{d}$ meson is shown. Only the unitary points appear in the figure. A full summary of the mass-squared splittings is given in Tables XV and XVI. The promised statistical precision is observed. Even though the errors on the masses themselves are of the same order as the mass difference, the splitting is statistically well resolved

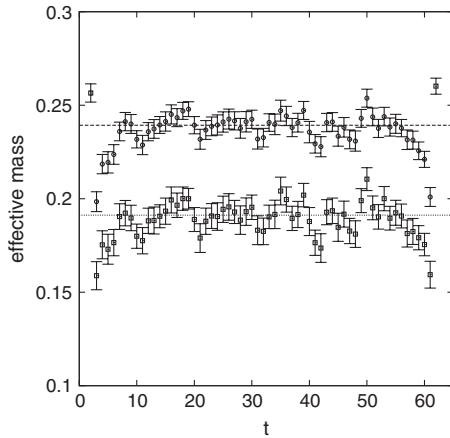


FIG. 3. Representative effective masses. Lattice size 24^3 . $m_{\text{sea}} = 0.005$, $m_1 = m_3 = 0.01$, $q_1 = 1/3$ and $q_3 = 0$ (upper points) and $m_{\text{sea}} = m_1 = m_3 = 0.005$, $q_1 = 1/3$ and $q_3 = -1/3$ (lower points). The horizontal lines represent the fit result.

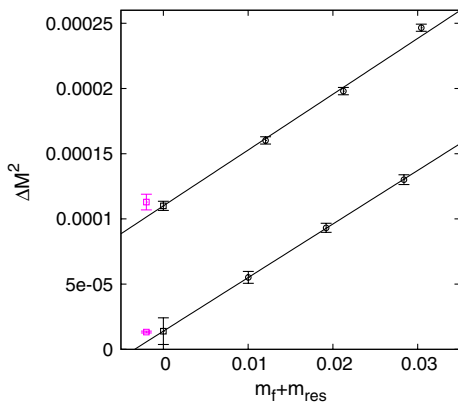


FIG. 4 (color online). ΔM^2 for the $d\bar{d}$ meson, with $L_s = 16$ (upper set of line and plots) and 32 , 16^3 lattice size from the SU(3) fit. The extrapolated values (box) are $e^2 \delta_{m_{\text{res}}} (q_1^2 + q_3^2)$. For comparison, we also show the values of $B_0 C_2 e^2 (q_1^2 + q_3^2)$ obtained from the Ward-Takahashi Identity (values are slightly shifted horizontally to the left for clarity). $\delta_{m_{\text{res}}}$ is obtained from the fit range of 0.01 – 0.02 for $L_s = 16$ and 0.01 – 0.03 for $L_s = 32$. The error on $B_0 C_2 e^2 (q_1^2 + q_3^2)$ comes mostly from the error on B_0 .

under the jackknife analysis thanks to the strong statistical correlation between $e = 0$ and $e \neq 0$.

We pause to compare the observed explicit chiral symmetry breaking effects to those expected from the discussion of the residual mass in the previous section. In the chiral limit, $m_f = -m_{\text{res}}(\text{QCD})$, and in the absence of EM induced explicit chiral symmetry breaking ($L_s \rightarrow \infty$), the neutral meson mass squared should vanish (up to α_{em}^2 corrections which we ignore), and so too should the splittings. But it is clear from Figs. 4 and 5 that the $d\bar{d}$ mass-squared splitting does not (the same is true for the $u\bar{u}$ meson). Following the discussion in Sec. IVA and from the result of the pseudoscalar mass squared at the lowest order in chiral perturbation theory, the shift in the splitting in the chiral limit should be $2B_0 C_2 e^2 q_d^2$ or $2BC_2 e^2 q_d^2$, depending on whether we choose SU(3) or SU(2) chiral perturbation theory. A simple linear fit, also shown in Fig. 4, suggests this is true. Note that at NLO there are no logs in the splitting of neutral mesons made from only connected quark propagators, that is, a charged meson whose net charge happens to be zero. Further, by making L_s larger, this lattice artifact should be (exponentially) reduced, which is also clear from Fig. 4 where for $L_s = 32$ the shift has been reduced by roughly a factor of 10, and the splitting nearly vanishes. Similar results hold for the $u\bar{u}$ mesons. The result based on the Ward-Takahashi Identity depends also on the value of B_0 or B , depending on whether we choose SU(3) or SU(2) chiral perturbation theory, which introduces some uncertainty. On the other hand, Figs. 4 and 5 clearly show that this effect is due to finite L_s chiral symmetry breaking, and that it can be precisely subtracted from the physical splitting by introducing a new lattice-artifact LEC to the fit, $e^2 \delta_{m_{\text{res}}} (q_i^2 + q_j^2)$. We conclude that the explicit chiral symmetry breaking artifacts induced by finite L_s and QED interactions are precisely quantifiable at NLO in chiral perturbation theory and that higher order terms can be safely neglected, so these artifacts can be robustly eliminated, just as in the case for pure (DWF) QCD.

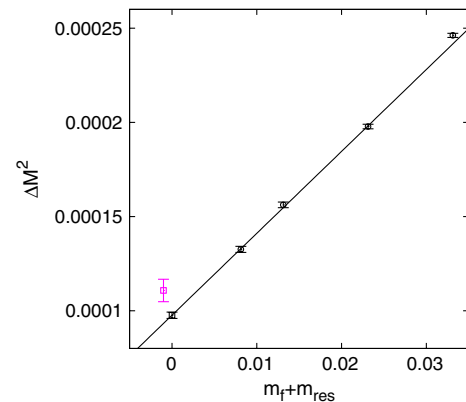


FIG. 5 (color online). Same as Fig. 4 but for lattice size 24^3 and $L_s = 16$.

1. Infinite volume fits

In Figs. 6 and 7, the meson mass-squared splittings are shown for the unitary quark mass points, for both 16^3 and 24^3 ensembles, respectively. For now, we concentrate on the 24^3 ensemble, and fit the mass-squared splittings to the infinite volume, NLO, chiral perturbation theory formulas described in Sec. II. The formulas require the values for the pure QCD LEC's, some of which we have not computed. The pure QCD LEC's, including F_0 , F , B_0 , B , and the Gasser-Leutwyler L 's, have been calculated already by the RBC and UKQCD collaborations from a larger ensemble of which the present one is a subset. We use these values in our fits, in a combined super-jackknife analysis so that the statistical errors on the QCD parameters are fed into our analysis.

Figure 7 shows the fit to the full $SU(3)_L \times SU(3)_R$ NLO formula, which is summarized in Tables IV and V. The quark mass range in the fit is $m_1, m_3 \leq 0.01$, and the χ^2/dof for these uncorrelated fits is about two. χ^2 degrades significantly if larger quark mass points are used in the fits.

Only unitary points are shown in the figure for clarity while all of the (allowed) quark mass and charge combinations for the mesons have been used in the analysis. For the 24^3 ensemble, this amounts to 52 data points for $m_1, m_3 \leq 0.01$. The charged-meson splittings should not vanish in the chiral limit, $m_f = -m_{\text{res}}$; this is just the LO Dashen term proportional to α_{em} and the lattice-artifact chiral symmetry breaking. The neutral meson splittings do not vanish either due to the latter. The chiral logarithms reduce the LO Dashen term relative to the value given by a simple linear ansatz. Recall that the splittings of neutral mesons made from connected quark diagrams only do not contain logs at NLO, so their chiral behavior is particularly simple.

Figures 7 and 8 show similar fits for $SU(2)_L \times SU(2)_R$ -plus-kaon chiral perturbation theory for the pions and kaons, respectively. Here we use the same range for the light quark masses, and for the kaons the valence strange quark is fixed to either 0.02 or 0.03. χ^2/dof is similar to the $SU(3)$ case for the pion and also significantly degrades when the quark mass range is extended upwards. For the

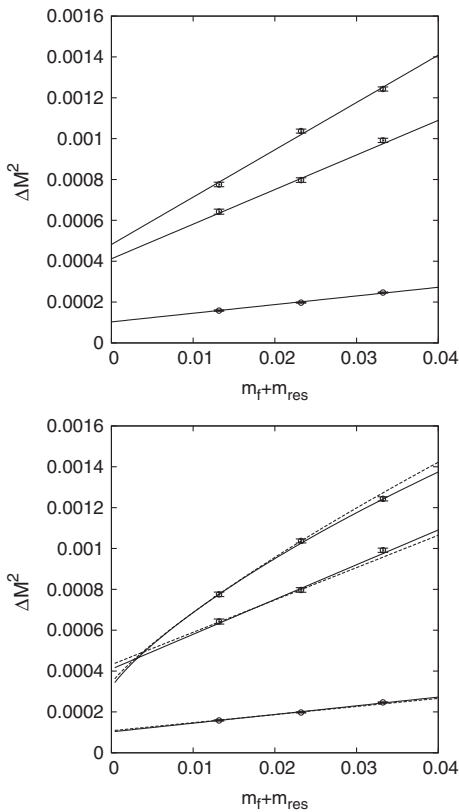


FIG. 6. Meson mass-squared splittings. 16^3 lattice size. Infinite volume linear fit (upper panel) and infinite volume $SU(3)$ chiral log fit (lower panel). The fit range of the linear fit is 0.01–0.03. Fit ranges of chiral log fits, 0.01–0.03 (solid line) and 0.01–0.02 (dashed line). Data points correspond to $u\bar{d}$, $u\bar{u}$ and $d\bar{d}$ mesons, respectively, from top to bottom. Only unitary points are shown, although all of the partially quenched points were used in the fit.

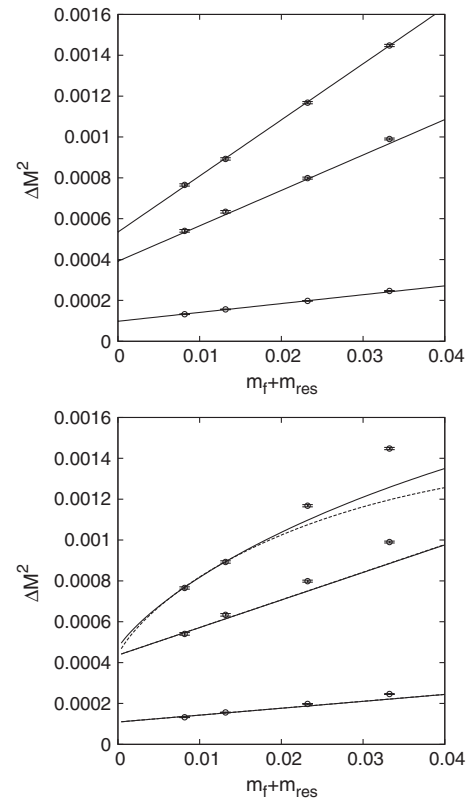


FIG. 7. Meson mass-squared splittings. 24^3 lattice size. Infinite volume linear fit (upper panel), and infinite volume $SU(3)$ and $SU(2)$ chiral log fits (lower panel). The fit range of the linear fit is 0.005–0.03. Fit range of chiral log fits is 0.005–0.01. The solid (dashed) line in the lower panel represents the $SU(3)$ [$SU(2)$] fit. Data points correspond to $u\bar{d}$, $u\bar{u}$ and $d\bar{d}$ mesons, respectively, from top to bottom. Only unitary points are shown, although all of the partially quenched points were used in the fit.

TABLE IV. The QCD LEC's from RBC/UKQCD collaboration's infinite volume fits on 24^3 lattices with SU(3) and SU(2) PQ χ PT [17]. They were computed from a larger ensemble of lattices than used in [7]. All of the QCD LEC's are defined at the chiral scale $\Lambda_\chi = 1$ GeV. The labels in the first column correspond to SU(3) definitions; the analogous LEC for SU(2) is given in the third column.

	SU(3) inf.v	SU(2) inf.v
$10^0 B_0$	2.15(11)	2.348(44)
$10^2 F_0$	3.43(19)	4.55(10)
$10^6(2L_6 - L_4)$	-2.6(29.6)	2.9(45.3)
$10^4(2L_8 - L_5)$	5.42(29)	4.36(31)
$10^5 L_4$	1.7(5.5)	2.48(89)
$10^4 L_5$	2.02(63)	5.49(47)
$10^3 m_{\text{res}}$	3.131(27)	3.131(27)
$a^{-1}(\text{GeV})$	1.784(44)	1.784(44)

TABLE V. The SU(3) PQ χ PT and SU(2) pion PQ χ PT QED LEC's from fits of the mass-squared splittings measured on the 24^3 lattices. All of the LEC's are defined at chiral scale $\Lambda_\chi = 1$ GeV and are given in lattice units. The quark mass range in the fits is $m_{1,3} \leq 0.01$. "inf.v." and "f.v." means infinite and finite-volume fits, respectively. "SU(3) + phenomen" refers to a parameter set presented based on phenomenology and using SU(3) χ PT [11]. Labels in the first column correspond to SU(3) definitions. "Dashen's term" is the LO result for the mass splitting in the chiral limit.

	SU(3)		SU(2)		SU(3) + phenomen.
	inf.v.	f.v.	inf.v.	f.v.	
$10^7 C$	2.2(2.0)	9.3(2.4)	18.3(1.8)	32.9(2.3)	41
$10^2 Y_2$	1.63(10)	1.451(92)	1.416(50)	1.301(49)	0.19
$10^3 Y_3$	-11.85(74)	-5.37(70)	-10.61(62)	-4.00(62)	1.25
$10^3 Y_4$	13.4(1.7)	9.7(1.7)	10.6(1.1)	8.3(1.1)	2.17
$10^3 Y_5$	2.06(72)	1.12(74)	1.95(50)	1.61(54)	-1.17
$10^3 \delta_{m_{\text{res}}}$	5.356(98)	5.357(98)	5.355(98)	5.355(98)	...
Dashen's term(MeV)	0.40(37)	1.68(39)	1.88(18)	3.38(23)	3.7
χ^2/dof	2.11(73)	2.12(78)	2.27(78)	2.19(82)	...

kaon fits χ^2 is small. The total number of data points in the fits are 52 for the pions and 36 for the kaons. The SU(2) LEC's are also summarized in Tables IV, V, and VI.

Before proceeding, we address a subtlety in the kaon fits that was not recognized until after the correlation functions had already been computed. Our original plan was to use an SU(3) chiral perturbation theory analysis only, for quark masses in the range 0.005–0.03, and nondegenerate meson correlation functions were computed for these masses in all possible combinations. However, learning first from the pure QCD analysis [7,15,16], and later from our own, it became clear that 0.02 and 0.03 were too heavy, and that SU(2) chiral perturbation theory would be needed to access the physical strange quark mass regime. We decided to include a lighter valence mass point, 0.001, to augment our fits, but since this was a new, separate calculation, only the mass-degenerate mesons could be computed. Thus, in our kaon fits, we have only two valence and two sea quark mass combinations available for the region $m_{u,d} \leq 0.01$. Now the subtlety: it turns out these combinations of quark masses and charges are not enough to constrain all 10 LEC's appearing in Eq. (23). There is one direction in the

multidimensional parameter space that is not linearly independent from the rest. Fixing any one of the LEC's to zero, except $A_5^{(s,1,1)}$ or $A_5^{(s,2)}$, results in a stable fit with the same χ^2 , but with different values of the LEC's. While these fits all agree exactly when evaluated at the data points used in the fits, they differ elsewhere. There are two ways to fix this problem of an accidental flat direction in the χ^2 function at our disposal. First, keeping the same quark mass range, use the technique of singular-value decomposition [35] (SVD) to determine all 10 LEC's. Second, increase the number of sea or valence quark mass points in the fit, so the parameter directions are all linearly independent. While treating the (next available) mass 0.02 quark simultaneously as light and strange contradicts our assumption that $m_l/m_s \ll 1$, nevertheless it allows the LEC's to be linearly independent, and only slightly increases χ^2 which is still small. In practice, we only added the 0.02 valence quark mass to the kaon fit, keeping the light sea quark mass ≤ 0.01 . As it happens, the quark masses determined from these two methods agree well, giving confidence that the SVD fit procedure, which we use for our central values, is reliable. Further, in the case where

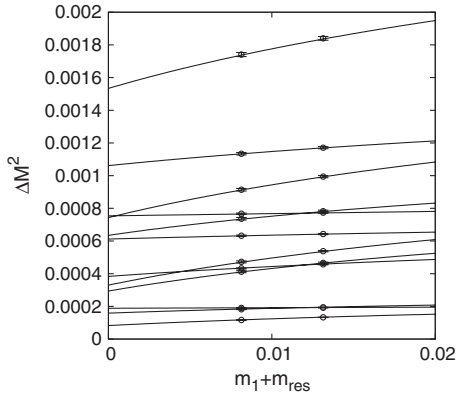


FIG. 8. Kaon mass-squared splitting and infinite volume SU(2) kaon fit. The mass of the strange valence quark is fixed at 0.03, and $m_{\text{sea}} = 0.005$. Different lines in the plot correspond to different charge combinations of the valence quarks.

0.02 data points were used, setting each of the LEC's to zero in turn resulted in much bigger χ^2 values except for $x_6^{(K)} - x_8^{(K)}$, the ones related to sea quark masses which are not constrained as well. $x_8^{(K)} = 0$ gave the smallest χ^2 . In each of these cases the quark masses agreed within statistical errors to the full SVD fit. We use the difference in the central values of the quark masses from the two procedures as an estimate of one of the systematic errors due to fitting.

From Table V, we can see a large effect on C going from SU(3), where it is almost zero, to SU(2) where it is almost 10 times larger. Recall that in the SU(2) theory the contributions of the strange quark terms in the SU(3) theory are absorbed into $C^{(2)}$ [see Eq. (19)]. This situation is

reminiscent of the pion decay constant in pure QCD computed on these lattices and for the same range of quark masses; the logs in that case also tend to significantly reduce the LO contribution over a simple analytic function, and the physical value [7,15,16]. Here, especially in the SU(3) case, the effect is even more dramatic. The other pion electromagnetic LEC's are roughly the same in both theories. In the SU(2) case, the size of the NLO EM correction turns out to be smaller than the LO one, showing compatibility with the chiral expansion. Finally, in Table V, we show LEC's corresponding to the phenomenological parameter set presented in Ref. [11]. The fact that the SU(3) NLO LEC's computed here (left-most column) do not agree is not surprising since the LO LEC, C , is clearly underestimated by a large degree. Note that to compare values of C , a factor of a^{-4} needs to be introduced, as well. We discuss the Dashen term further in Sec. V, after presenting the finite-volume fits.

2. Finite-volume fits

Next we include in our fits the finite-volume corrections to the chiral logarithms using Eq. (12) for the SU(3) fit, and Eq. (22) for the pion and the results in Appendix B 2 for the kaon in the SU(2) fit. We continue to use the pure QCD, infinite volume, LEC's from [17]. Since the finite-volume effects in QCD are very small compared to the QED ones, we ignore the former. Figure 9 shows the modified fits for the pions and kaons on the 24^3 lattice. The LEC's are given in Tables V and VI. The largest change by far is in C , the LO Dashen term, which roughly doubles in the SU(2) case and increases by a factor of 4 in the SU(3) case. Note, it is

TABLE VI. Kaon QCD and QED LEC's extracted from 24^3 lattice size data. LEC's are in lattice units. The kaon is composed by one light- (m_1) and one strange- (m_3) quark. We choose $m_1 \leq 0.01$ and $m_3 = 0.02$ or 0.03 . The light sea quark is chosen as $m^{\text{sea}} \leq 0.01$. The mass of the strange sea quark is fixed at 0.04. The kaon QCD LEC's are quoted from RBC/UKQCD's work [17]. χ^2/dof refers to the fit using the SVD method [35].

m_s^{val}	inf.v			f.v		
	0.02	0.03	m_s^{phys}	0.02	0.03	m_s^{phys}
$10^2 M^2$	4.804(88)	6.89(10)	7.37(36)
$10^1 A_3$	-2.199(44)	-2.198(45)	-2.198(46)
$10^2 A_4$	-1.89(45)	-2.15(52)	-2.21(56)
$10^3 A_K^{(1,1)}$	-9.1(1.1)	-8.9(1.3)	-8.8(1.4)	-6.4(1.0)	-5.8(1.2)	-5.7(1.3)
$10^3 A_K^{(2,1)}$	8.29(86)	8.15(99)	8.1(1.0)	7.16(81)	6.92(93)	6.87(99)
$10^2 A_K^{(s,1,1)}$	0.958(26)	1.254(30)	1.321(64)	1.241(26)	1.577(31)	1.653(70)
$10^3 A_K^{(s,2)}$	-4.22(20)	-4.68(22)	-4.79(25)	-6.74(20)	-7.56(23)	-7.75(28)
$10^2 x_3^{(K)}$	1.41(32)	1.93(39)	2.05(46)	2.34(35)	3.00(42)	3.15(52)
$10^2 x_4^{(K)}$	4.60(36)	5.06(47)	5.16(50)	3.52(38)	3.83(49)	3.90(51)
$10^1 x_5^{(K)}$	0.376(42)	0.366(51)	0.364(53)	0.361(41)	0.350(50)	0.348(53)
$10^2 x_6^{(K)}$	-0.83(0.94)	-0.99(1.01)	-1.0(1.0)	-0.086(0.959)	-0.14(1.02)	-0.16(1.05)
$10^2 x_7^{(K)}$	-0.11(1.82)	-0.27(2.00)	-0.30(2.05)	-0.81(1.82)	-1.0(2.0)	-1.1(2.0)
$10^2 x_8^{(K)}$	-8.28(47)	-8.65(78)	-8.73(86)	-8.23(47)	-8.60(78)	-8.69(86)
χ^2/dof	0.4578(52)	0.2869(40)	...	0.4578(52)	0.2869(40)	...

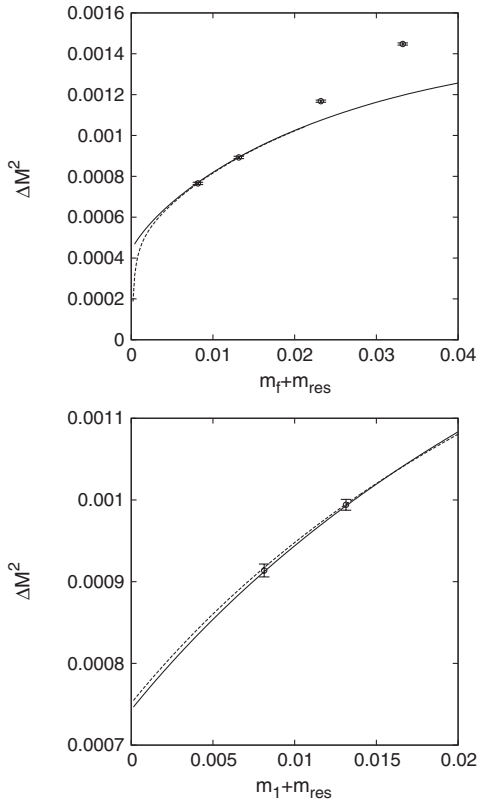


FIG. 9. 24^3 SU(2) chiral log infinite volume and finite-volume fits for pion (upper) and kaon (lower) mass-squared splittings. Lines correspond to fit results. The fit range is 0.005–0.01. The solid (dashed) line represents the infinite (finite) volume fit. In the upper panel, the fit curves are evaluated for degenerate unitary light quarks. For the lower panel, the curves are evaluated for $m_{\text{sea}} = 0.005$ and $m_3 = 0.03$. Data points in the plot correspond to $q_1 = 2/3$ and $q_3 = -1/3$, but all partially quenched points allowed by the fit range were used in the fit.

still much larger for the SU(2) fit. This is consistent with the observed large effect in the charged-meson splitting compared to the neutral. Fortunately, this huge change does not greatly affect the values of the quark masses, as we shall see.

TABLE VII. The u , d and s quark masses determined from QCD + QED interaction on 24^3 lattices. The values are given in MeV and the $\overline{\text{MS}}$ scheme at renormalization scale $\mu = 2$ GeV. SU(3) or SU(2) mean quark masses from SU(3) PQ χ PT or SU(2) PQ χ PT + kaon theory.

	SU(3)		SU(2)	
	inf.v	f.v	inf.v	f.v
m_u	2.606(89)	2.318(91)	2.54(10)	2.24(10)
m_d	4.50(16)	4.60(16)	4.53(15)	4.65(15)
m_s	89.1(3.6)	89.1(3.6)	97.7(2.9)	97.6(2.9)
$m_d - m_u$	1.900(99)	2.28(11)	1.993(67)	2.411(65)
m_{ud}	3.55(12)	3.46(12)	3.54(12)	3.44(12)
m_u/m_d	0.578(11)	0.503(12)	0.5608(87)	0.4818(96)
m_s/m_{ud}	25.07(36)	25.73(36)	27.58(27)	28.31(29)

C. Quark masses

Having determined the LEC's to NLO describing the pseudoscalar masses in chiral perturbation theory, we now turn to fixing the physical quark masses at the (arbitrary) low-energy scale of 2 GeV. First, the bare quark masses are determined by solving Eq. (4) or Eqs. (20) and (23) evaluated at the physical meson masses [4] (in MeV)

$$M_{\pi^\pm} = 139.570\,18 \pm 0.000\,35 \quad (28)$$

$$M_{K^0} = 497.614 \pm 0.024 \quad (29)$$

$$M_{K^\pm} = 493.667 \pm 0.016, \quad (30)$$

where only the central values are used in our analysis since the errors are negligible compared to the lattice results. Using $a^{-1} = 1.784(44)$ GeV and the pure QCD nonperturbative renormalization constant $Z_m = 1.546(2)(43)$ [17] computed by the RBC and UKQCD collaborations, $\overline{\text{MS}}$ light quark masses are given in Table VII, for infinite volume, finite-volume, SU(3), and SU(2) fits. We have not included the $O(\alpha_{\text{em}})$ renormalization of the quark mass from QED interactions. These are similar to those found in our earlier two-flavor work [2], also using DWF, but which used a more crude chiral perturbation theory analysis that did not include logarithms. The strange quark mass is somewhat lower here, which may be a real flavor-dependent effect [1,2]. We also note that in the combined continuum limit analysis mentioned earlier, the RBC and UKQCD collaborations found that the strange quark mass is even smaller [15–17]. The average light quark mass is close to the value determined in pure QCD [7,15,16].

V. SYSTEMATIC ERRORS

In this section we examine the important systematic errors in our calculation: the chiral extrapolations, finite volume, nonzero lattice spacing, and QED quenching. In each case we estimate the size of the effect on the values of the quark masses and investigate the effect on the LO

electromagnetic LEC's. Similar systematic uncertainties have been given for the pure QCD sector [7,15,16].

To estimate the systematic errors, the change in a quantity is computed under the influence of a change in how that quantity is computed, for example, by using a different fit formula. Since the data is the same, or there is significant overlap, in each case, we compute the change under the super-jackknife procedure in order to assess its significance. Central values of all quantities are quoted for the finite volume, SU(2) chiral perturbation theory fits which we believe give the most accurate results. The systematic errors computed in the following come from comparison to these central values.

A. Chiral extrapolations

Previous studies have used the difference in analytic and chiral perturbation theory fits to estimate the chiral extrapolation error that stems from using unphysical heavy quarks [7,14,15,17,36,37]. One can also estimate the error in chiral perturbation theory alone by comparing the relative sizes of LO, NLO, or even NNLO corrections to a given quantity. For the latter to work, the estimates of the higher order contributions must be accurate.

It is perhaps not surprising to find that the meson mass-squared splittings show little trace of the chiral logarithms. For the mass range of pions in this study, it is well known that low-energy observables like the meson mass squared or decay constant exhibit more or less linear dependence on the quark mass. In Fig. 7, the charged pseudoscalar splitting appears linear over the range of unitary points shown in the figure. Nevertheless, the fits to our data do show that NLO chiral perturbation theory (chiral logs) is consistent with the data. A similar conclusion was reached in the pure QCD case [7,15–17]. To NLO in chiral perturbation theory, there are no logs for the neutral mesons made from connected quark propagators like those studied here, and indeed the neutral splittings, too, appear to be quite linear.

We do point out one aspect of the EM logs that leads one to expect a noticeable affect. They behave like $\alpha m \log m$, not $m^2 \log m$ as the pure QCD logs do. A factor of α has replaced a factor of the quark mass. In fact they are like the quenched logs in pure QCD in this respect.

The first step in estimating the systematic error is to determine the fit range, or range of quark masses included in the fit. The available ranges are summarized in Table I. In Refs. [7,14–17] it was shown that for the same ensembles used in this work, SU(3) and SU(2) chiral perturbation theories give sensible fit results for pion masses less than about 400 MeV, or for bare quark masses satisfying $m_f \leq 0.01$. It is possible that the range is different, perhaps larger, for the EM splittings. After all, most of the pure QCD contributions at LO and NLO completely cancel in the EM splittings (some of the pure QCD LEC's survive at $O(\alpha_{\text{em}} m)$). We work with uncorrelated fits, though our data

are highly correlated, because there are too many mass and charge combinations to accurately determine the correlations on this finite statistical ensemble. The uncorrelated fits have been shown to agree with correlated ones when the covariance matrix is well determined, and when it is not, the correlated fits break down [17,38]. As already mentioned, when the quark mass range is extended upwards, for both SU(3) and SU(2) [pion] fits, χ^2/dof increases noticeably, by more than a factor of 2. Since we use uncorrelated fits, this χ^2 is not an absolute test of goodness of fit, though we expect changes do indicate relative goodness of fit. Thus, we stick with the range $m_1, m_3 \leq 0.01$ for the light quarks to quote central values and to estimate systematic errors. One of the systematic errors is the difference in the central values for the quark masses determined from this restricted range and those values computed from the range $m_1, m_3 \leq 0.02$ for the light quarks. $m_1, m_3 \leq 0.01$ corresponds to valence pions in the range 250–420 MeV.

For the mass range $m_1, m_3 \leq 0.01$, the most important change, which is anticipated in Fig. 7, is that the Dashen term increases significantly when the logs are omitted from the SU(3) fit. C increases by about a factor of 5, although it is still small compared to the value one would obtain from the physical splitting. For SU(2), the situation is much different; C changes very little, about 2%. Presumably, the large logs containing the strange quark mass contribute to the LO term in this case, and the remaining effect of the light logs is not as important. The higher order terms

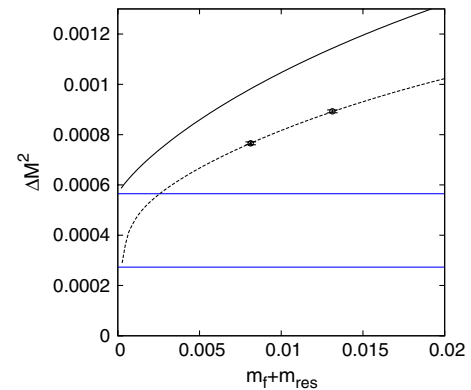


FIG. 10 (color online). The LO and NLO in finite-volume SU(2) chiral perturbation theory contributions to the EM meson mass splitting. The dashed line corresponds to the finite-volume fit result. The data points shown are for charged mesons with $q_1 = 2/3$ and $q_3 = -1/3$. The lower horizontal line gives the contribution of the lattice artifact $e^2 \delta_{m_{\text{res}}}(q_1^2 + q_3^2)$ while the upper horizontal line gives the sum of this contribution and Dashen's term (in other words, their difference is just the LO contribution). The solid line corresponds to the total LO + NLO + $e^2 \delta_{m_{\text{res}}}(q_1^2 + q_3^2)$ contributions based on the fitted, finite-volume LEC's, but evaluated with the infinite volume logarithms. The fit curves are evaluated for degenerate unitary light quarks.

TABLE VIII. Summary of quark mass systematic errors. Central values quoted from the finite-volume, SU(2), chiral perturbation theory fit. Masses given in MeV. The quark mass renormalization error comes from the nonperturbative QCD result [17] plus a 1% error from QED, added in quadrature. Systematic errors are given as a percent (%). The algebraic sign of each change comes from the difference (quantity under change)—(central value).

	Value (stat. error)	Fit	fv	Lat. spacing	QED quenching	m_s quenching	Renorm
m_u	2.24(10)	+4.02	+13.50	4	2	...	2.8
m_d	4.65(15)	+3.55	-2.48	4	2	...	2.8
m_s	97.6(2.9)	+0.23	+0.07	4	2	2	2.8
$m_d - m_u$	2.411(65)	+7.77	-17.35	4	2	...	2.8
m_{ud}	3.44(12)	+2.75	+2.71	4	2	...	2.8
m_u/m_d	0.4818(96)	+5.45	+16.40	4
m_s/m_{ud}	28.31(29)	+2.91	-2.56	4	2	2	...

change more, but without logs to affect their running, there is not much sense in comparing the changes.

In Fig. 10 the LO and NLO contributions in finite-volume SU(2)_L × SU(2)_R chiral perturbation theory for the charged pion mass splittings are shown. At the values of quark masses used in our calculation, after accounting for the $\delta_{m_{\text{res}}}$ contribution, the NLO contributions are about 50–100% of the LO contribution. It is interesting to see how $m_d - m_u$ is affected at the various orders in chiral perturbation theory. Using the LEC's determined in the full SU(2)_L × SU(2)_R-plus-kaon fits, we find that the NLO contributions increase $m_d - m_u$ by a bit less than 2%.

Taking all the above uncertainties due to fitting into account, we estimate systematic errors of about four and zero percent for the up and down, and strange quark masses, respectively. These are collected in Table VIII.

B. Finite volume

The effect of finite volume on the measured charged-meson splittings is large, as we have seen. In Fig. 11 the

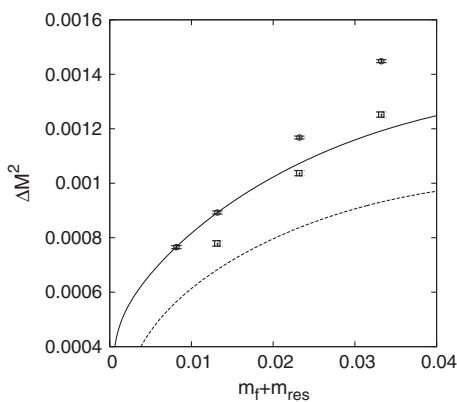


FIG. 11. Finite-volume effect in the measured EM splittings. All of the data points have $q_1 = 2/3$ and $q_3 = -1/3$. Circles and squares correspond to 24^3 and 16^3 lattice sizes, respectively. The solid line is from the finite-volume fit on 24^3 ensembles. The dashed line is the theoretical prediction for 16^3 lattices based on the LEC's extracted from 24^3 finite-volume fit. The fit curves are evaluated for degenerate unitary light quarks.

difference between the measured 16^3 and 24^3 EM splittings is about 15–20%. The LO LEC C changes dramatically, by about a factor of 2, when the finite-volume corrections at NLO are included in the chiral perturbation theory fits (see Table V and Fig. 10). Besides the usual special functions that replace the infinite volume logs, a large, negative constant appears in the finite-volume formula, $-3\kappa q_{13}^2/4\pi L^2$ [10] with $\kappa \approx 2.837$, which cancels against an enhanced value of C .

To estimate how reliable the NLO finite-volume corrections are, one can use the LEC's from the 24^3 fits to predict the finite-volume shift in the 16^3 splitting. The fit and prediction are shown in Fig. 11. First, the SU(2) fit agrees well with the 24^3 results for $m_f \leq 0.01$ which is the quark mass range used in the fit. For larger masses the fit deviates significantly from the data and suggests that NLO chiral perturbation theory is not reliable for these masses. Even for $m_f = 0.01$, where we may trust NLO chiral perturbation theory, the theory over-predicts the shift on the 16^3 lattice by about a factor of 2. The NLO LEC's Y_3 and Y_5 also have large finite-volume shifts.

From Table VI the shifts in the kaon mass-squared LEC's are much smaller, especially the ones representing the LO Dashen term ($A_K^{(1,1)}$, $A_K^{(2,1)}$, $A_K^{(s,1,1)}$, and $A_K^{(s,2)}$).

Even though some of the LEC's show large finite-volume shifts, the ultimate shifts in the quark masses are smaller. The largest, about 14%, occurs for the up quark mass. The down quark mass is affected much less, about 3%, and the shift in the strange quark mass is negligible.

From the pure QCD calculations, we know the finite-volume effects in the 24^3 meson masses are at about the 1% level [15–17], and therefore the QED finite-volume corrections dominate.

The finite-volume errors on the quark masses are summarized in Table VIII.

C. Nonzero lattice spacing

Since our calculation has only been done at a single lattice spacing, we cannot estimate the nonzero lattice spacing errors directly. However, by now there is much evidence that these $O(a^2 + m_{\text{res}}a)$ discretization errors are

small in pure DWF QCD, and they should largely cancel in the splittings. Even assuming they do not cancel, there is no reason to expect they are enhanced over the pure QCD case. In the first QCD calculation using the 24^3 ensemble, it was estimated that scaling errors were at about the 4% level for low-energy quantities like the pion decay constant and the kaon [7]. Since then, a new calculation at the same physical volume but smaller lattice spacing has shown this estimate was about right, or perhaps a bit conservative [15–17]. Of course, here we are interested only in the mass splittings. The pion and kaon masses are fixed to their continuum values, so they have no scaling errors. Instead, the lattice spacing errors enter in the LEC's and the physical quark masses. Therefore, we assign a robust 4% scaling error to the quark masses, which will be eliminated in upcoming calculations on the finer lattice spacing ensemble [15–17]. This error also encompasses the uncertainty in setting the lattice scale itself, which as mentioned earlier differs by about 2 ~ 3 percent from the scale given in Ref. [7].

The nonzero lattice spacing errors on the quark masses are summarized in Table VIII.

D. QED quenching

As mentioned our calculation is done in quenched QED where the sea quarks are neutral. In chiral perturbation theory, we have neglected terms of order $O(\alpha_{\text{em}} m_{\text{sea}})$, including logs. From a weak-coupling perturbation theory perspective in QCD + QED, we have neglected vacuum polarization effects at order $O(\alpha_{\text{em}} \alpha_s)$. For the pions, the consequence is that the single (linear combination) LEC Y_1 cannot be determined. For the kaons there are several LEC's that cannot be determined [see Eq. (23)]. However, we do note that sea quark charge effects from the logs can be included *a posteriori* in our determination of the quark masses.

Since the LEC's absorb changes of scale in the logs, one way to estimate the effect of the missing LEC's, or counter-terms, is to mark the change in the quark masses when these logs are included, or not. This leads to a negligible change in the quark masses. From Table V, the other EM LEC's have magnitudes roughly in the range 0.01 to 0.001. Setting Y_1 at the high end, $Y_1 = \pm 0.01$, the quark masses again change very little. Of course, the LEC's calculated with $q_{\text{sea}} = 0$ will differ from those with $q_{\text{sea}} \neq 0$, by $O(\alpha_{\text{em}})$. This is higher order for all the LEC's determined here except C for the pions and $A_K^{(1,1)}$, $A_K^{(2,1)}$, $A_K^{(s,1,1)}$, and $A_K^{(s,2)}$ for the kaons. Taking all of the above into account, we quote a conservative 2% systematic error in our quark mass determination, stemming from the quenched approximation to QED.

Of course the above is only a rough estimate, so presently we are investigating the use of so-called reweighting techniques to eliminate the quenching effects [23–25,27,28,39]. Reweighting is simply the use of ratio(s)

of fermion determinants in observable averages in order to include the desired dynamical-quark effects. The calculation of a determinant which is nonlocal in the fields is quite expensive, so stochastic estimators must be used to make the calculation tractable. Reweighting in the strange quark mass to the *a posteriori* determined physical value has proved quite useful and efficient in recent 2 + 1 flavor simulations [15–17,26].

VI. QUARK MASSES

We use finite-volume SU(2) chiral perturbation theory and the light quark mass range $m \leq 0.01$ to obtain our central values of the physical quark masses.

The physical strange quark mass is determined from the kaon mass squared which is an implicit function of the bare sea and valence strange quark masses, through its LEC's which are calculated for fixed valence strange quark masses 0.02 and 0.03 and fixed sea strange quark mass 0.04. Assuming that the m_s dependence is modest in this region, the physical kaon mass squared is determined from a linear extrapolation in the valence strange quark mass. A similar procedure was carried out in [7] where three data points in the range 0.02–0.04 showed the kaon mass squared is well approximated by a linear function (it turns out that the physical strange quark corresponds to about 0.035). Because we have only carried out calculations at a single strange sea quark mass value of 0.04, the kaon mass squared cannot be evaluated at the physical strange sea quark mass. This partial quenching leads to a small systematic error that was conservatively estimated in [7] to be 2% for m_s which we adopt here. It is added in quadrature to the total systematic error for m_s which appears below. The systematic error on the light quark masses is about 0.7% which is negligible compared to the other systematic errors, so we ignore it.

The statistical errors come from fits underneath a standard jackknife analysis. The QCD LEC's come from an analysis of the extended RBC/UKQCD 24^3 ensembles; the results are consistent with those in Ref. [7]. All of the fits and corresponding LEC's are analyzed under a super-jackknife analysis so that statistical errors on all quantities, from all ensembles, are included. The systematic errors assigned have been discussed in this section. The mass-independent quark mass renormalization factor is

$$Z_m^{\overline{\text{MS}}}(\mu = 2 \text{ GeV}) = 1.546(2)(43), \quad (31)$$

which is obtained via nonperturbative renormalization using the RI/SMOM $_{\gamma_\mu}$ scheme [17,40–44]. The second error is systematic, including $O((\mu a)^2)$, which will be removed when we take the continuum limit in future work (the $O(\alpha_{\text{em}})$ QED correction to Z_m is omitted). The final values are

$$m_u = 2.24 \pm 0.10 \pm 0.34 \text{ MeV}, \quad (32)$$

$$m_d = 4.65 \pm 0.15 \pm 0.32 \text{ MeV}, \quad (33)$$

$$m_s = 97.6 \pm 2.9 \pm 5.5 \text{ MeV}, \quad (34)$$

$$m_d - m_u = 2.411 \pm 0.065 \pm 0.476 \text{ MeV}, \quad (35)$$

$$m_{ud} = 3.44 \pm 0.12 \pm 0.22 \text{ MeV}, \quad (36)$$

$$m_u/m_d = 0.4818 \pm 0.0096 \pm 0.0860, \quad (37)$$

$$m_s/m_{ud} = 28.31 \pm 0.29 \pm 1.77, \quad (38)$$

where the first error is statistical, and the second is a total systematic error, derived by adding the individual errors summarized in Table VIII in quadrature. We remind the reader that these central values are obtained from our SU(2), finite-volume fits on the 24^3 ensembles.

We note that the up quark mass obtained here is different from zero by more than 6 standard deviations, which seems to rule out the $m_u = 0$ solution to the strong CP problem. However, there is an extensive literature concerning this scenario to which we refer the interested reader. For a discussion of extracting the up quark mass by using chiral perturbation theory, and its consequences, see [45–47]. The possibility of instanton effects additively shifting the up quark mass is discussed in many places [48–51]. In [52], renormalization scheme dependence of the renormalized quark mass was discussed in the context the isospin breaking. The effect vanishes in the (perturbative) $\overline{\text{MS}}$ scheme. At this point, there seem to be no common consensus on if there is any nonperturbative contribution, which is related to the aforementioned instanton effects, and how large it might be. Our results are potentially susceptible to this uncertainty, as are all other quark masses renormalized in a perturbative scheme.

VII. MESON MASS SPLITTINGS

In Table V we give the contribution to the charged pion mass splitting in the chiral limit, or Dashen's term. The physical splitting, given in Eq. (1), is 4.5936 (5) MeV. The SU(3) fit gives a very small value, about half an MeV. The finite-volume fit dramatically increases the value, but it is less than half the physical value. The SU(2) fit gives a bigger value still, and after including finite-volume corrections, it gives the LO EM correction to the pion mass difference $(m_{\pi^\pm} - m_{\pi^0})_{\text{QED}} = 3.38(23)$ MeV. Coincidentally, this is about the same value obtained from the linear fit, 3.22(25) MeV. The value of $m_{\pi^\pm}^2$ in the chiral limit, which comes from the LO EM correction is 929(64) MeV² and is similar to the values, using a sum rule and lattice-computed vector and axial-vector correlation functions in pure QCD, reported in [53,54]. Our value for $(m_{\pi^\pm} - m_{\pi^0})_{\text{QED}}$ is roughly consistent with, but two statistical standard deviations smaller

than, the value from phenomenology and SU(3) chiral perturbation theory reported in [11], 3.7 MeV.

The above suggests that NLO contributions at the physical quark masses may be as large as 25% of the total pion mass difference, $m_{\pi^\pm} - m_{\pi^0}$. Away from the chiral limit, there are corrections to m_{π^0} that we have not computed in the lattice calculation (disconnected diagrams), nor in chiral perturbation theory (logs). However, we can estimate some of them by evaluating Eq. (20) for $m_u = m_d = m_{ud}$, $q_1 = q_3 = q_u$ and averaging it with the case for $q_1 = q_3 = q_d$

$$\begin{aligned} \bar{M}^2(q_1, q_3; m_1) &\equiv \frac{1}{2}\{M^2(m_1, q_1, m_1, q_1) \\ &+ M^2(m_1, q_3, m_1, q_3)\}. \end{aligned} \quad (39)$$

This form can be inferred for the π^0 made with degenerate light valence quarks ($m_3 = m_1$) in our current study in which only the connected valence quark diagram is computed and QED is quenched. We focus on the one-particle irreducible two-point function $\Sigma_{\pi^0}(p^2)$ of π^0 , and pick out the part depending on the valence EM charges induced from the connected diagram. $\Sigma_{\pi^0}(p^2)$ can be divided into a pure QCD part $\Sigma_{\pi^0}^{\text{QCD}}(p^2)$ and a QED correction $\Sigma_{\pi^0}^{\text{QED}}(p^2)$ at order e^2 ,

$$\Sigma_{\pi^0}(p^2) = \Sigma_{\pi^0}^{\text{QCD}}(p^2) + \Sigma_{\pi^0}^{\text{QED}}(p^2), \quad (40)$$

$$\Sigma_{\pi^0}^{\text{QCD}}(p^2) = \left(\frac{1}{\sqrt{2}}\right)^2 \text{tr}((\tau_3)^2) A_{\text{QCD}}(p^2) = A_{\text{QCD}}(p^2), \quad (41)$$

$$\begin{aligned} \Sigma_{\pi^0}^{\text{QED}}(p^2) &= \left(\frac{1}{\sqrt{2}}\right)^2 \text{tr}(\tau_3 Q \tau_3 Q) D_1(p^2) + 2 \\ &\quad \times \left(\frac{1}{\sqrt{2}}\right)^2 \text{tr}((\tau_3)^2 Q^2) D_2(p^2) \\ &= \frac{1}{2}(q_1^2 + q_3^2) D_1(p^2) + (q_1^2 + q_3^2) D_2(p^2), \end{aligned} \quad (42)$$

where τ_a ($a = 1, 2, 3$) denote the Pauli matrices and $Q = \text{diag}(q_1, q_3)$. In Eq. (42), the first term originates from the Feynman diagram in which a virtual photon is exchanged between two valence quark lines, while a photon propagates on the same valence quark lines and induces the second term. Because the functions $D_{1,2}(p^2)$ are given by QCD dynamics weighted by the photon propagator, the self-energy $\Sigma_{\pi^\pm}(p^2)$ of the charged pion is also expressed in terms of these functions

$$\Sigma_{\pi^\pm}(p^2) = \Sigma_{\pi^\pm}^{\text{QCD}}(p^2) + \Sigma_{\pi^\pm}^{\text{QED}}(p^2), \quad (43)$$

$$\begin{aligned} \Sigma_{\pi^\pm}^{\text{QED}}(p^2) &= \text{tr}(\tau_+ Q \tau_- Q) D_1(p^2) \\ &\quad + \text{tr}((\tau_+ \tau_- + \tau_- \tau_+) Q^2) D_2(p^2) \\ &= q_1 q_3 D_1(p^2) + (q_1^2 + q_3^2) D_2(p^2). \end{aligned} \quad (44)$$

From Eqs. (40)–(44), the charge dependence of $m_{\pi^0}^2$ and $m_{\pi^\pm}^2 = M^2(m_1, q_1, m_1, q_3)$, to the order relevant to us, is found as

$$\begin{aligned}
M^2(m_1, q_1, m_1, q_3) &= K + q_1 q_3 F_1 + (q_1^2 + q_3^2) F_2, \\
m_{\pi^0}^2 &= K + \frac{1}{2}(q_1^2 + q_3^2) F_1 + (q_1^2 + q_3^2) F_2 \\
&= \bar{M}^2(q_1, q_3; m_1),
\end{aligned} \tag{45}$$

where K denotes the QCD part to NLO of chiral perturbation, and $F_{1,2}$ the $O(e^2)$ and $O(e^2 m_l)$ part. The chiral symmetry as well as QED gauge invariance should give $F_1|_{m_l=0} = -2F_2|_{m_l=0}$ to reproduce the EM charge dependence $(q_1 - q_3)^2$ of the LO EM correction to $m_{\pi^+}^2$. Using Eq. (39) for $m_{\pi^0}^2$, we find the LO + NLO EM pion mass difference at the physical point to be $m_{\pi^+} - m_{\pi^0} = 4.50(23)$ MeV. Phenomenology predicts that a small part of the total NLO correction is due to $m_u - m_d \neq 0$, 0.17 (3) MeV [55] and 0.32(20) MeV [56].

For the kaons, the pure EM mass difference is $m_{K^+} - m_{K^0} = 1.87(10)$ MeV, while the contribution from $m_u - m_d \neq 0$ is $-5.840(96)$ MeV. Here, of course, the result includes all NLO corrections, and LEC's from the finite-volume fit are used. These values are obtained by taking the SU(2) formula for the kaon mass squared $M_K^2(m_1, q_1, m_3, q_3)$, Eq. (23)

$$\begin{aligned}
M_K^2(m_u, \frac{2}{3} m_s, -\frac{1}{3}) - M_K^2(m_d, -\frac{1}{3} m_s, -\frac{1}{3}) \\
= \Delta^{(\text{EM})} M_K^2 + \Delta^{(m_u - m_d)} M_K^2 + \mathcal{O}(e^2(m_u - m_d)),
\end{aligned} \tag{46}$$

where the contributions to the mass-squared splitting are defined as

$$\begin{aligned}
\Delta^{(\text{EM})} M_K^2 &= M_K^2(m_{ud}, \frac{2}{3} m_{ud}, -\frac{1}{3}) \\
&\quad - M_K^2(m_{ud}, -\frac{1}{3} m_{ud}, -\frac{1}{3}),
\end{aligned} \tag{47}$$

$$\begin{aligned}
\Delta^{(m_u - m_d)} M_K^2 &= M_K^2(m_u, 0, m_s, 0) \\
&\quad - M_K^2(m_d, 0, m_s, 0).
\end{aligned} \tag{48}$$

$\Delta^{(\text{EM})}/(m_u - m_d) M_K^2 / (M_{K^0} + M_{K^\pm})$ are quoted above. So out of a physical mass-squared splitting $(M_{K^0})^2 - (M_{K^\pm})^2 = 3902.7$ MeV², about $-47(2)\%$ is $\Delta^{(\text{EM})} M_K^2$ and $+148(2)\%$ is $\Delta^{(m_u - m_d)} M_K^2$.

The breaking of Dashen's theorem can also be parametrized by ΔE [57],

$$\Delta E = \frac{M_K^2(m_1, q_1, m_3, q_3) - M_K^2(m_1, q_3, m_3, q_3)}{M^2(m_1, q_1, m_1, q_3) - M^2(m_1, q_3, m_1, q_3)} - 1, \tag{49}$$

where m_1 is the light quark mass and m_3 is the strange. $M^2(m_1, q_3, m_1, q_3)$ is used here to represent $m_{\pi^0}^2$; no significant change of ΔE is observed in our numerical study even when the average (39) is adopted for $m_{\pi^0}^2$ in place of $M^2(m_1, q_3, m_1, q_3)$. In the SU(3) chiral limit $\Delta E = 0$ since the LO Dashen terms are the same in the numerator and denominator. If the strange quark mass is fixed to its physical value, then it does not vanish, and can be much larger than zero, even in the light quark chiral limit. Notice

that ΔE vanishes trivially in both SU(2) and SU(3) theories when $m_1 \rightarrow m_3$.

We show ΔE for our data in Fig. 12 where the artifact $\delta_{m_{\text{res}}}(q_1^2 + q_3^2)$ has been subtracted for each value of the meson mass squared. In the upper panel, fit results are shown for SU(3). The fit evaluated at the simulated mass points does a reasonable job of reproducing the data, though as m_3 increases differences emerge. This is not surprising since only $m_1, m_3 \leq 0.01$ points were used in the fit, and including larger values yielded significantly poorer fits. More troublesome is the light quark extrapolation which yields a large value of ΔE at the physical point, which can be understood from two primary causes. First, the numerator is quite large since m_3 is evaluated at the physical strange quark mass, leading to a large $O(\alpha m)$ correction to the charged kaon mass squared. Second, the denominator becomes quite small because the LO Dashen term is quite small in the SU(3) fit (compared to NLO terms). Both facts, of course, signal a breakdown in SU(3)

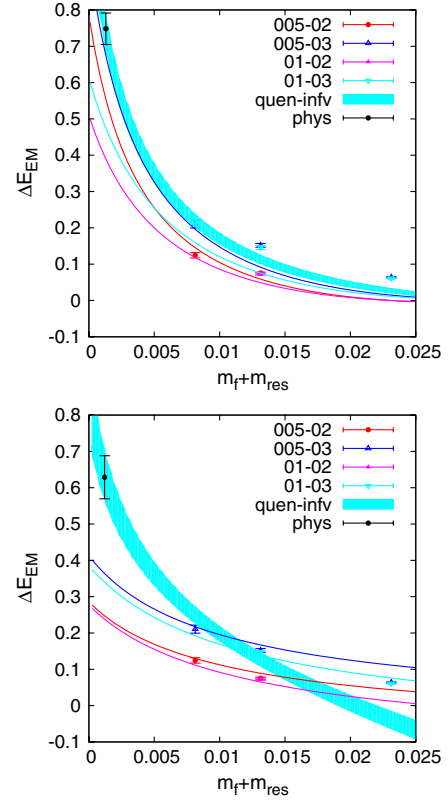


FIG. 12 (color online). Breaking of Dashen's theorem for the quenched QED case. The unphysical contribution $\delta_{m_{\text{res}}}(q_1^2 + q_3^2)$ has been subtracted from the data. Data for two values of the strange quark, 0.02 and 0.03, are shown. The curves correspond to the SU(3) fits (upper panel) and SU(2) fits (lower panel). The cyan bands denote the infinite volume extrapolations with 1 standard deviation statistical errors, using the LEC's extracted from the finite-volume fits; the sea and strange quark masses are fixed at their physical values.

chiral perturbation theory which renders the SU(3) ΔE unreliable. As noted in [11], the sea quark charge LEC's drop out of ΔE , and only known logarithms remain. Adding these to the (cyan) physical curve in Fig. 12 changes it only slightly.

In the lower panel of Fig. 12 we show analogous results for the SU(2) fits. While the SU(2) fits are more reliable since the LO contribution is larger compared to NLO, the latter corrections are still large (recall Fig. 10). As expected, the fit agrees better with the data points for larger values of m_1 , but the extrapolated value at the physical point and infinite volume is still much larger than the data points. We find in quenched QED that $\Delta E = 0.628(59)$ where the error is statistical only. This is much larger than the value reported in our previous two-flavor paper [2] and not much smaller than phenomenology and SU(3) chiral perturbation theory [11]. The main difference is that here we use full NLO chiral perturbation theory with finite-volume corrections while in [2] only simple analytic fits were used. To properly address these large corrections, one needs to simulate with larger volumes and smaller quark masses, a project that is now underway.

Perhaps more useful for other pure QCD simulations are the ‘‘physical’’ values of m_π and m_K in pure QCD deduced from our SU(2) fits with $m_u = m_d = m_{ud}$:

$$m_\pi^{\text{(QCD)}} = 134.98(23) \text{ MeV}, \quad (50)$$

$$m_K^{\text{(QCD)}} = 494.521(58) \text{ MeV}. \quad (51)$$

The small statistical errors result because the physical pion and kaon meson masses were used to determine the physical quark masses from our fit.

Finally, based on the quark masses in Eqs. (32)–(34) and (36), we examine the ratio introduced in Ref. [58],

$$\kappa_{\text{quark mass}} \equiv \frac{m_d - m_u}{m_s - m_{ud}} \frac{2m_{ud}}{m_s + m_{ud}}, \quad (52)$$

which is equal to

$$\begin{aligned} \kappa_{\text{meson}} &\equiv \frac{(M_{K^0}^2 - M_{K^\pm}^2)_{\text{QCD}}}{M_K^2 - M_\pi^2} \frac{M_\pi^2}{M_K^2}, \quad (53) \\ &= \frac{M_K^2(m_d, 0, m_s, 0) - M_K^2(m_u, 0, m_s, 0)}{M_K^2(m_s, 0, m_{ud}, 0) - M_K^2(m_{ud}, 0, m_{ud}, 0)} \\ &\quad \times \frac{M^2(m_{ud}, 0, m_{ud}, 0)}{M_K^2(m_s, 0, m_{ud}, 0)}, \quad (54) \end{aligned}$$

up to NNLO in SU(3) ChPT [55]. For SU(3) we obtain

$$\kappa_{\text{quark mass}} = 0.00201(3), \quad (55)$$

$$\kappa_{\text{meson}} = 0.00201(3), \quad (56)$$

while for SU(2),

$$\kappa_{\text{quark mass}} = 0.00176(4), \quad (57)$$

$$\kappa_{\text{meson}} = 0.00191(3), \quad (58)$$

where the errors are statistical only. For SU(3) the values are quite consistent with each other, while for SU(2) there is a small difference. In [58], κ extracted from $\eta \rightarrow \pi^0 \pi^+ \pi^-$ decays is 0.0019(3) while the $O(p^6)$ analysis in [56] gives $\kappa = 0.00260$ at $m_s/m_{ud} = 24$.

VIII. ISOSPIN BREAKING EFFECTS ON THE KAON DECAY CONSTANT

In our results the up quark mass is about 35% smaller than average of the up and down quark masses, m_{ud} . In principle, this isospin breaking effect may cause visible effects on phenomenologically important quantities when they are measured with sufficient accuracy. As we saw in the previous section, a major part of the Kaon mass splitting comes from the quark mass difference, $m_u - m_d$.

Here we examine isospin breaking effects on the Kaon decay constant, f_K . By combining the experimental decay widths, $\Gamma(K \rightarrow \nu\mu(\gamma))$ and $\Gamma(\pi \rightarrow \nu\mu(\gamma))$, and f_π and f_K , one can extract the corresponding ratio of Cabibbo-Kobayashi-Maskawa matrix elements [59]. In the latest global analysis by the FlaviaNet Working Group on Kaon Decays [60], $\frac{f_K}{f_\pi} \left| \frac{V_{us}}{V_{ud}} \right|$ is obtained from experimental results with an accuracy of 0.2%. The ratio of the decay constants used are from their world average of lattice QCD simulations, and is

$$\frac{f_K}{f_\pi} = 1.193(5) \quad [0.4\%]. \quad (59)$$

We address a question: how far does the value of f_K shift when the light quark mass in the Kaon is changed from m_{ud} to m_u ? Some lattice determinations of f_K use m_{ud} as the light quark mass while the experiments measure decays of the *charged* Kaon to obtain f_{K^\pm} , which is made of an up (and strange) quark. So it is relevant to know if the shift $f_K(m_{ud}) - f_K(m_u)$ is comparable in size to the total error on the ratio, 0.4%. We note the analyses of V_{us}/V_{ud} in [59,60] (see also [61]) correct for the QED effects of the decay constants, and we only consider the decay constant for $e = 0$ but $m_u \neq m_d$ in this section.

In Fig. 13, $f_K(m_x)$ obtained by the RBC/UKQCD Collaboration [7] is plotted as a function of valence light quark mass m_x . The sea and valence strange quark masses are fixed. The square points are from light sea quark mass $m_l = 0.01$ (~40 MeV) while the circle data are for $m_l = 0.005$ (~22 MeV). The curves are from the partially quenched SU(2) ChPT fits. The upper two curves denote $f_K(m_x)$ at fixed degenerate sea quark masses $m_l = 0.01$ (upper) and 0.005 (lower), while the dotted curve is evaluated for unitary quark mass, $m_x = m_l$. The lower three, almost degenerate, curves are for $m_l = 0.7m_{ud}$, m_{ud} , and $1.3m_{ud}$.

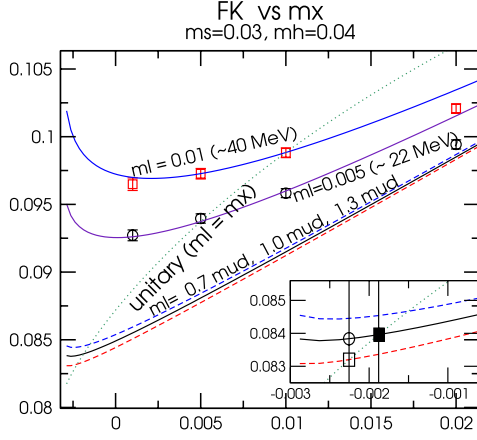


FIG. 13 (color online). Kaon decay constant in pure QCD [7] computed from the same ensembles as used in this work. The valence strange quark mass is fixed to 0.03 and the sea strange quark mass is 0.04.

The inset magnifies the region close to the physical point. The filled square is f_K for equal up and down quark masses, $m_l = m_x = m_{ud}$. When the valence quark mass is decreased to a 30% smaller value, $0.7 \times m_{ud}$, f_K decreases by about 1%, if we simultaneously decrease the light sea quark masses to $0.7 \times m_{ud}$ (empty square). This setting of quark masses (empty square) underestimates the value of f_K in Nature, since the down sea quark mass is also decreased to $0.7 \times m_{ud}$ for the empty square.⁴

The more accurate estimation of f_K for nondegenerate valence up and down quark masses is the empty circle, where the degenerate sea quark mass is fixed to $m_l = m_{ud}$, and only the valence quark mass is set to the lighter mass, $m_x = 0.7m_{ud}$. We note that the nondegenerate quark mass effect in the sea sector is suppressed by $(m_u - m_d)^2$, and setting degenerate sea quark mass to $m_l = m_{ud}$ is a good approximation to estimate the f_K shift due to the isospin breaking in the up and down quark masses. Because of the (accidental) decrease in the slope of $f_K(m_x)$ around the physical sea quark mass $m_l = m_{ud}$, the difference between $f_K(m_{ud})$ and $f_K(0.7 \times m_{ud})$ is only about -0.2% , which is nevertheless sizable compared to the total error of 0.4% in the current world average of f_K/f_π .

A similar analysis was done in [57], where f_{K^+} was properly estimated at $m_x = m_u$. An indirect error on f_{K^+} induced from (their) EM uncertainty in m_u/m_d ($\sim 19\%$) was estimated to be $\sim 0.07\%$. So their shift of f_K due to the quark mass difference between m_{ud} and m_u would be roughly $0.07/0.19 \times (m_{ud}/m_u - 1) \sim 0.25\%$ from their value of $m_u/m_{ud} \approx 0.6$. This shift is slightly larger than our estimation, 0.2% , in part because m_u/m_{ud} in [57] is smaller than ours by about 10% .

⁴We thank C. Sachrajda for pointing this out.

IX. NUCLEON MASS SPLITTINGS

Isospin breaking also occurs in the nucleon system. The proton is slightly lighter than the neutron, which makes the proton a stable particle. In conjunction with baryon PQ χ PT, the lattice simulation helps us understand the relation between the baryon masses and their quark content [62].

In Nature, $m_p - m_n = -1.293\,321(4)$ MeV as determined by experiments, and it is explained by two mechanisms. One is the EM interaction. The proton is a charged particle, but the neutron is neutral, so the QED interaction makes the proton heavier. The other is due to nondegenerate u, d quark masses. The valence quark content in the proton and neutron is uud and udd , respectively. So the proton is lighter than the neutron due to the fact that the d quark is heavier than the u . Combining these two effects in our lattice calculations, we can compute the p - n mass splitting.

For nondegenerate quark masses, we study the splitting using the pure QCD configurations. The nucleon mass in two-flavor QCD is given by baryon PQ χ PT, to NLO [62],

$$m_p = M_0 + \frac{1}{3}(5\alpha + 2\beta)m_u + \frac{1}{3}(\alpha + 4\beta)m_d + \frac{1}{2}\sigma(m_j + m_l), \quad (60)$$

$$m_n = M_0 + \frac{1}{3}(\alpha + 4\beta)m_u + \frac{1}{3}(5\alpha + 2\beta)m_d + \frac{1}{2}\sigma(m_j + m_l), \quad (61)$$

where m_u, m_d are the masses of the valence quarks and m_j, m_l are the masses of the sea quarks. The mass difference between the proton and the neutron is

$$(m_p - m_n)_{(m_d - m_u)} = -\frac{1}{3}(4\alpha - 2\beta)(m_d - m_u). \quad (62)$$

We note only the sum of sea quark masses, $m_j + m_l$, appears in Eqs. (60) and (61) and the difference $m_j - m_l$ appears first at NNLO in any observable due to the symmetry under switching sea up quark to sea down quark. So our degenerate sea up and down quark mass is enough to extract the isospin breaking to NLO (We will ignore possible contributions of $O(e^2(m_u - m_d))$).

Next, we test the EM induced mass splitting on QCD + QED configurations with unitary (and therefore degenerate) mass points. The lowest-order mass difference is parametrized as

$$(m_p - m_n)_{\text{QED}} = \alpha_{\text{em}}(A_0 + A_1 m_{ud}), \quad (63)$$

where $m_{ud} = (m_u + m_d)/2$, and the dependence on α_{em} is made explicit to remind ourselves that the splitting vanishes in the absence of QED.

All of the above LEC's here can be extracted from fits to lattice data.

We first extract the nucleon masses from the two-point correlation function. The correlation function measured on

the lattice with antiperiodic boundary condition in time has the form [63]:

$$G(t) = (1 + \gamma_4)A_{B^+}e^{-M_{B^+}t} - (1 - \gamma_4)A_{B^+}e^{-M_{B^+}(N_t-t)} \\ + (1 + \gamma_4)A_{B^-}e^{-M_{B^-}(N_t-t)} - (1 - \gamma_4)A_{B^-}e^{-M_{B^-}t}, \quad (64)$$

where B^+ represents the nucleon state which has positive parity and B^- represents the excited state of the nucleon which has negative parity. N_t is the time size of the lattice. Since the mass of the excited state is much heavier than the ground state, we neglect its contribution. The nucleon and antinucleon terms left in the correlation function are picked up by multiplying $G(t)$ by the projection operator $1 \pm \gamma_4$ and taking the trace. Then we average these two terms by taking $t \rightarrow N_t - t$ for the antinucleon to improve the statistics of our measurements. The $\pm e$ trick is also used when QED configurations are included. Finally the nucleon masses are extracted from single state fits to point-sink correlation functions as

$$G(t) = Ae^{-Mt}, \quad (65)$$

where M is the ground state nucleon mass, and A measures the overlap between the nucleon state and the nucleon interpolation operator.

Initially, nucleon correlation functions were computed from the same wall source propagators used for the meson splitting analysis. However, on the 24^3 ensembles these exhibited poor plateaus and had poor signals for the EM neutron-proton mass difference. We then switched to box sources (of size 16^3), which gave much better plateaus and signals, but only on the unitary points because of the additional computational cost. Thus, for the 16^3 and 24^3 QCD configurations the masses come from wall source correlation functions while for the 24^3 QCD + QED configurations, the masses are from box source correlation functions. The configuration information of the additional measurements is listed in Table IX. Figure 14 shows representative plateaus for the sea quark mass 0.005 ensemble.

The nucleon masses are listed in Tables XVII and XVIII. They come from a standard χ^2 minimization with correlated fit, and the error on the mass is from the standard jackknife method. The results in Table XVII for the unitary masses and nonzero α_{em} on the 24^3 ensembles are consistent with the pure QCD results obtained on the same

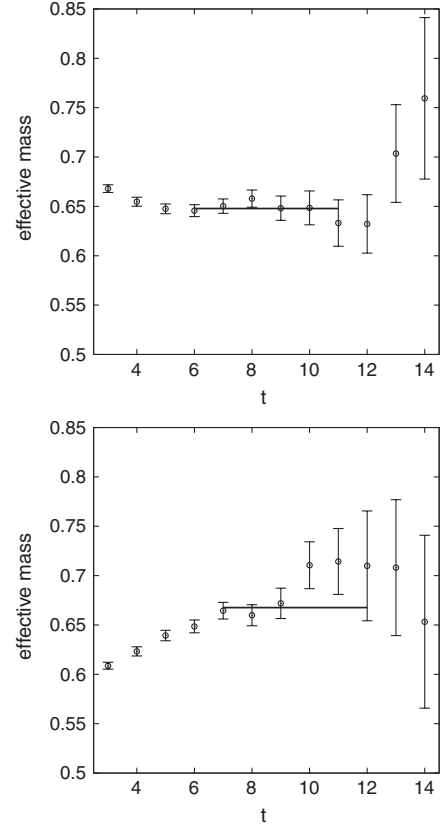


FIG. 14. Proton effective masses, 24^3 lattice size, $m_l = 0.005$. The upper panel is for the unitary point and box source. The lower panel is for a nondegenerate case and wall source.

ensembles reported in Refs. [7,17], except for the $m_l = 0.005$ case. The proton and neutron masses are about 3 standard deviations smaller than in the pure QCD case, or roughly 3%. It is of interest to further investigate how large the EM effect is on the nucleon masses themselves, as well as on the mass difference. Of course, in Nature there is no way to measure the nucleon mass due to QCD alone.

Figure 15 shows the mass difference between the proton and neutron due to the QED interaction for the unitary points. If there is no QED interaction and $m_u = m_d$, then $m_n = m_p$, which is the result of isospin symmetry. When the QED interaction is included, the proton is heavier than the neutron, and the mass difference decreases with quark mass as observed in Fig. 15. The 24^3 result is larger than the 16^3 result, once again signaling finite-volume

TABLE IX. Summary of additional configurations used for the box source nucleon calculation on the 24^3 lattices. QCD gauge configurations generated by the RBC and UKQCD collaborations [7,17,30]. Δ is the separation between measurements in molecular dynamics time units. The Iwasaki gauge coupling is $\beta = 2.13$.

Lat	m_{sea}	m_{val}	Trajectories	Δ	N_{meas}	t_{src}
24^3	0.005	0.005	900–8000	20	355	0
24^3	0.01	0.01	1460–8540	40	534	0, 16, 32
24^3	0.02	0.02	1800–3560	20	534	0, 8, 16, 24, 32, 48
24^3	0.03	0.03	1260–3020	20	534	0, 8, 16, 24, 32, 48

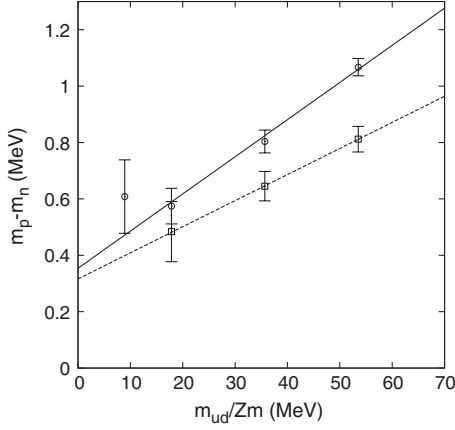


FIG. 15. The proton-neutron mass difference due to the QED interaction computed for unitary points. 24^3 (circle) and 16^3 (square) lattice sizes. The solid (dashed) line corresponds to a linear fit to the 24^3 (16^3) data points.

corrections. This simulation is on the unitary points, but $m_u \neq m_d$ in nature. When we extrapolate $(m_p - m_n)_{\text{QED}}$ to the physical point, we use the average light quark mass m_{ud} , as determined in the previous section. Finally, we find that $(m_p - m_n)_{\text{QED}}$ is about 0.4 MeV (see Table X). From Fig. 15 there is a visible flattening of the splitting at the lightest quark mass for the 24^3 lattice size. Using only the lightest two quark masses in the extrapolation, we obtain $(m_p - m_n)_{\text{QED}} = 0.63(23)$ MeV. The difference between the two results is used to estimate the systematic error in the chiral extrapolation.

Since the photon is not confined, the EM proton-neutron mass difference could suffer from a large finite-volume effect. In order to estimate this artifact, we use the Cottingham formula [9,64],

$$\delta m_{\text{ele}} = 2\pi\alpha m \frac{1}{L^3} \sum_{q \neq 0} \frac{G_E(q)^2}{|q|} \cdot \left[\frac{2}{q^2 + 4m^2} + \frac{1}{2m^2} \left(\sqrt{1 + \frac{4m^2}{q^2}} - 1 \right) \right], \quad (66)$$

$$\delta m_{\text{mag}} = -\frac{\pi\alpha}{2m^3} \frac{1}{L^3} \sum_{q \neq 0} |q| G_M(q)^2 \cdot \left(\sqrt{1 + \frac{4m^2}{q^2}} - 1 - \frac{1}{2} \frac{1}{1 + q^2/4m^2} \right), \quad (67)$$

where δm_{ele} (δm_{mag}) is the electric (magnetic) contribution to the nucleon mass m . We evaluate the above formulae at the physical point, using the dipole form for the nucleon electromagnetic form factors, $G_E^p(Q^2) = G_M^p(Q^2)/\mu_p = G_M^n(Q^2)/\mu_n = G_D(Q^2)$, where μ_p (μ_n), are proton (neutron) magnetic moment, and $G_D(Q^2) = 1/(1 + Q^2/\Lambda^2)^2$ with $\Lambda^2 = 0.71 \text{ GeV}^2$. For $G_E^n(Q^2)$, we use the Galster parametrization of $G_E^n(Q^2) = A Q^2/(4m^2 + B Q^2) \cdot G_D(Q^2)$ with $A = 1.70$, $B = 3.30$ [65]. We obtain $(m_p - m_n)_{\text{QED}}^{\text{(Cott.)}} = 0.04 \text{ MeV}$ for 16^3 volume, and $(m_p - m_n)_{\text{QED}}^{\text{(Cott.)}} = 0.16 \text{ MeV}$ for 24^3 volume. Since the formula yields $(m_p - m_n)_{\text{QED}}^{\text{(Cott.)}} = 0.77 \text{ MeV}$ for the infinite volume limit, the finite-volume artifact corresponds to an underestimate of 0.73 MeV and 0.61 MeV for 16^3 and 24^3 , respectively. The tendency for the larger volume to correspond to larger $(m_p - m_n)_{\text{QED}}$ is qualitatively consistent with the lattice results presented here.

Next we compute the mass splitting due to nondegenerate u and d quark masses, which is expected to switch the sign of the mass difference, in accord with Nature. Figure 16 shows the fit of the proton and neutron mass difference due to nondegenerate u , d quark masses computed on the QCD configurations. The LEC's and values of the splitting at the physical point are summarized in Table XI. Figure 16 confirms that $(m_p - m_n)_{(m_d - m_u)}$ is proportional to $m_d - m_u$, which is predicted by baryon PQ χ PT [Eq. (62)]. The slope is extracted and the physical $(m_p - m_n)_{(m_d - m_u)}$ is estimated by setting $m_d - m_u$ to its physical value, again as determined in the previous section. Our result is in good agreement with the one in Ref. [62].

The quark mass dependence of $m_p - m_n$ is simple in baryon chiral perturbation theory [62] to NLO in pure QCD, as seen in Eq. (60). The leading quark mass dependence for the EM splitting is unknown, so we assume that it is linear, and at this stage the measured values likely cannot be used to discern a more complicated form anyway. In contrast, chiral perturbation theory for the nucleon mass itself predicts several nonanalytic terms at NLO, and the careful extrapolation to the physical point is an important topic of current calculations. Because we have few data points, and our quark masses are relatively heavy, we do not attempt such an extrapolation here.

Combining the contributions from the EM interaction and nondegenerate u , d quark masses, we give the physical p - n mass splitting. We find $m_p - m_n = -1.93(12)$

TABLE X. Proton and neutron mass difference due to the QED interaction. The LEC's are extracted from the nucleon data on the unitary points. $(m_p - m_n)_{\text{QED}}$ is given at the physical quark mass m_{ud} determined in this work.

Lattice size	$10^2 A_0$	A_1	χ^2/dof	$(m_p - m_n)_{\text{QED}}(\text{MeV})$
16^3	2.42(95)	1.26(38)	0.002(96)	0.33(11)
24^3	2.72(55)	1.80(22)	0.7(1.2)	0.383(68)

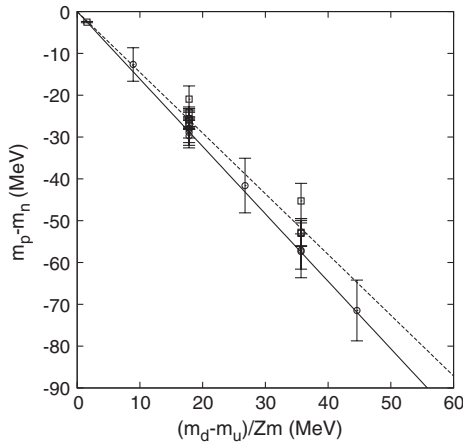


FIG. 16. The proton-neutron mass difference for $m_u - m_d \neq 0$ and $e = 0$. The solid (dashed) line corresponds to a linear fit to the 24^3 (16^3) data points, shown by circles (squares).

and $-2.13(16)$ MeV, for 16^3 and 24^3 lattice sizes, respectively, which is larger than the experimental result ($-1.293\,321(4)$ MeV), but remarkable given that compared to the mass itself, the splitting is a 0.1% effect in Nature. The errors above are statistical only, and their small size is due to the facts that the difference is calculated on exactly the same configurations and with the $\pm e$ averaging trick.

To estimate the systematic error on the EM splitting from the chiral extrapolation we take the difference between the extrapolation using all of the data points (on the 24^3 lattice) and the lightest two mass points, or roughly 0.3 MeV. The finite-volume effects, while quite noticeable at the simulated quark masses, are smaller in the quark mass extrapolated result. To roughly estimate the finite-volume effect, we consider the difference in the 16^3 and 24^3 results which is about 0.05 MeV when all of the data are used in the fits, and roughly 0.3 MeV if only the lightest points on the 24^3 lattice are used. In light of the much

larger artifact predicted by the Cottingham formula, we take the more conservative estimate of 0.3 MeV. The finite-volume error on the pure QCD splitting appears to be under better control, and we simply take the difference of the two as an additional finite-volume effect, or ~ 0.25 MeV. The QCD splitting depends somewhat strongly on the value of $m_u - m_d$, and given the $\sim 20\%$ uncertainty in this quantity, we estimate the systematic error due to the extrapolation by varying $m_u - m_d$ over this range. This yields roughly a 0.5 MeV uncertainty. Adding all of these errors in quadrature, we find $m_p - m_n = -2.13(16)(70)$ MeV. The result and errors are summarized in Table XII. Clearly further calculations are needed, at smaller quark masses to improve the extrapolation, with a different lattice spacing to take the continuum limit, and on a larger volume to improve the infinite volume extrapolation.

X. CONCLUSION

In this paper we have investigated the EM mass splittings of the low-lying hadrons from first principles in the framework of lattice QCD + QED. Our simulations were based on the 2 + 1 flavor DWF QCD configurations generated by the RBC and UKQCD collaborations and quenched, noncompact, QED configurations generated by us. The mass splittings could be determined with very high statistical accuracy since the QCD part of the fluctuations in the hadron masses largely cancels in the splittings. The precision is further enhanced by applying our $\pm e$ trick [2,34] to cancel $O(e)$ noise on each configuration, before averaging over the QCD ensemble. The statistical errors on the pseudoscalar splittings are at an impressive sub-one-percent level, as are the errors on the masses themselves.

The explicit chiral symmetry breaking induced by the finite extra fifth dimension of DWF was studied in detail and shown to be under good control. This is important because the leading $O(\alpha_{\text{em}} m_{\text{res}})$ effect is comparable in size to the physical effects under investigation.

TABLE XI. Proton-neutron mass difference due to nondegenerate u , d quark masses, computed on QCD configurations only. $(m_p - m_n)_{(m_d - m_u)}$ is calculated at the physical value of $(m_d - m_u)$ determined in this work.

Lattice size	$-\frac{1}{3}(4\alpha - 2\beta)$	χ^2/dof	$(m_p - m_n)_{(m_d - m_u)}$ (MeV)
16^3	$-1.452(45)$	1.1(1.2)	$-2.265(70)$
24^3	$-1.612(92)$	0.06(24)	$-2.51(14)$

TABLE XII. Estimated result of the proton-neutron mass difference in Nature (systematic errors as described in the text).

Lattice size	$m_p - m_n$ (MeV)	Fit error (MeV)	Finite vol. error (MeV)
16^3	$-1.93(12)$
24^3	$-2.13(16)$	0.58	0.39

We fit the pseudoscalar meson mass-squared splittings to the theoretical predictions of partially quenched chiral perturbation theory, including photons, to extract the EM low-energy constants of the effective theory, up to NLO. We presented new analytic results for the kaon mass squared in Sec. II and in Appendix B. The fits were done to both $SU(3)_L \times SU(3)_R$ and $SU(2)_L \times SU(2)_R$ -plus-kaon theories, the latter being necessary to determine the strange quark mass [7,14–19]. When using the finite-volume $PQ\chi PT$ formulas, we found that the NLO corrections relative to LO are about 25% for the physical pion masses, neglecting $O(\alpha_{\text{em}}^2)$ terms in the π^0 mass that come from the axial anomaly (disconnected graphs) and are expected to be small [11]. Simple linear fits also work as well as the complicated NLO chiral perturbation theory ones, as has been seen in the case of pure QCD [7,15–17]. Indeed, our data do not show significant curvature, so while they do not seem to require the presence of chiral logs from a theoretical point of view, they are consistent with them. The EM splittings and LEC's are significantly affected by the finite volume of the lattice, as expected since the long range interactions of the photons are not confined. For our final values, we used the finite-volume formulas for the chiral logs computed in Ref. [10]. The lattice-extracted, $SU(3)_L \times SU(3)_R$ LEC's were found to be somewhat inconsistent with the result of the phenomenological analysis in Ref. [11], although the latter were fit using an *ad hoc* set of choices for the LEC's. This may also be due to a lack of convergence of $SU(3)$ chiral perturbation theory in the range of quark masses used here, or finite-volume effects, or both.

The masses of the light quarks were also determined from our calculation. This is the first time EM interactions have been included directly in the quark masses determined from $2 + 1$ flavor calculations. We employed the physical masses of the π^\pm , K^0 and K^\pm mesons as input to fix the quark masses in $PQ\chi PT$. The $SU(2)_L \times SU(2)_R$ -plus-kaon theory was used to quote our final values since the physical strange quark mass is outside the range of convergence of $SU(3)_L \times SU(3)_R$ chiral perturbation theory. They are given in Eqs. (32)–(36), along with statistical and systematic errors. The down-up mass difference and quark mass ratios are given in Eqs. (35)–(38). These quark masses, up to EM effects, are consistent with the pure QCD values given in Ref. [7], which is not surprising since the pure QCD LEC's were taken from an identical analysis of extended ensembles of configurations [17] used there. Concerning the solution of the strong CP problem, it is of interest that our value for the up quark mass is different from zero by many (~ 6 – 7) standard deviations.

The Dashen term, or LO EM contribution to the pion mass difference is $(m_{\pi^\pm} - m_{\pi^0})_{\text{QED}} = 3.38(23)$ MeV in

our calculation, coming from the $SU(2)$ chiral perturbation theory, finite-volume-corrected fit, which is our most reliable one. The error is statistical only. However, the value from the linear chiral fit agrees within errors. It is also consistent with the values of $m_{\pi^\pm}^2$ in the chiral limit recently reported in [53,54], but somewhat smaller than the value from phenomenology and $SU(3)$ chiral perturbation theory [11] and the value we reported for two-flavor QCD in Ref. [2]. This suggests that NLO contributions at the physical quark masses may be as large as 25% of the total pion mass difference, and approximating the π^0 mass from the LEC's computed here, we find the LO + NLO EM contribution at the physical point is $m_{\pi^+} - m_{\pi^0} = 4.50(23)$ MeV. Phenomenology predicts that a small part of the NLO correction is due to $m_u - m_d \neq 0$, 0.17 (3) MeV [55] and 0.32(20) MeV [56]. Similarly, we find for the kaons that the pure EM mass difference is $(m_{K^\pm} - m_{K^0})_{\text{QED}} = 1.87(10)$ MeV, while the contribution from $m_u - m_d \neq 0$ is $-5.840(96)$ MeV. While these values are interesting, there is still systematic uncertainty in them which can only be removed by calculations with lighter quark masses and larger volumes.

Finally, we also computed the proton-neutron mass difference, again for the first time in $2 + 1$ flavor QCD + QED. Our result is somewhat bigger than the experimental one, but encouraging. We found $m_p - m_n = 0.383(68)$ MeV for the EM mass splitting, and $-2.51(14)$ MeV from $m_u \neq m_d$, both on the larger lattice (errors are statistical). Part of the systematic error, stemming mainly from finite volume and chiral extrapolations of the splittings, was estimated. The total splitting was found to be $m_p - m_n = -2.13(16)(70)$ MeV, where the first error is statistical and the second, part of the systematic error. The central value is from the 24^3 lattice; we have not attempted either continuum limit or infinite volume extrapolations. The sign and relative size of the EM effect compared to the $m_d - m_u$ mass difference effect is as expected.

In this work, quenched QED configurations were used to account for the EM interactions of the valence quarks, i.e., the sea quarks were neutral in our calculation. The systematic error due to this approximation can be removed by the reweighing method [23,25]. We are now undertaking such a study. In similar spirit to the most recent RBC/UKQCD pure QCD calculation [15–17] on a finer lattice ensemble, $a \approx 0.086$ fm, the analysis presented here is being replicated on those ensembles in order to take the continuum limit. Similarly, calculations on a third set of ensembles being generated by the RBC and UKQCD collaborations are ongoing, with a new modified Iwasaki gauge action [66], to better explore the chiral regime.

ACKNOWLEDGMENTS

We thank E. Scholz and the RBC and UKQCD collaborations for providing us with the pure QCD LEC's used in this work. T. B. thanks N. Christ for helpful discussions on the EM induced part of the residual mass. T. I. thanks C. Bernard, M. Creutz, and E. Eichten for illuminating discussions. T. B. and T. I. thank G. Colangelo for helpful discussions on finite-volume chiral perturbation theory. T. B. and T. I. thank the organizers of the CERN Theory Institute ‘‘Future directions in Lattice Gauge Theory—LGT10,’’ where a part of this paper was finalized. T. B. and T. I. also appreciate discussions on f_K/f_π (Sec. VIII) with G. Colangelo, A. Juettner, L. Lellouch, C. Sachrajda, and Y. Kuramashi held at the workshop. T. I. also thanks W. Marciano concerning this section. We are grateful to USQCD and the RBRC for providing time on the DOE and RBRC QCDOC supercomputers at BNL for the computations reported here. T. B. and R. Z. were supported in part by the U.S. DOE under Contract No. DE-FG02-92ER40716, T. D. by JSPS Grant-in-Aid No. 21.5985, M. H. by JSPS Grant-in-Aid of Scientific Research (C) Grant No. 20540261 and (S) Grant No. 22224003, T. I. and N. Y. by Grant-in-Aid of the Japanese Ministry of Education (Nos. 20105001, 20105002, 22740183), and S. U. by the JSPS Grant-in-Aid No. 227180 and Nagoya University Global COE program, Quest for Fundamental Principles in the Universe. This manuscript has been authored by an employee (T. I.) of Brookhaven Science Associates, LLC under Contract No. DE-AC02-98CH10886 with the U.S. Department of Energy.

TABLE XIII. Summary of pseudoscalar meson masses obtained from fits to the pseudoscalar two-point correlation functions on the 16^3 QCD + QED lattice configurations. Fit range is $9 \leq t \leq N_t/2$ in each case. m_{sea} is the mass of the light quark in the sea sector. m_1 and m_3 are the masses of the valence quarks. The mass of the strange sea quark is fixed at 0.04. ‘‘cov’’ and ‘‘uncov’’ refer to covariant and uncovariant fits, respectively.

m_{sea}	m_1	m_3	$q_1(\frac{1}{3})$	$q_3(\frac{1}{3})$	M (cov)	χ^2/dof (cov)	M (uncov)	χ^2/dof (uncov)
0.010	0.010	0.010	0	1	0.2430(14)	1.21(89)	0.2420(16)	0.02(4)
0.010	0.010	0.020	0	1	0.2837(13)	1.39(96)	0.2828(15)	0.03(5)
0.010	0.010	0.030	0	1	0.3196(12)	1.50(99)	0.3188(14)	0.04(6)
0.010	0.010	0.010	0	0	0.2427(14)	1.21(89)	0.2417(16)	0.02(4)
0.010	0.020	0.020	0	1	0.3193(12)	1.55(1.01)	0.3185(13)	0.04(6)
0.010	0.020	0.030	0	1	0.3518(11)	1.62(1.03)	0.3510(12)	0.04(6)
0.010	0.030	0.030	0	1	0.3817(11)	1.65(1.05)	0.3809(11)	0.04(6)
0.010	0.010	0.020	0	0	0.2834(13)	1.39(96)	0.2825(15)	0.03(5)
0.010	0.010	0.020	1	0	0.2836(13)	1.39(96)	0.2827(15)	0.03(5)
0.010	0.010	0.030	1	0	0.3196(12)	1.50(99)	0.3187(14)	0.04(6)
0.010	0.020	0.030	1	0	0.3518(11)	1.62(1.03)	0.3509(12)	0.04(6)
0.010	0.010	0.010	1	1	0.2430(14)	1.22(89)	0.2420(16)	0.02(4)
0.010	0.010	0.020	1	1	0.2838(13)	1.39(96)	0.2828(15)	0.03(5)
0.010	0.010	0.030	1	1	0.3197(12)	1.50(99)	0.3188(14)	0.03(6)
0.010	0.020	0.020	1	1	0.3194(12)	1.55(1.01)	0.3186(13)	0.04(6)
0.010	0.020	0.030	1	1	0.3519(11)	1.62(1.04)	0.3510(12)	0.04(6)
0.010	0.010	0.030	0	0	0.3194(12)	1.50(99)	0.3185(14)	0.04(6)
0.010	0.030	0.030	1	1	0.3818(10)	1.66(1.05)	0.3810(11)	0.04(6)
0.010	0.010	0.010	1	-1	0.2434(14)	1.21(89)	0.2424(16)	0.02(4)
0.010	0.010	0.020	1	-1	0.2841(13)	1.39(96)	0.2832(15)	0.03(5)
0.010	0.010	0.030	1	-1	0.3200(12)	1.50(99)	0.3191(14)	0.04(6)
0.010	0.020	0.020	1	-1	0.3198(12)	1.55(1.01)	0.3189(13)	0.04(6)
0.010	0.020	0.030	1	-1	0.3522(11)	1.62(1.04)	0.3514(12)	0.04(6)
0.010	0.030	0.030	1	-1	0.3821(11)	1.66(1.05)	0.3813(11)	0.04(6)
0.010	0.020	0.020	0	0	0.3191(12)	1.55(1.01)	0.3182(13)	0.04(6)
0.010	0.020	0.030	0	0	0.3516(11)	1.62(1.03)	0.3507(12)	0.04(6)
0.010	0.030	0.030	0	0	0.3814(11)	1.65(1.04)	0.3806(11)	0.04(6)
0.010	0.010	0.020	-2	-1	0.2842(13)	1.40(96)	0.2833(15)	0.03(5)
0.010	0.020	0.010	2	1	0.2844(13)	1.40(96)	0.2835(15)	0.03(5)
0.010	0.010	0.030	-2	-1	0.3201(12)	1.51(1.00)	0.3192(14)	0.03(6)
0.010	0.030	0.010	2	1	0.3204(12)	1.51(1.00)	0.3195(14)	0.03(6)
0.010	0.020	0.020	-2	-1	0.3200(12)	1.56(1.02)	0.3191(13)	0.04(6)

TABLE XIII. (Continued)

m_{sea}	m_1	m_3	$q_1(\frac{1}{3})$	$q_3(\frac{1}{3})$	M (cov)	χ^2/dof (cov)	M (uncov)	χ^2/dof (uncov)
0.010	0.020	0.030	-2	-1	0.3524(11)	1.63(1.04)	0.3515(12)	0.04(6)
0.010	0.030	0.020	2	1	0.3525(11)	1.63(1.04)	0.3517(12)	0.04(6)
0.010	0.030	0.030	-2	-1	0.3823(10)	1.66(1.05)	0.3815(11)	0.04(6)
0.010	0.010	0.010	2	0	0.2437(14)	1.22(89)	0.2427(16)	0.02(4)
0.010	0.010	0.020	2	0	0.2843(13)	1.40(96)	0.2834(15)	0.03(5)
0.010	0.010	0.030	2	0	0.3201(12)	1.50(1.00)	0.3193(14)	0.04(6)
0.010	0.020	0.020	2	0	0.3201(12)	1.56(1.01)	0.3192(13)	0.04(6)
0.010	0.020	0.030	2	0	0.3524(11)	1.63(1.04)	0.3516(12)	0.04(6)
0.010	0.030	0.030	2	0	0.3824(10)	1.66(1.05)	0.3816(11)	0.04(6)
0.010	0.010	0.010	2	1	0.2436(14)	1.22(90)	0.2426(16)	0.02(4)
0.010	0.010	0.010	2	-1	0.2443(14)	1.21(89)	0.2433(16)	0.02(4)
0.010	0.010	0.020	2	-1	0.2849(13)	1.39(96)	0.2840(15)	0.03(5)
0.010	0.020	0.010	2	-1	0.2851(13)	1.39(96)	0.2841(15)	0.03(5)
0.010	0.010	0.030	2	-1	0.3208(12)	1.50(1.00)	0.3199(14)	0.04(6)
0.010	0.030	0.010	2	-1	0.3210(12)	1.50(99)	0.3201(14)	0.04(6)
0.010	0.020	0.020	2	-1	0.3206(12)	1.56(1.01)	0.3198(13)	0.04(6)
0.010	0.020	0.030	2	-1	0.3530(11)	1.63(1.04)	0.3522(12)	0.04(6)
0.010	0.030	0.020	2	-1	0.3532(11)	1.63(1.04)	0.3523(12)	0.04(6)
0.010	0.030	0.030	2	-1	0.3830(11)	1.67(1.05)	0.3822(11)	0.04(6)
0.010	0.020	0.010	-2	0	0.2845(13)	1.39(96)	0.2836(15)	0.03(5)
0.010	0.030	0.010	-2	0	0.3205(12)	1.50(1.00)	0.3196(14)	0.03(6)
0.010	0.030	0.020	-2	0	0.3526(11)	1.63(1.04)	0.3518(12)	0.04(6)
0.010	0.010	0.010	-2	-2	0.2440(14)	1.23(90)	0.2430(16)	0.02(4)
0.010	0.010	0.020	-2	-2	0.2847(13)	1.41(96)	0.2838(14)	0.03(5)
0.010	0.010	0.030	-2	-2	0.3206(12)	1.52(1.00)	0.3197(14)	0.03(6)
0.010	0.020	0.020	-2	-2	0.3204(12)	1.57(1.02)	0.3195(13)	0.04(6)
0.010	0.020	0.030	-2	-2	0.3528(11)	1.64(1.04)	0.3520(12)	0.04(6)
0.010	0.030	0.030	-2	-2	0.3827(10)	1.67(1.05)	0.3819(11)	0.04(6)
0.010	0.010	0.010	-2	2	0.2454(14)	1.21(89)	0.2444(16)	0.02(4)
0.010	0.010	0.020	-2	2	0.2860(13)	1.39(96)	0.2851(15)	0.03(5)
0.010	0.010	0.030	-2	2	0.3219(12)	1.50(1.00)	0.3211(14)	0.04(6)
0.010	0.020	0.020	-2	2	0.3217(12)	1.56(1.02)	0.3208(13)	0.04(6)
0.010	0.020	0.030	-2	2	0.3542(11)	1.63(1.04)	0.3533(12)	0.04(6)
0.010	0.030	0.030	-2	2	0.3841(11)	1.67(1.05)	0.3833(11)	0.04(6)
0.020	0.010	0.010	0	1	0.2521(14)	1.07(84)	0.2528(15)	0.10(12)
0.020	0.010	0.020	0	1	0.2918(12)	1.02(82)	0.2923(13)	0.11(13)
0.020	0.010	0.030	0	1	0.3271(12)	0.94(79)	0.3274(12)	0.10(12)
0.020	0.010	0.010	0	0	0.2519(14)	1.07(84)	0.2525(15)	0.10(12)
0.020	0.020	0.020	0	1	0.3267(11)	1.01(82)	0.3270(11)	0.11(12)
0.020	0.020	0.030	0	1	0.3587(10)	0.97(80)	0.3588(11)	0.09(11)
0.020	0.030	0.030	0	1	0.3881(10)	0.97(80)	0.3882(10)	0.07(9)
0.020	0.010	0.020	0	0	0.2916(12)	1.02(82)	0.2920(13)	0.11(13)
0.020	0.010	0.020	1	0	0.2918(12)	1.03(82)	0.2922(13)	0.11(13)
0.020	0.010	0.030	1	0	0.3270(12)	0.94(79)	0.3273(12)	0.10(12)
0.020	0.020	0.030	1	0	0.3586(10)	0.97(80)	0.3588(11)	0.09(11)
0.020	0.010	0.010	1	1	0.2522(14)	1.07(84)	0.2528(15)	0.10(12)
0.020	0.010	0.020	1	1	0.2919(12)	1.03(83)	0.2923(13)	0.11(13)
0.020	0.010	0.030	1	1	0.3271(12)	0.95(79)	0.3274(12)	0.10(12)
0.020	0.020	0.020	1	1	0.3268(11)	1.02(82)	0.3270(11)	0.11(12)
0.020	0.020	0.030	1	1	0.3587(10)	0.97(80)	0.3589(11)	0.09(11)
0.020	0.010	0.030	0	0	0.3268(12)	0.94(79)	0.3271(12)	0.10(12)
0.020	0.030	0.030	1	1	0.3882(10)	0.97(80)	0.3883(10)	0.07(9)
0.020	0.010	0.010	1	-1	0.2526(14)	1.07(84)	0.2532(15)	0.10(12)

TABLE XIII. (Continued)

m_{sea}	m_1	m_3	$q_1(\frac{1}{3})$	$q_3(\frac{1}{3})$	M (cov)	χ^2/dof (cov)	M (uncov)	χ^2/dof (uncov)
0.020	0.010	0.020	1	-1	0.2922(12)	1.03(82)	0.2927(13)	0.11(13)
0.020	0.010	0.030	1	-1	0.3275(12)	0.95(79)	0.3277(12)	0.10(12)
0.020	0.020	0.020	1	-1	0.3271(11)	1.02(82)	0.3274(11)	0.11(12)
0.020	0.020	0.030	1	-1	0.3591(10)	0.97(80)	0.3592(11)	0.09(11)
0.020	0.030	0.030	1	-1	0.3885(10)	0.97(80)	0.3887(10)	0.07(9)
0.020	0.020	0.020	0	0	0.3265(11)	1.01(82)	0.3267(11)	0.11(12)
0.020	0.020	0.030	0	0	0.3584(10)	0.97(80)	0.3586(11)	0.09(11)
0.020	0.030	0.030	0	0	0.3879(10)	0.96(80)	0.3880(10)	0.07(9)
0.020	0.010	0.020	-2	-1	0.2924(12)	1.04(83)	0.2928(13)	0.12(13)
0.020	0.020	0.010	2	1	0.2925(12)	1.03(83)	0.2929(13)	0.12(13)
0.020	0.010	0.030	-2	-1	0.3275(12)	0.95(80)	0.3278(12)	0.10(12)
0.020	0.030	0.010	2	1	0.3278(12)	0.95(79)	0.3281(12)	0.10(12)
0.020	0.020	0.020	-2	-1	0.3273(11)	1.02(82)	0.3276(11)	0.11(12)
0.020	0.020	0.030	-2	-1	0.3592(10)	0.97(80)	0.3594(11)	0.09(11)
0.020	0.030	0.020	2	1	0.3593(10)	0.97(80)	0.3595(11)	0.09(11)
0.020	0.030	0.030	-2	-1	0.3887(10)	0.97(80)	0.3889(10)	0.07(9)
0.020	0.010	0.010	2	0	0.2529(14)	1.08(84)	0.2536(15)	0.10(12)
0.020	0.010	0.020	2	0	0.2925(12)	1.03(83)	0.2929(13)	0.12(13)
0.020	0.010	0.030	2	0	0.3276(12)	0.95(79)	0.3279(12)	0.10(12)
0.020	0.020	0.020	2	0	0.3275(11)	1.02(82)	0.3277(11)	0.11(12)
0.020	0.020	0.030	2	0	0.3593(10)	0.97(80)	0.3595(11)	0.09(11)
0.020	0.030	0.030	2	0	0.3889(10)	0.97(80)	0.3890(10)	0.07(9)
0.020	0.010	0.010	2	1	0.2528(14)	1.08(85)	0.2534(15)	0.10(12)
0.020	0.010	0.010	2	-1	0.2535(14)	1.08(84)	0.2542(15)	0.10(12)
0.020	0.010	0.020	2	-1	0.2931(12)	1.03(83)	0.2935(13)	0.12(13)
0.020	0.020	0.010	2	-1	0.2933(12)	1.03(83)	0.2937(13)	0.12(13)
0.020	0.010	0.030	2	-1	0.3283(12)	0.95(79)	0.3285(12)	0.10(12)
0.020	0.030	0.010	2	-1	0.3285(12)	0.95(79)	0.3288(12)	0.10(12)
0.020	0.020	0.020	2	-1	0.3281(11)	1.02(82)	0.3283(11)	0.11(12)
0.020	0.020	0.030	2	-1	0.3599(10)	0.97(80)	0.3601(11)	0.09(11)
0.020	0.030	0.020	2	-1	0.3600(10)	0.97(80)	0.3602(11)	0.09(11)
0.020	0.030	0.030	2	-1	0.3895(10)	0.97(80)	0.3896(10)	0.07(9)
0.020	0.020	0.010	-2	0	0.2927(12)	1.03(83)	0.2931(13)	0.12(13)
0.020	0.030	0.010	-2	0	0.3279(12)	0.95(79)	0.3282(12)	0.10(12)
0.020	0.030	0.020	-2	0	0.3595(10)	0.97(80)	0.3596(11)	0.09(11)
0.020	0.010	0.010	-2	-2	0.2531(14)	1.09(85)	0.2538(15)	0.10(12)
0.020	0.010	0.020	-2	-2	0.2928(12)	1.04(83)	0.2932(13)	0.12(13)
0.020	0.010	0.030	-2	-2	0.3280(11)	0.96(80)	0.3283(12)	0.10(12)
0.020	0.020	0.020	-2	-2	0.3277(11)	1.03(83)	0.3280(11)	0.11(12)
0.020	0.020	0.030	-2	-2	0.3596(10)	0.98(81)	0.3598(11)	0.09(11)
0.020	0.030	0.030	-2	-2	0.3891(10)	0.97(80)	0.3892(10)	0.07(9)
0.020	0.010	0.010	-2	2	0.2547(14)	1.08(85)	0.2554(15)	0.11(13)
0.020	0.010	0.020	-2	2	0.2943(12)	1.04(83)	0.2947(13)	0.12(13)
0.020	0.010	0.030	-2	2	0.3295(12)	0.96(80)	0.3297(12)	0.10(12)
0.020	0.020	0.020	-2	2	0.3292(11)	1.03(82)	0.3294(11)	0.11(12)
0.020	0.020	0.030	-2	2	0.3611(10)	0.98(81)	0.3613(11)	0.09(11)
0.020	0.030	0.030	-2	2	0.3906(10)	0.98(81)	0.3907(10)	0.07(9)
0.030	0.010	0.010	0	1	0.2505(15)	2.00(1.16)	0.2507(16)	0.16(12)
0.030	0.010	0.020	0	1	0.2901(13)	2.00(1.16)	0.2901(14)	0.12(10)
0.030	0.010	0.030	0	1	0.3256(12)	2.02(1.16)	0.3254(13)	0.10(9)
0.030	0.010	0.010	0	0	0.2503(15)	2.00(1.16)	0.2504(16)	0.16(12)
0.030	0.020	0.020	0	1	0.3249(12)	2.05(1.17)	0.3247(12)	0.10(9)
0.030	0.020	0.030	0	1	0.3570(11)	2.12(1.19)	0.3567(12)	0.09(8)

TABLE XIII. (Continued)

m_{sea}	m_1	m_3	$q_1(\frac{1}{3})$	$q_3(\frac{1}{3})$	M (cov)	χ^2/dof (cov)	M (uncov)	χ^2/dof (uncov)
0.030	0.030	0.030	0	1	0.3865(10)	2.20(1.21)	0.3862(11)	0.09(7)
0.030	0.010	0.020	0	0	0.2899(13)	2.00(1.16)	0.2898(14)	0.12(10)
0.030	0.010	0.020	1	0	0.2901(13)	2.00(1.16)	0.2901(14)	0.12(10)
0.030	0.010	0.030	1	0	0.3255(12)	2.02(1.16)	0.3253(13)	0.10(9)
0.030	0.020	0.030	1	0	0.3569(11)	2.12(1.19)	0.3567(12)	0.09(8)
0.030	0.010	0.010	1	1	0.2506(15)	2.00(1.16)	0.2507(16)	0.16(12)
0.030	0.010	0.020	1	1	0.2902(13)	2.00(1.16)	0.2901(14)	0.12(10)
0.030	0.010	0.030	1	1	0.3256(12)	2.02(1.16)	0.3254(13)	0.10(9)
0.030	0.020	0.020	1	1	0.3249(12)	2.06(1.17)	0.3248(12)	0.10(9)
0.030	0.020	0.030	1	1	0.3570(11)	2.12(1.19)	0.3568(12)	0.09(8)
0.030	0.010	0.030	0	0	0.3253(12)	2.02(1.16)	0.3251(13)	0.10(9)
0.030	0.030	0.030	1	1	0.3866(10)	2.20(1.21)	0.3863(11)	0.09(7)
0.030	0.010	0.010	1	-1	0.2510(15)	2.00(1.16)	0.2511(16)	0.16(12)
0.030	0.010	0.020	1	-1	0.2905(13)	2.00(1.16)	0.2905(14)	0.12(10)
0.030	0.010	0.030	1	-1	0.3259(12)	2.02(1.16)	0.3258(13)	0.10(9)
0.030	0.020	0.020	1	-1	0.3253(12)	2.06(1.17)	0.3251(12)	0.10(9)
0.030	0.020	0.030	1	-1	0.3574(11)	2.12(1.19)	0.3571(12)	0.09(8)
0.030	0.030	0.030	1	-1	0.3870(10)	2.20(1.21)	0.3866(11)	0.09(7)
0.030	0.020	0.020	0	0	0.3246(12)	2.05(1.17)	0.3245(12)	0.10(9)
0.030	0.020	0.030	0	0	0.3567(11)	2.12(1.19)	0.3564(12)	0.09(8)
0.030	0.030	0.030	0	0	0.3863(10)	2.20(1.21)	0.3860(11)	0.09(7)
0.030	0.010	0.020	-2	-1	0.2907(13)	2.01(1.16)	0.2906(14)	0.12(10)
0.030	0.020	0.010	2	1	0.2908(13)	2.01(1.16)	0.2908(14)	0.12(10)
0.030	0.010	0.030	-2	-1	0.3260(12)	2.04(1.17)	0.3259(13)	0.10(9)
0.030	0.030	0.010	2	1	0.3263(12)	2.03(1.17)	0.3261(13)	0.10(9)
0.030	0.020	0.020	-2	-1	0.3255(12)	2.06(1.17)	0.3253(12)	0.10(9)
0.030	0.020	0.030	-2	-1	0.3575(11)	2.13(1.19)	0.3573(11)	0.09(8)
0.030	0.030	0.020	2	1	0.3576(11)	2.13(1.19)	0.3574(11)	0.09(8)
0.030	0.030	0.030	-2	-1	0.3872(10)	2.21(1.21)	0.3868(11)	0.09(7)
0.030	0.010	0.010	2	0	0.2513(15)	2.00(1.16)	0.2514(16)	0.16(12)
0.030	0.010	0.020	2	0	0.2908(13)	2.01(1.16)	0.2907(14)	0.12(10)
0.030	0.010	0.030	2	0	0.3261(12)	2.03(1.17)	0.3259(13)	0.10(9)
0.030	0.020	0.020	2	0	0.3256(12)	2.06(1.17)	0.3255(12)	0.10(9)
0.030	0.020	0.030	2	0	0.3576(11)	2.13(1.19)	0.3574(12)	0.09(8)
0.030	0.030	0.030	2	0	0.3873(10)	2.21(1.21)	0.3870(11)	0.09(7)
0.030	0.010	0.010	2	1	0.2512(15)	2.01(1.16)	0.2513(16)	0.16(12)
0.030	0.010	0.010	2	-1	0.2519(15)	2.00(1.16)	0.2521(16)	0.16(12)
0.030	0.010	0.020	2	-1	0.2914(13)	2.00(1.16)	0.2914(14)	0.12(10)
0.030	0.020	0.010	2	-1	0.2916(13)	2.00(1.16)	0.2915(14)	0.12(10)
0.030	0.010	0.030	2	-1	0.3267(12)	2.03(1.16)	0.3266(13)	0.10(9)
0.030	0.030	0.010	2	-1	0.3270(12)	2.02(1.16)	0.3268(13)	0.10(9)
0.030	0.020	0.020	2	-1	0.3262(12)	2.06(1.17)	0.3261(12)	0.10(9)
0.030	0.020	0.030	2	-1	0.3582(11)	2.13(1.19)	0.3580(12)	0.09(8)
0.030	0.030	0.020	2	-1	0.3584(11)	2.13(1.19)	0.3581(12)	0.09(8)
0.030	0.030	0.030	2	-1	0.3879(10)	2.21(1.21)	0.3876(11)	0.09(7)
0.030	0.020	0.010	-2	0	0.2910(13)	2.00(1.16)	0.2909(14)	0.12(10)
0.030	0.030	0.010	-2	0	0.3264(12)	2.02(1.16)	0.3263(13)	0.10(9)
0.030	0.030	0.020	-2	0	0.3578(11)	2.13(1.19)	0.3575(12)	0.09(8)
0.030	0.010	0.010	-2	-2	0.2515(15)	2.02(1.16)	0.2517(16)	0.16(12)
0.030	0.010	0.020	-2	-2	0.2911(13)	2.02(1.16)	0.2911(14)	0.12(10)
0.030	0.010	0.030	-2	-2	0.3265(12)	2.04(1.17)	0.3264(13)	0.10(9)
0.030	0.020	0.020	-2	-2	0.3259(11)	2.07(1.18)	0.3257(12)	0.10(9)
0.030	0.020	0.030	-2	-2	0.3580(11)	2.14(1.19)	0.3577(11)	0.10(8)

TABLE XIV. Same as for Table XIII, except for lattice size 24^3 .

m_{sea}	m_1	m_3	$q_1(\frac{1}{3})$	$q_3(\frac{1}{3})$	M (cov)	χ^2/dof (cov)	M (uncov)	χ^2/dof (uncov)
0.005	0.005	0.020	-1	0	0.2605(4)	0.92(40)	0.2605(5)	0.07(7)
0.005	0.005	0.030	-1	0	0.2984(4)	0.99(42)	0.2985(5)	0.05(5)
0.005	0.010	0.010	-1	0	0.2393(4)	0.97(41)	0.2393(5)	0.08(8)
0.005	0.010	0.020	-1	0	0.2798(4)	0.94(41)	0.2799(5)	0.06(5)
0.005	0.010	0.030	-1	0	0.3154(4)	0.98(42)	0.3156(5)	0.04(4)
0.005	0.020	0.020	-1	0	0.3153(3)	0.89(40)	0.3154(5)	0.04(3)
0.005	0.020	0.030	-1	0	0.3475(3)	0.91(40)	0.3477(4)	0.04(3)
0.005	0.010	0.030	0	0	0.3152(4)	0.98(42)	0.3154(5)	0.04(4)
0.005	0.030	0.030	-1	0	0.3773(3)	0.91(40)	0.3776(4)	0.04(3)
0.005	0.001	0.001	-1	0	0.1399(6)	1.05(43)	0.1396(7)	0.14(10)
0.005	0.005	0.005	-1	1	0.1912(5)	0.96(41)	0.1912(6)	0.13(10)
0.005	0.005	0.010	-1	1	0.2169(4)	0.95(41)	0.2169(5)	0.10(9)
0.005	0.005	0.020	-1	1	0.2610(4)	0.91(40)	0.2611(5)	0.07(7)
0.005	0.005	0.030	-1	1	0.2989(4)	0.99(42)	0.2990(5)	0.05(5)
0.005	0.010	0.010	-1	1	0.2398(4)	0.97(41)	0.2398(5)	0.08(8)
0.005	0.010	0.020	-1	1	0.2803(4)	0.93(41)	0.2804(5)	0.06(5)
0.005	0.010	0.030	-1	1	0.3160(4)	0.97(42)	0.3161(5)	0.04(4)
0.005	0.020	0.020	-1	1	0.3157(3)	0.88(40)	0.3159(5)	0.04(3)
0.005	0.020	0.030	-1	1	0.3480(3)	0.90(40)	0.3482(4)	0.04(3)
0.005	0.020	0.020	0	0	0.3150(3)	0.89(40)	0.3151(5)	0.04(3)
0.005	0.030	0.030	-1	1	0.3778(3)	0.91(40)	0.3780(4)	0.04(3)
0.005	0.001	0.001	-1	1	0.1405(6)	1.05(43)	0.1402(7)	0.15(10)
0.005	0.005	0.005	-1	-1	0.1907(5)	0.97(41)	0.1907(6)	0.13(10)
0.005	0.005	0.010	-1	-1	0.2165(4)	0.96(41)	0.2165(5)	0.10(9)
0.005	0.005	0.020	-1	-1	0.2606(4)	0.92(40)	0.2606(5)	0.07(7)
0.005	0.005	0.030	-1	-1	0.2985(4)	0.99(42)	0.2986(5)	0.05(5)
0.005	0.010	0.010	-1	-1	0.2393(4)	0.97(41)	0.2394(5)	0.08(8)
0.005	0.010	0.020	-1	-1	0.2798(4)	0.94(41)	0.2799(5)	0.06(5)
0.005	0.010	0.030	-1	-1	0.3155(4)	0.98(42)	0.3157(5)	0.04(4)
0.005	0.020	0.020	-1	-1	0.3153(3)	0.89(40)	0.3154(5)	0.04(3)
0.005	0.020	0.030	-1	-1	0.3476(3)	0.91(40)	0.3478(4)	0.04(3)
0.005	0.020	0.030	0	0	0.3473(3)	0.91(40)	0.3475(4)	0.04(3)
0.005	0.030	0.030	-1	-1	0.3774(3)	0.92(40)	0.3776(4)	0.04(3)
0.005	0.001	0.001	-1	-1	0.1399(6)	1.05(43)	0.1396(7)	0.15(10)
0.005	0.005	0.005	0	0	0.1904(5)	0.96(41)	0.1903(6)	0.13(10)
0.005	0.030	0.030	0	0	0.3771(3)	0.91(40)	0.3773(4)	0.04(3)
0.005	0.001	0.001	0	0	0.1395(6)	1.05(43)	0.1392(7)	0.14(10)
0.005	0.005	0.005	0	1	0.1907(5)	0.96(41)	0.1906(6)	0.13(10)
0.005	0.005	0.010	0	1	0.2164(4)	0.95(41)	0.2164(5)	0.10(9)
0.005	0.005	0.020	0	1	0.2606(4)	0.92(40)	0.2606(5)	0.07(7)
0.005	0.005	0.030	0	1	0.2985(4)	0.99(42)	0.2986(5)	0.05(5)
0.005	0.010	0.020	0	1	0.2798(4)	0.94(41)	0.2799(5)	0.06(5)
0.005	0.010	0.030	0	1	0.3155(4)	0.98(42)	0.3157(5)	0.04(4)
0.005	0.020	0.030	0	1	0.3476(3)	0.91(40)	0.3477(4)	0.04(3)
0.005	0.005	0.010	0	0	0.2161(4)	0.95(41)	0.2161(6)	0.10(9)
0.005	0.005	0.020	0	0	0.2603(4)	0.92(40)	0.2603(5)	0.07(7)
0.005	0.005	0.010	1	0	0.2164(4)	0.95(41)	0.2164(5)	0.10(9)
0.005	0.005	0.030	0	0	0.2982(4)	0.99(42)	0.2983(5)	0.05(5)
0.005	0.010	0.010	0	0	0.2390(4)	0.97(41)	0.2391(5)	0.08(8)
0.005	0.010	0.020	0	0	0.2795(4)	0.94(41)	0.2796(5)	0.06(5)
0.005	0.005	0.010	-2	0	0.2172(4)	0.95(41)	0.2172(5)	0.10(9)
0.005	0.005	0.020	-2	0	0.2611(4)	0.92(40)	0.2612(5)	0.07(7)
0.005	0.005	0.030	-2	0	0.2990(4)	0.99(42)	0.2991(5)	0.05(5)

TABLE XIV. (Continued)

m_{sea}	m_1	m_3	$q_1(\frac{1}{3})$	$q_3(\frac{1}{3})$	M (cov)	χ^2/dof (cov)	M (uncov)	χ^2/dof (uncov)
0.005	0.010	0.010	-2	0	0.2401(4)	0.97(41)	0.2402(5)	0.08(8)
0.005	0.001	0.001	-2	0	0.1410(6)	1.04(42)	0.1407(7)	0.15(11)
0.005	0.010	0.020	-2	0	0.2805(4)	0.93(41)	0.2806(5)	0.06(5)
0.005	0.010	0.030	-2	0	0.3161(4)	0.97(42)	0.3162(5)	0.04(4)
0.005	0.020	0.020	-2	0	0.3160(3)	0.89(40)	0.3162(5)	0.04(3)
0.005	0.020	0.030	-2	0	0.3482(3)	0.90(40)	0.3484(4)	0.04(3)
0.005	0.030	0.030	-2	0	0.3781(3)	0.91(40)	0.3784(4)	0.04(3)
0.005	0.005	0.005	-2	1	0.1924(5)	0.96(41)	0.1923(6)	0.13(10)
0.005	0.005	0.010	-2	1	0.2180(4)	0.95(41)	0.2180(5)	0.10(9)
0.005	0.010	0.005	-2	1	0.2181(4)	0.95(41)	0.2181(5)	0.10(9)
0.005	0.005	0.020	-2	1	0.2619(4)	0.91(40)	0.2619(5)	0.07(7)
0.005	0.020	0.005	-2	1	0.2621(4)	0.91(40)	0.2622(5)	0.07(7)
0.005	0.005	0.030	-2	1	0.2997(4)	0.98(42)	0.2998(5)	0.05(5)
0.005	0.030	0.005	-2	1	0.3001(4)	0.98(42)	0.3002(5)	0.05(5)
0.005	0.010	0.010	-2	1	0.2408(4)	0.96(41)	0.2409(5)	0.08(8)
0.005	0.001	0.001	-2	1	0.1419(6)	1.04(42)	0.1416(7)	0.15(11)
0.005	0.010	0.020	-2	1	0.2812(4)	0.92(40)	0.2813(5)	0.06(5)
0.005	0.020	0.010	-2	1	0.2814(4)	0.93(40)	0.2814(5)	0.06(5)
0.005	0.010	0.030	-2	1	0.3168(4)	0.96(41)	0.3169(5)	0.04(4)
0.005	0.030	0.010	-2	1	0.3171(4)	0.97(42)	0.3172(5)	0.04(4)
0.005	0.020	0.020	-2	1	0.3167(3)	0.88(39)	0.3169(5)	0.04(3)
0.005	0.020	0.030	-2	1	0.3489(3)	0.90(40)	0.3491(4)	0.04(3)
0.005	0.030	0.020	-2	1	0.3491(3)	0.90(40)	0.3492(4)	0.04(3)
0.005	0.030	0.030	-2	1	0.3788(3)	0.91(40)	0.3790(4)	0.04(3)
0.005	0.005	0.005	-2	-1	0.1914(5)	0.97(41)	0.1913(6)	0.13(10)
0.005	0.005	0.010	-2	-1	0.2170(4)	0.96(41)	0.2170(5)	0.10(9)
0.005	0.010	0.005	2	1	0.2171(4)	0.96(41)	0.2171(5)	0.10(9)
0.005	0.005	0.020	-2	-1	0.2610(4)	0.92(40)	0.2611(5)	0.07(7)
0.005	0.020	0.005	2	1	0.2613(4)	0.92(40)	0.2613(5)	0.07(7)
0.005	0.005	0.030	-2	-1	0.2989(4)	0.99(42)	0.2990(5)	0.05(5)
0.005	0.030	0.005	2	1	0.2992(4)	1.00(42)	0.2993(5)	0.05(5)
0.005	0.010	0.010	-2	-1	0.2399(4)	0.97(41)	0.2400(5)	0.08(8)
0.005	0.001	0.001	-2	-1	0.1408(6)	1.04(42)	0.1404(7)	0.15(11)
0.005	0.010	0.020	-2	-1	0.2803(4)	0.94(41)	0.2804(5)	0.06(5)
0.005	0.020	0.010	2	1	0.2805(4)	0.94(41)	0.2806(5)	0.06(5)
0.005	0.010	0.030	-2	-1	0.3160(4)	0.98(42)	0.3161(5)	0.04(4)
0.005	0.030	0.010	2	1	0.3162(4)	0.98(42)	0.3164(5)	0.04(4)
0.005	0.020	0.020	-2	-1	0.3159(3)	0.89(40)	0.3160(5)	0.04(3)
0.005	0.020	0.030	-2	-1	0.3481(3)	0.91(40)	0.3483(4)	0.04(3)
0.005	0.030	0.020	2	1	0.3482(3)	0.91(40)	0.3484(4)	0.04(3)
0.005	0.030	0.030	-2	-1	0.3780(3)	0.92(40)	0.3782(4)	0.04(3)
0.005	0.005	0.005	2	0	0.1916(5)	0.96(41)	0.1915(6)	0.13(10)
0.005	0.010	0.005	-2	0	0.2173(4)	0.95(41)	0.2173(5)	0.10(9)
0.005	0.020	0.005	-2	0	0.2615(4)	0.92(40)	0.2615(5)	0.07(7)
0.005	0.030	0.005	-2	0	0.2995(4)	0.99(42)	0.2996(5)	0.05(5)
0.005	0.020	0.010	-2	0	0.2807(4)	0.93(41)	0.2808(5)	0.06(5)
0.005	0.030	0.010	-2	0	0.3165(4)	0.98(42)	0.3166(5)	0.04(4)
0.005	0.030	0.020	-2	0	0.3484(3)	0.90(40)	0.3486(4)	0.04(3)
0.005	0.005	0.005	2	-2	0.1938(5)	0.95(41)	0.1937(6)	0.13(10)
0.005	0.005	0.010	2	-2	0.2193(4)	0.94(41)	0.2193(5)	0.10(9)
0.005	0.005	0.020	2	-2	0.2632(4)	0.90(40)	0.2633(5)	0.07(7)
0.005	0.005	0.030	2	-2	0.3011(4)	0.97(42)	0.3012(5)	0.05(5)
0.005	0.010	0.010	2	-2	0.2421(4)	0.95(41)	0.2421(5)	0.08(8)

TABLE XIV. (*Continued*)

m_{sea}	m_1	m_3	$q_1(\frac{1}{3})$	$q_3(\frac{1}{3})$	M (cov)	χ^2/dof (cov)	M (uncov)	χ^2/dof (uncov)
0.005	0.010	0.020	2	-2	0.2825(4)	0.92(40)	0.2826(5)	0.05(5)
0.005	0.010	0.030	2	-2	0.3181(4)	0.96(41)	0.3183(5)	0.04(4)
0.005	0.020	0.020	2	-2	0.3179(3)	0.87(39)	0.3180(5)	0.04(3)
0.005	0.020	0.030	2	-2	0.3502(3)	0.89(40)	0.3504(4)	0.04(3)
0.005	0.030	0.030	2	-2	0.3800(3)	0.90(40)	0.3803(4)	0.04(4)
0.005	0.001	0.001	2	-2	0.1436(6)	1.03(42)	0.1433(7)	0.15(11)
0.005	0.005	0.005	2	2	0.1918(5)	0.97(41)	0.1917(6)	0.13(10)
0.005	0.005	0.010	2	2	0.2175(4)	0.96(41)	0.2175(5)	0.10(9)
0.005	0.005	0.020	2	2	0.2615(4)	0.93(40)	0.2616(5)	0.07(7)
0.005	0.005	0.030	2	2	0.2994(4)	1.00(42)	0.2995(5)	0.05(5)
0.005	0.010	0.010	2	2	0.2403(4)	0.98(41)	0.2403(5)	0.08(8)
0.005	0.010	0.020	2	2	0.2808(4)	0.94(41)	0.2809(5)	0.05(5)
0.005	0.010	0.030	2	2	0.3165(4)	0.99(42)	0.3166(5)	0.04(4)
0.005	0.020	0.020	2	2	0.3162(3)	0.90(40)	0.3164(5)	0.04(3)
0.005	0.020	0.030	2	2	0.3485(3)	0.92(40)	0.3487(4)	0.04(3)
0.005	0.030	0.030	2	2	0.3784(3)	0.93(41)	0.3786(4)	0.04(3)
0.005	0.001	0.001	2	2	0.1413(6)	1.03(42)	0.1409(7)	0.15(11)
0.010	0.010	0.010	0	1	0.2409(3)	2.98(73)	0.2411(5)	0.27(18)
0.010	0.001	0.001	-1	0	0.1414(5)	4.03(85)	0.1419(8)	0.56(31)
0.010	0.010	0.020	0	1	0.2811(3)	2.77(71)	0.2815(5)	0.23(16)
0.010	0.001	0.001	-1	1	0.1421(5)	4.05(85)	0.1426(8)	0.56(32)
0.010	0.010	0.030	0	1	0.3167(3)	2.54(68)	0.3173(5)	0.20(15)
0.010	0.001	0.001	-1	-1	0.1414(5)	4.04(85)	0.1419(8)	0.56(31)
0.010	0.010	0.010	0	0	0.2406(3)	2.98(74)	0.2408(5)	0.27(18)
0.010	0.020	0.020	0	1	0.3165(3)	2.41(66)	0.3169(5)	0.20(15)
0.010	0.001	0.001	0	0	0.1410(5)	4.02(85)	0.1415(8)	0.55(31)
0.010	0.020	0.030	0	1	0.3488(3)	2.18(63)	0.3493(4)	0.18(15)
0.010	0.030	0.030	0	1	0.3786(3)	1.99(60)	0.3791(4)	0.17(15)
0.010	0.010	0.020	0	0	0.2808(3)	2.78(71)	0.2813(5)	0.23(16)
0.010	0.010	0.020	1	0	0.2811(3)	2.77(71)	0.2815(5)	0.23(16)
0.010	0.010	0.030	1	0	0.3166(3)	2.54(68)	0.3172(5)	0.20(15)
0.010	0.020	0.030	1	0	0.3487(3)	2.18(63)	0.3492(4)	0.18(15)
0.010	0.010	0.010	1	1	0.2410(3)	2.97(73)	0.2411(5)	0.27(18)
0.010	0.010	0.020	1	1	0.2811(3)	2.76(71)	0.2816(5)	0.23(16)
0.010	0.010	0.030	1	1	0.3167(3)	2.54(68)	0.3173(5)	0.20(15)
0.010	0.020	0.020	1	1	0.3165(3)	2.41(66)	0.3170(5)	0.20(15)
0.010	0.020	0.030	1	1	0.3488(3)	2.18(63)	0.3493(4)	0.18(15)
0.010	0.010	0.030	0	0	0.3164(3)	2.55(68)	0.3170(5)	0.20(15)
0.010	0.030	0.030	1	1	0.3786(3)	1.99(60)	0.3791(4)	0.17(15)
0.010	0.010	0.010	1	-1	0.2414(3)	2.98(73)	0.2416(5)	0.27(18)
0.010	0.010	0.020	1	-1	0.2816(3)	2.76(71)	0.2820(5)	0.23(16)
0.010	0.010	0.030	1	-1	0.3171(3)	2.53(68)	0.3177(5)	0.20(15)
0.010	0.020	0.020	1	-1	0.3169(3)	2.40(66)	0.3174(5)	0.20(15)
0.010	0.020	0.030	1	-1	0.3492(3)	2.17(63)	0.3497(4)	0.18(15)
0.010	0.030	0.030	1	-1	0.3791(3)	1.99(60)	0.3795(4)	0.17(15)
0.010	0.020	0.020	0	0	0.3162(3)	2.42(66)	0.3167(5)	0.20(15)
0.010	0.020	0.030	0	0	0.3485(3)	2.19(63)	0.3490(4)	0.18(15)
0.010	0.030	0.030	0	0	0.3783(3)	2.00(60)	0.3788(4)	0.17(15)
0.010	0.010	0.020	-2	-1	0.2817(3)	2.74(71)	0.2821(5)	0.22(16)
0.010	0.020	0.010	2	1	0.2818(3)	2.75(71)	0.2822(5)	0.22(16)
0.010	0.010	0.030	-2	-1	0.3172(3)	2.52(68)	0.3177(5)	0.20(15)
0.010	0.030	0.010	2	1	0.3174(3)	2.52(68)	0.3180(5)	0.20(15)
0.010	0.020	0.020	-2	-1	0.3171(3)	2.40(66)	0.3176(5)	0.20(15)

TABLE XIV. (Continued)

m_{sea}	m_1	m_3	$q_1(\frac{1}{3})$	$q_3(\frac{1}{3})$	M (cov)	χ^2/dof (cov)	M (uncov)	χ^2/dof (uncov)
0.010	0.020	0.030	-2	-1	0.3493(3)	2.17(63)	0.3498(4)	0.18(15)
0.010	0.030	0.020	2	1	0.3495(3)	2.17(63)	0.3499(4)	0.18(15)
0.010	0.001	0.001	-2	0	0.1425(5)	4.07(86)	0.1430(8)	0.57(32)
0.010	0.030	0.030	-2	-1	0.3792(3)	1.98(60)	0.3797(4)	0.17(15)
0.010	0.010	0.010	2	0	0.2418(3)	2.96(73)	0.2419(5)	0.27(18)
0.010	0.010	0.020	2	0	0.2818(3)	2.75(71)	0.2822(5)	0.22(16)
0.010	0.010	0.030	2	0	0.3173(3)	2.52(68)	0.3179(5)	0.20(15)
0.010	0.020	0.020	2	0	0.3173(3)	2.40(66)	0.3177(5)	0.20(15)
0.010	0.020	0.030	2	0	0.3495(3)	2.16(63)	0.3500(4)	0.18(15)
0.010	0.030	0.030	2	0	0.3794(3)	1.98(60)	0.3799(4)	0.17(15)
0.010	0.010	0.010	2	1	0.2416(3)	2.95(73)	0.2417(5)	0.27(18)
0.010	0.001	0.001	-2	1	0.1435(5)	4.09(86)	0.1440(8)	0.58(32)
0.010	0.010	0.010	2	-1	0.2425(3)	2.96(73)	0.2426(5)	0.27(18)
0.010	0.010	0.020	2	-1	0.2825(3)	2.74(71)	0.2829(5)	0.22(16)
0.010	0.020	0.010	2	-1	0.2827(3)	2.74(71)	0.2831(5)	0.22(16)
0.010	0.010	0.030	2	-1	0.3180(3)	2.50(68)	0.3186(5)	0.20(15)
0.010	0.030	0.010	2	-1	0.3183(3)	2.50(68)	0.3189(5)	0.20(15)
0.010	0.020	0.020	2	-1	0.3180(3)	2.38(66)	0.3184(5)	0.20(15)
0.010	0.020	0.030	2	-1	0.3502(3)	2.15(63)	0.3507(4)	0.18(15)
0.010	0.030	0.020	2	-1	0.3503(3)	2.15(63)	0.3508(4)	0.18(15)
0.010	0.030	0.030	2	-1	0.3801(3)	1.97(60)	0.3806(4)	0.17(15)
0.010	0.001	0.001	-2	-1	0.1422(5)	4.07(86)	0.1428(8)	0.56(32)
0.010	0.020	0.010	-2	0	0.2820(3)	2.75(71)	0.2824(5)	0.22(16)
0.010	0.030	0.010	-2	0	0.3176(3)	2.52(68)	0.3182(5)	0.20(15)
0.010	0.030	0.020	-2	0	0.3496(3)	2.16(63)	0.3501(4)	0.18(15)
0.010	0.001	0.001	2	-2	0.1453(5)	4.14(86)	0.1457(8)	0.59(33)
0.010	0.001	0.001	2	2	0.1427(5)	4.09(86)	0.1433(8)	0.56(32)
0.010	0.010	0.010	-2	-2	0.2420(3)	2.92(73)	0.2421(5)	0.26(18)
0.010	0.010	0.020	-2	-2	0.2821(3)	2.73(70)	0.2825(5)	0.22(16)
0.010	0.010	0.030	-2	-2	0.3177(3)	2.51(68)	0.3182(5)	0.20(15)
0.010	0.020	0.020	-2	-2	0.3175(3)	2.39(66)	0.3179(4)	0.20(15)
0.010	0.020	0.030	-2	-2	0.3498(3)	2.16(63)	0.3503(4)	0.18(15)
0.010	0.030	0.030	-2	-2	0.3796(3)	1.98(60)	0.3801(4)	0.17(14)
0.010	0.010	0.010	-2	2	0.2438(3)	2.95(73)	0.2439(5)	0.27(18)
0.010	0.010	0.020	-2	2	0.2839(3)	2.71(70)	0.2843(5)	0.22(16)
0.010	0.010	0.030	-2	2	0.3194(3)	2.46(67)	0.3199(5)	0.19(15)
0.010	0.020	0.020	-2	2	0.3192(3)	2.35(66)	0.3196(5)	0.20(15)
0.010	0.020	0.030	-2	2	0.3515(3)	2.12(62)	0.3520(4)	0.18(15)
0.010	0.030	0.030	-2	2	0.3814(3)	1.95(59)	0.3818(4)	0.17(15)
0.020	0.020	0.020	-1	0	0.3222(3)	1.21(46)	0.3220(5)	0.06(6)
0.020	0.020	0.020	-1	1	0.3227(3)	1.21(46)	0.3225(5)	0.06(6)
0.020	0.020	0.020	-1	-1	0.3222(3)	1.20(46)	0.3220(5)	0.06(6)
0.020	0.020	0.020	0	0	0.3219(3)	1.21(46)	0.3217(5)	0.06(6)
0.020	0.020	0.020	-2	0	0.3230(3)	1.20(46)	0.3228(5)	0.06(6)
0.020	0.020	0.020	-2	1	0.3237(3)	1.20(46)	0.3235(5)	0.06(6)
0.020	0.020	0.020	-2	-1	0.3228(3)	1.19(46)	0.3226(5)	0.06(6)
0.020	0.020	0.020	2	-2	0.3250(3)	1.20(46)	0.3248(5)	0.06(6)
0.020	0.020	0.020	2	2	0.3232(3)	1.18(46)	0.3229(5)	0.06(6)
0.030	0.030	0.030	-1	0	0.3891(4)	1.27(47)	0.3890(4)	0.06(5)
0.030	0.030	0.030	-1	1	0.3896(4)	1.28(47)	0.3895(4)	0.06(5)
0.030	0.030	0.030	-1	-1	0.3891(4)	1.27(47)	0.3890(4)	0.06(5)
0.030	0.030	0.030	0	0	0.3888(4)	1.27(47)	0.3887(4)	0.06(5)
0.030	0.030	0.030	-2	0	0.3899(4)	1.28(47)	0.3898(4)	0.06(5)

TABLE XV. Summary of pseudoscalar meson mass-squared splittings ($\times 10^3$) obtained from the masses in Table XIII. Lattice size 16^3 .

m_{sea}	m_1	m_3	$q_1(\frac{1}{3})$	$q_3(\frac{1}{3})$	$\Delta M^2(\times 10^3)$ (cov)	$\Delta M^2(\times 10^3)$ (uncov)
0.010	0.010	0.010	0	1	0.1210(14)	0.1207(16)
0.010	0.010	0.020	0	1	0.1515(13)	0.1510(14)
0.010	0.010	0.030	0	1	0.1820(14)	0.1812(14)
0.010	0.020	0.020	0	1	0.1532(13)	0.1529(13)
0.010	0.020	0.030	0	1	0.1844(13)	0.1838(12)
0.010	0.030	0.030	0	1	0.1869(13)	0.1865(12)
0.010	0.010	0.020	1	0	0.1222(15)	0.1222(16)
0.010	0.010	0.030	1	0	0.1236(17)	0.1237(17)
0.010	0.020	0.030	1	0	0.1551(13)	0.1549(13)
0.010	0.010	0.010	1	1	0.1596(27)	0.1583(31)
0.010	0.010	0.020	1	1	0.1800(25)	0.1788(28)
0.010	0.010	0.030	1	1	0.2013(27)	0.2001(29)
0.010	0.020	0.020	1	1	0.2005(24)	0.1997(26)
0.010	0.020	0.030	1	1	0.2223(25)	0.2216(26)
0.010	0.030	0.030	1	1	0.2449(26)	0.2444(26)
0.010	0.010	0.010	1	-1	0.3244(43)	0.3245(47)
0.010	0.010	0.020	1	-1	0.3674(43)	0.3675(44)
0.010	0.010	0.030	1	-1	0.4100(44)	0.4095(44)
0.010	0.020	0.020	1	-1	0.4123(42)	0.4120(41)
0.010	0.020	0.030	1	-1	0.4566(43)	0.4558(41)
0.010	0.030	0.030	1	-1	0.5027(43)	0.5015(41)
0.010	0.010	0.020	-2	-1	0.4582(68)	0.4562(75)
0.010	0.010	0.020	1	2	0.5448(57)	0.5416(62)
0.010	0.010	0.030	-2	-1	0.4730(76)	0.4716(82)
0.010	0.010	0.030	1	2	0.6460(59)	0.6421(61)
0.010	0.020	0.020	-2	-1	0.5585(58)	0.5565(61)
0.010	0.020	0.030	-2	-1	0.5747(63)	0.5734(65)
0.010	0.020	0.030	1	2	0.6614(59)	0.6590(59)
0.010	0.030	0.030	-2	-1	0.6797(62)	0.6783(61)
0.010	0.010	0.010	2	0	0.4899(59)	0.4885(65)
0.010	0.010	0.020	2	0	0.4947(61)	0.4944(65)
0.010	0.010	0.030	2	0	0.5002(68)	0.5003(70)
0.010	0.020	0.020	2	0	0.6176(53)	0.6164(52)
0.010	0.020	0.030	2	0	0.6252(55)	0.6244(53)
0.010	0.030	0.030	2	0	0.7513(54)	0.7495(49)
0.010	0.010	0.010	2	1	0.4456(66)	0.4425(75)
0.010	0.010	0.010	2	-1	0.775(10)	0.775(11)
0.010	0.010	0.020	2	-1	0.833(10)	0.834(10)
0.010	0.010	0.020	-1	2	0.920(10)	0.919(10)
0.010	0.010	0.030	2	-1	0.891(10)	0.891(10)
0.010	0.010	0.030	-1	2	1.064(10)	1.061(10)
0.010	0.020	0.020	2	-1	0.9828(97)	0.9820(95)
0.010	0.020	0.030	2	-1	1.0441(98)	1.0426(94)
0.010	0.020	0.030	-1	2	1.1309(99)	1.1283(95)
0.010	0.030	0.030	2	-1	1.1964(98)	1.1934(93)
0.010	0.010	0.020	0	-2	0.6106(54)	0.6086(56)
0.010	0.010	0.030	0	-2	0.7317(57)	0.7284(57)
0.010	0.020	0.030	0	-2	0.7412(53)	0.7389(50)
0.010	0.010	0.010	-2	-2	0.648(10)	0.642(12)
0.010	0.010	0.020	-2	-2	0.728(10)	0.723(11)
0.010	0.010	0.030	-2	-2	0.812(11)	0.807(11)
0.010	0.020	0.020	-2	-2	0.8092(98)	0.805(10)

TABLE XV. (Continued)

m_{sea}	m_1	m_3	$q_1(\frac{1}{3})$	$q_3(\frac{1}{3})$	$\Delta M^2(\times 10^3)$ (cov)	$\Delta M^2(\times 10^3)$ (uncov)
0.010	0.020	0.030	-2	-2	0.895(10)	0.892(10)
0.010	0.030	0.030	-2	-2	0.984(10)	0.982(10)
0.010	0.010	0.010	-2	2	1.309(17)	1.310(19)
0.010	0.010	0.020	-2	2	1.480(17)	1.481(17)
0.010	0.010	0.030	-2	2	1.650(18)	1.648(17)
0.010	0.020	0.020	-2	2	1.659(17)	1.658(16)
0.010	0.020	0.030	-2	2	1.835(17)	1.832(16)
0.010	0.030	0.030	-2	2	2.019(17)	2.014(16)
0.020	0.010	0.010	0	1	0.1292(15)	0.1289(16)
0.020	0.010	0.020	0	1	0.1577(13)	0.1575(13)
0.020	0.010	0.030	0	1	0.1874(14)	0.1875(14)
0.020	0.020	0.020	0	1	0.1588(13)	0.1586(13)
0.020	0.020	0.030	0	1	0.1893(13)	0.1893(13)
0.020	0.030	0.030	0	1	0.1913(13)	0.1915(13)
0.020	0.010	0.020	1	0	0.1296(16)	0.1290(17)
0.020	0.010	0.030	1	0	0.1304(18)	0.1299(19)
0.020	0.020	0.030	1	0	0.1601(14)	0.1601(14)
0.020	0.010	0.010	1	1	0.1606(47)	0.1595(34)
0.020	0.010	0.020	1	1	0.1788(29)	0.1779(31)
0.020	0.010	0.030	1	1	0.1990(30)	0.1983(31)
0.020	0.020	0.020	1	1	0.1980(26)	0.1975(27)
0.020	0.020	0.030	1	1	0.2190(26)	0.2188(26)
0.020	0.030	0.030	1	1	0.2410(25)	0.2408(25)
0.020	0.010	0.010	1	-1	0.3563(43)	0.3558(45)
0.020	0.010	0.020	1	-1	0.3957(42)	0.3950(43)
0.020	0.010	0.030	1	-1	0.4366(43)	0.4364(44)
0.020	0.020	0.020	1	-1	0.4370(41)	0.4368(41)
0.020	0.020	0.030	1	-1	0.4797(41)	0.4800(42)
0.020	0.030	0.030	1	-1	0.5243(42)	0.5250(42)
0.020	0.010	0.020	-2	-1	0.4642(78)	0.4615(84)
0.020	0.010	0.020	1	2	0.5478(64)	0.5461(67)
0.020	0.010	0.030	-2	-1	0.4766(85)	0.4740(90)
0.020	0.010	0.030	1	2	0.6457(62)	0.6449(64)
0.020	0.020	0.020	-2	-1	0.5590(63)	0.5578(65)
0.020	0.020	0.030	-2	-1	0.5733(94)	0.5725(67)
0.020	0.020	0.030	1	2	0.6596(59)	0.6593(60)
0.020	0.030	0.030	-2	-1	0.6765(60)	0.6763(60)
0.020	0.010	0.010	2	0	0.5227(61)	0.5212(64)
0.020	0.010	0.020	2	0	0.5240(66)	0.5217(70)
0.020	0.010	0.030	2	0	0.5274(75)	0.5252(78)
0.020	0.020	0.020	2	0	0.6398(54)	0.6392(55)
0.020	0.020	0.030	2	0	0.6453(57)	0.6451(58)
0.020	0.030	0.030	2	0	0.7691(53)	0.7697(53)
0.020	0.010	0.010	2	1	0.4556(75)	0.4531(82)
0.020	0.010	0.010	2	-1	0.847(10)	0.846(10)
0.020	0.010	0.020	2	-1	0.898(10)	0.896(10)
0.020	0.010	0.020	-1	2	0.9822(96)	0.9811(99)
0.020	0.010	0.030	2	-1	0.952(10)	0.950(10)
0.020	0.010	0.030	-1	2	1.1218(99)	1.122(10)
0.020	0.020	0.020	2	-1	1.0376(94)	1.0372(96)
0.020	0.020	0.030	2	-1	1.0954(96)	1.0959(97)
0.020	0.020	0.030	-1	2	1.1819(96)	1.1828(97)
0.020	0.030	0.030	2	-1	1.2440(96)	1.2456(97)

TABLE XV. (*Continued*)

m_{sea}	m_1	m_3	$q_1(\frac{1}{3})$	$q_3(\frac{1}{3})$	$\Delta M^2(\times 10^3)$ (cov)	$\Delta M^2(\times 10^3)$ (uncov)
0.020	0.010	0.020	0	-2	0.6357(54)	0.6349(56)
0.020	0.010	0.030	0	-2	0.7535(56)	0.7538(57)
0.020	0.020	0.030	0	-2	0.7609(53)	0.7612(53)
0.020	0.010	0.010	-2	-2	0.651(12)	0.647(13)
0.020	0.010	0.020	-2	-2	0.723(11)	0.719(12)
0.020	0.010	0.030	-2	-2	0.803(12)	0.800(12)
0.020	0.020	0.020	-2	-2	0.799(10)	0.797(11)
0.020	0.020	0.030	-2	-2	0.882(10)	0.880(10)
0.020	0.030	0.030	-2	-2	0.968(19)	0.968(10)
0.020	0.010	0.010	-2	2	1.436(17)	1.434(18)
0.020	0.010	0.020	-2	2	1.593(16)	1.591(17)
0.020	0.010	0.030	-2	2	1.756(17)	1.755(17)
0.020	0.020	0.020	-2	2	1.757(16)	1.757(16)
0.020	0.020	0.030	-2	2	1.928(16)	1.929(16)
0.020	0.030	0.030	-2	2	2.105(16)	2.108(17)
0.030	0.010	0.010	0	1	0.1292(15)	0.1289(16)
0.030	0.010	0.020	0	1	0.1588(13)	0.1584(14)
0.030	0.010	0.030	0	1	0.1886(13)	0.1882(14)
0.030	0.020	0.020	0	1	0.1599(13)	0.1594(14)
0.030	0.020	0.030	0	1	0.1907(13)	0.1901(13)
0.030	0.030	0.030	0	1	0.1932(13)	0.1924(13)
0.030	0.010	0.020	1	0	0.1291(16)	0.1289(17)
0.030	0.010	0.030	1	0	0.1297(18)	0.1295(19)
0.030	0.020	0.030	1	0	0.1615(14)	0.1610(14)
0.030	0.010	0.010	1	1	0.1590(31)	0.1587(33)
0.030	0.010	0.020	1	1	0.1790(28)	0.1790(30)
0.030	0.010	0.030	1	1	0.1995(28)	0.1998(30)
0.030	0.020	0.020	1	1	0.2008(25)	0.2010(27)
0.030	0.020	0.030	1	1	0.2228(24)	0.2232(26)
0.030	0.030	0.030	1	1	0.2462(24)	0.2465(25)
0.030	0.010	0.010	1	-1	0.3579(46)	0.3569(49)
0.030	0.010	0.020	1	-1	0.3968(44)	0.3955(47)
0.030	0.010	0.030	1	-1	0.4371(45)	0.4354(47)
0.030	0.020	0.020	1	-1	0.4387(42)	0.4367(44)
0.030	0.020	0.030	1	-1	0.4815(42)	0.4788(44)
0.030	0.030	0.030	1	-1	0.5265(42)	0.5232(44)
0.030	0.010	0.020	-2	-1	0.4629(75)	0.4627(80)
0.030	0.010	0.020	1	2	0.5510(71)	0.5504(65)
0.030	0.010	0.030	-2	-1	0.4751(80)	0.4759(86)
0.030	0.010	0.030	1	2	0.6500(59)	0.6499(63)
0.030	0.020	0.020	-2	-1	0.5659(59)	0.5659(63)
0.030	0.020	0.030	-2	-1	0.5824(62)	0.5828(66)
0.030	0.020	0.030	1	2	0.6690(56)	0.6690(60)
0.030	0.030	0.030	-2	-1	0.6889(57)	0.6889(61)
0.030	0.010	0.010	2	0	0.5229(63)	0.5215(68)
0.030	0.010	0.020	2	0	0.5224(66)	0.5213(71)
0.030	0.010	0.030	2	0	0.5247(73)	0.5238(77)
0.030	0.020	0.020	2	0	0.6446(53)	0.6427(56)
0.030	0.020	0.030	2	0	0.6509(56)	0.6489(58)
0.030	0.030	0.030	2	0	0.7767(53)	0.7738(55)
0.030	0.010	0.010	2	1	0.4527(74)	0.4517(80)
0.030	0.010	0.010	2	-1	0.850(10)	0.848(11)
0.030	0.010	0.020	2	-1	0.899(10)	0.896(11)

TABLE XV. (Continued)

m_{sea}	m_1	m_3	$q_1(\frac{1}{3})$	$q_3(\frac{1}{3})$	$\Delta M^2(\times 10^3)$ (cov)	$\Delta M^2(\times 10^3)$ (uncov)
0.030	0.010	0.020	-1	2	0.987(10)	0.984(10)
0.030	0.010	0.030	2	-1	0.950(10)	0.947(11)
0.030	0.010	0.030	-1	2	1.126(10)	1.121(10)
0.030	0.020	0.020	2	-1	1.0424(96)	1.037(10)
0.030	0.020	0.030	2	-1	1.1003(98)	1.094(10)
0.030	0.020	0.030	-1	2	1.1871(97)	1.181(10)
0.030	0.030	0.030	2	-1	1.2503(97)	1.243(10)
0.030	0.010	0.020	0	-2	0.6403(55)	0.6386(57)
0.030	0.010	0.030	0	-2	0.7586(55)	0.7567(57)
0.030	0.020	0.030	0	-2	0.7669(52)	0.7643(54)
0.030	0.010	0.010	-2	-2	0.645(12)	0.644(13)
0.030	0.010	0.020	-2	-2	0.724(11)	0.724(12)
0.030	0.010	0.030	-2	-2	0.805(11)	0.806(12)
0.030	0.020	0.020	-2	-2	0.810(10)	0.811(10)
0.030	0.020	0.030	-2	-2	0.8978(98)	0.899(10)
0.030	0.030	0.030	-2	-2	0.9899(96)	0.991(10)
0.030	0.010	0.010	-2	2	1.442(18)	1.438(19)
0.030	0.010	0.020	-2	2	1.598(17)	1.592(18)
0.030	0.010	0.030	-2	2	1.758(18)	1.751(19)
0.030	0.020	0.020	-2	2	1.765(16)	1.756(17)
0.030	0.020	0.030	-2	2	1.935(17)	1.924(17)
0.030	0.030	0.030	-2	2	2.114(17)	2.101(17)

APPENDIX A: TABLES OF HADRON MASSES AND SPLITTINGS

TABLE XVI. Summary of pseudoscalar meson mass-squared splittings ($\times 10^3$) obtained from the masses in Table XIV. Lattice size 24^3 .

m_{sea}	m_1	m_3	$q_1(\frac{1}{3})$	$q_3(\frac{1}{3})$	$\Delta M^2(\times 10^3)$ (cov)	$\Delta M^2(\times 10^3)$ (uncov)
0.005	0.005	0.020	-1	0	0.1148(11)	0.1147(11)
0.005	0.005	0.030	-1	0	0.1161(15)	0.1166(15)
0.005	0.010	0.010	-1	0	0.129 45(77)	0.129 39(78)
0.005	0.010	0.020	-1	0	0.130 90(92)	0.130 96(87)
0.005	0.010	0.030	-1	0	0.1327(10)	0.1331(10)
0.005	0.020	0.020	-1	0	0.163 04(85)	0.163 35(76)
0.005	0.020	0.030	-1	0	0.166 15(87)	0.166 38(80)
0.005	0.030	0.030	-1	0	0.199 80(86)	0.199 90(80)
0.005	0.001	0.001	-1	0	0.102 28(85)	0.102 35(96)
0.005	0.005	0.005	-1	1	0.3233(22)	0.3226(24)
0.005	0.005	0.010	-1	1	0.3447(23)	0.3440(25)
0.005	0.005	0.020	-1	1	0.3876(27)	0.3878(27)
0.005	0.005	0.030	-1	1	0.4310(31)	0.4325(30)
0.005	0.010	0.010	-1	1	0.3665(24)	0.3662(24)
0.005	0.010	0.020	-1	1	0.4109(27)	0.4114(26)
0.005	0.010	0.030	-1	1	0.4558(30)	0.4572(28)
0.005	0.020	0.020	-1	1	0.4583(29)	0.4592(26)
0.005	0.020	0.030	-1	1	0.5062(30)	0.5074(28)
0.005	0.030	0.030	-1	1	0.5566(31)	0.5578(29)
0.005	0.001	0.001	-1	1	0.2880(23)	0.2889(27)
0.005	0.005	0.005	-1	-1	0.1332(14)	0.1326(16)

TABLE XVI. (*Continued*)

m_{sea}	m_1	m_3	$q_1(\frac{1}{3})$	$q_3(\frac{1}{3})$	$\Delta M^2(\times 10^3)$ (cov)	$\Delta M^2(\times 10^3)$ (uncov)
0.005	0.005	0.010	-1	-1	0.1416(14)	0.1414(15)
0.005	0.005	0.020	-1	-1	0.1603(17)	0.1607(17)
0.005	0.005	0.030	-1	-1	0.1818(20)	0.1821(20)
0.005	0.010	0.010	-1	-1	0.1511(14)	0.1512(14)
0.005	0.010	0.020	-1	-1	0.1713(15)	0.1718(14)
0.005	0.010	0.030	-1	-1	0.1936(17)	0.1938(15)
0.005	0.020	0.020	-1	-1	0.1937(15)	0.1940(12)
0.005	0.020	0.030	-1	-1	0.2176(15)	0.2173(13)
0.005	0.030	0.030	-1	-1	0.2425(15)	0.2417(13)
0.005	0.001	0.001	-1	-1	0.1208(18)	0.1202(20)
0.005	0.005	0.005	0	1	0.114 18(75)	0.113 84(82)
0.005	0.005	0.010	0	1	0.129 05(73)	0.128 98(77)
0.005	0.005	0.020	0	1	0.159 17(92)	0.159 54(85)
0.005	0.005	0.030	0	1	0.1903(11)	0.1907(10)
0.005	0.010	0.020	0	1	0.160 32(86)	0.160 69(78)
0.005	0.010	0.030	0	1	0.1920(10)	0.192 46(87)
0.005	0.020	0.030	0	1	0.195 85(90)	0.196 05(79)
0.005	0.005	0.010	1	0	0.114 13(85)	0.113 80(91)
0.005	0.005	0.010	-2	0	0.4624(34)	0.4611(36)
0.005	0.005	0.020	-2	0	0.4653(46)	0.4650(46)
0.005	0.005	0.030	-2	0	0.4705(59)	0.4723(59)
0.005	0.010	0.010	-2	0	0.5232(31)	0.5231(31)
0.005	0.001	0.001	-2	0	0.4156(34)	0.4159(38)
0.005	0.010	0.020	-2	0	0.5290(36)	0.5293(35)
0.005	0.010	0.030	-2	0	0.5365(42)	0.5379(40)
0.005	0.020	0.020	-2	0	0.6568(34)	0.6580(30)
0.005	0.020	0.030	-2	0	0.6691(34)	0.6701(32)
0.005	0.030	0.030	-2	0	0.8028(34)	0.8032(32)
0.005	0.005	0.005	-2	1	0.7671(51)	0.7654(56)
0.005	0.005	0.010	-2	1	0.7947(54)	0.7929(58)
0.005	0.005	0.010	1	-2	0.8391(53)	0.8381(57)
0.005	0.005	0.020	-2	1	0.8519(66)	0.8519(67)
0.005	0.005	0.020	1	-2	0.9837(62)	0.9850(62)
0.005	0.005	0.030	-2	1	0.9102(80)	0.9137(78)
0.005	0.005	0.030	1	-2	1.1305(73)	1.1342(71)
0.005	0.010	0.010	-2	1	0.8683(55)	0.8676(57)
0.005	0.001	0.001	-2	1	0.6851(55)	0.6869(62)
0.005	0.010	0.020	-2	1	0.9291(63)	0.9299(61)
0.005	0.010	0.020	1	-2	1.0165(63)	1.0183(60)
0.005	0.010	0.030	-2	1	0.9910(70)	0.9941(66)
0.005	0.010	0.030	1	-2	1.1670(70)	1.1705(66)
0.005	0.020	0.020	-2	1	1.0848(66)	1.0868(61)
0.005	0.020	0.030	-2	1	1.1539(68)	1.1565(64)
0.005	0.020	0.030	1	-2	1.2421(70)	1.2447(65)
0.005	0.030	0.030	-2	1	1.3172(70)	1.3196(67)
0.005	0.005	0.005	-2	-1	0.3861(35)	0.3846(38)
0.005	0.005	0.010	-2	-1	0.3878(38)	0.3870(41)
0.005	0.005	0.010	1	2	0.4322(33)	0.4321(34)
0.005	0.005	0.020	-2	-1	0.3967(48)	0.3970(49)
0.005	0.005	0.020	1	2	0.5282(38)	0.5299(34)
0.005	0.005	0.030	-2	-1	0.4112(61)	0.4122(63)
0.005	0.005	0.030	1	2	0.6312(46)	0.6322(39)
0.005	0.010	0.010	-2	-1	0.4367(34)	0.4370(34)

TABLE XVI. (Continued)

m_{sea}	m_1	m_3	$q_1(\frac{1}{3})$	$q_3(\frac{1}{3})$	$\Delta M^2(\times 10^3)$ (cov)	$\Delta M^2(\times 10^3)$ (uncov)
0.005	0.001	0.001	-2	-1	0.3500(42)	0.3489(48)
0.005	0.010	0.020	-2	-1	0.4492(39)	0.4499(36)
0.005	0.010	0.020	1	2	0.5365(36)	0.5381(31)
0.005	0.010	0.030	-2	-1	0.4658(45)	0.4664(42)
0.005	0.010	0.030	1	2	0.6417(40)	0.6425(33)
0.005	0.020	0.020	-2	-1	0.5546(35)	0.5556(29)
0.005	0.020	0.030	-2	-1	0.5758(37)	0.5755(31)
0.005	0.020	0.030	1	2	0.6639(36)	0.6635(29)
0.005	0.030	0.030	-2	-1	0.6878(36)	0.6864(30)
0.005	0.005	0.005	2	0	0.4626(30)	0.4614(32)
0.005	0.005	0.010	0	-2	0.5217(29)	0.5214(30)
0.005	0.005	0.020	0	-2	0.6413(37)	0.6428(34)
0.005	0.005	0.030	0	-2	0.7649(46)	0.7667(41)
0.005	0.010	0.020	0	-2	0.6458(34)	0.6474(31)
0.005	0.010	0.030	0	-2	0.7718(40)	0.7735(35)
0.005	0.020	0.030	0	-2	0.7870(36)	0.7878(32)
0.005	0.005	0.005	2	-2	1.3062(90)	1.3034(99)
0.005	0.005	0.010	2	-2	1.3910(94)	1.388(10)
0.005	0.005	0.020	2	-2	1.561(10)	1.563(11)
0.005	0.005	0.030	2	-2	1.734(12)	1.741(12)
0.005	0.010	0.010	2	-2	1.4780(98)	1.476(10)
0.005	0.010	0.020	2	-2	1.654(11)	1.657(10)
0.005	0.010	0.030	2	-2	1.833(12)	1.839(11)
0.005	0.020	0.020	2	-2	1.844(11)	1.847(10)
0.005	0.020	0.030	2	-2	2.034(12)	2.039(11)
0.005	0.030	0.030	2	-2	2.235(12)	2.240(12)
0.005	0.001	0.001	2	-2	1.1658(95)	1.169(10)
0.005	0.005	0.005	2	2	0.5427(59)	0.5406(64)
0.005	0.005	0.010	2	2	0.5757(59)	0.5753(62)
0.005	0.005	0.020	2	2	0.6498(68)	0.6516(67)
0.005	0.005	0.030	2	2	0.7349(80)	0.7361(79)
0.005	0.010	0.010	2	2	0.6135(57)	0.6142(57)
0.005	0.010	0.020	2	2	0.6934(61)	0.6953(55)
0.005	0.010	0.030	2	2	0.7816(68)	0.7823(60)
0.005	0.020	0.020	2	2	0.7820(59)	0.7834(50)
0.005	0.020	0.030	2	2	0.8764(62)	0.8754(52)
0.005	0.030	0.030	2	2	0.9747(62)	0.9718(52)
0.005	0.001	0.001	2	2	0.4943(70)	0.4920(80)
0.010	0.010	0.010	0	1	0.13426(85)	0.13325(75)
0.010	0.001	0.001	-1	0	0.1044(10)	0.1068(10)
0.010	0.010	0.020	0	1	0.16591(89)	0.16441(80)
0.010	0.001	0.001	-1	1	0.3012(32)	0.3008(35)
0.010	0.010	0.030	0	1	0.19850(99)	0.19621(91)
0.010	0.001	0.001	-1	-1	0.1162(17)	0.1262(20)
0.010	0.020	0.020	0	1	0.169 35(82)	0.166 67(80)
0.010	0.020	0.030	0	1	0.202 33(88)	0.199 32(88)
0.010	0.030	0.030	0	1	0.205 93(92)	0.202 82(90)
0.010	0.010	0.020	1	0	0.137 24(92)	0.134 65(81)
0.010	0.010	0.030	1	0	0.1403(10)	0.136 37(95)
0.010	0.020	0.030	1	0	0.172 74(88)	0.169 31(86)
0.010	0.010	0.010	1	1	0.1581(15)	0.1562(15)
0.010	0.010	0.020	1	1	0.1806(15)	0.1762(15)
0.010	0.010	0.030	1	1	0.2032(17)	0.1975(16)

TABLE XVI. (*Continued*)

m_{sea}	m_1	m_3	$q_1(\frac{1}{3})$	$q_3(\frac{1}{3})$	$\Delta M^2(\times 10^3)$ (cov)	$\Delta M^2(\times 10^3)$ (uncov)
0.010	0.020	0.020	1	1	0.2022(15)	0.1975(14)
0.010	0.020	0.030	1	1	0.2247(17)	0.2201(15)
0.010	0.030	0.030	1	1	0.2474(19)	0.2439(15)
0.010	0.010	0.010	1	-1	0.3787(25)	0.3767(25)
0.010	0.010	0.020	1	-1	0.4257(27)	0.4218(27)
0.010	0.010	0.030	1	-1	0.4746(30)	0.4675(29)
0.010	0.020	0.020	1	-1	0.4751(27)	0.4691(28)
0.010	0.020	0.030	1	-1	0.5253(29)	0.5170(30)
0.010	0.030	0.030	1	-1	0.5763(30)	0.5672(31)
0.010	0.010	0.020	-2	-1	0.4746(40)	0.4624(38)
0.010	0.010	0.020	1	2	0.5599(37)	0.5508(32)
0.010	0.010	0.030	-2	-1	0.4936(45)	0.4767(44)
0.010	0.010	0.030	1	2	0.6663(38)	0.6543(35)
0.010	0.020	0.020	-2	-1	0.5779(36)	0.5658(33)
0.010	0.020	0.030	-2	-1	0.5968(40)	0.5837(36)
0.010	0.020	0.030	1	2	0.6846(38)	0.6727(34)
0.010	0.001	0.001	-2	0	0.4239(40)	0.4338(41)
0.010	0.030	0.030	-2	-1	0.7039(44)	0.6938(36)
0.010	0.010	0.010	2	0	0.5426(34)	0.5386(30)
0.010	0.010	0.020	2	0	0.5546(37)	0.5441(32)
0.010	0.010	0.030	2	0	0.5671(41)	0.5510(37)
0.010	0.020	0.020	2	0	0.6821(33)	0.6714(32)
0.010	0.020	0.030	2	0	0.6956(35)	0.6819(34)
0.010	0.030	0.030	2	0	0.8275(37)	0.8150(36)
0.010	0.010	0.010	2	1	0.4556(37)	0.4508(35)
0.010	0.001	0.001	-2	1	0.7125(73)	0.7150(80)
0.010	0.010	0.010	2	-1	0.8982(58)	0.8925(58)
0.010	0.010	0.020	2	-1	0.9665(62)	0.9543(60)
0.010	0.010	0.020	-1	2	1.0517(63)	1.0429(63)
0.010	0.010	0.030	2	-1	1.0380(69)	1.0173(66)
0.010	0.010	0.030	-1	2	1.2109(71)	1.1953(70)
0.010	0.020	0.020	2	-1	1.1251(62)	1.1100(64)
0.010	0.020	0.030	2	-1	1.1991(65)	1.1785(68)
0.010	0.020	0.030	-1	2	1.2871(66)	1.2677(70)
0.010	0.030	0.030	2	-1	1.3631(69)	1.3416(71)
0.010	0.001	0.001	-2	-1	0.3431(43)	0.3653(47)
0.010	0.010	0.020	0	-2	0.6685(35)	0.6624(32)
0.010	0.010	0.030	0	-2	0.7980(39)	0.7886(36)
0.010	0.020	0.030	0	-2	0.8131(35)	0.8010(35)
0.010	0.001	0.001	2	-2	1.214(12)	1.216(14)
0.010	0.001	0.001	2	2	0.4768(71)	0.5156(81)
0.010	0.010	0.010	-2	-2	0.6414(61)	0.6339(62)
0.010	0.010	0.020	-2	-2	0.7300(63)	0.7129(61)
0.010	0.010	0.030	-2	-2	0.8197(68)	0.7972(66)
0.010	0.020	0.020	-2	-2	0.8159(61)	0.7970(57)
0.010	0.020	0.030	-2	-2	0.9051(68)	0.8864(60)
0.010	0.030	0.030	-2	-2	0.9947(75)	0.9806(63)
0.010	0.010	0.010	-2	2	1.529(10)	1.519(10)
0.010	0.010	0.020	-2	2	1.716(10)	1.698(10)
0.010	0.010	0.030	-2	2	1.911(12)	1.880(12)
0.010	0.020	0.020	-2	2	1.913(11)	1.887(11)
0.010	0.020	0.030	-2	2	2.112(11)	2.078(12)
0.010	0.030	0.030	-2	2	2.315(12)	2.278(12)

TABLE XVI. (Continued)

m_{sea}	m_1	m_3	$q_1(\frac{1}{3})$	$q_3(\frac{1}{3})$	$\Delta M^2(\times 10^3)$ (cov)	$\Delta M^2(\times 10^3)$ (uncov)
0.020	0.020	0.020	-1	0	0.1752(12)	0.17318(67)
0.020	0.020	0.020	-1	1	0.5002(36)	0.4947(23)
0.020	0.020	0.020	-1	-1	0.2007(22)	0.1978(12)
0.020	0.020	0.020	-2	0	0.7058(48)	0.6976(26)
0.020	0.020	0.020	-2	1	1.1807(83)	1.1680(53)
0.020	0.020	0.020	-2	-1	0.5811(53)	0.5732(28)
0.020	0.020	0.020	2	-2	2.011(14)	1.9905(95)
0.020	0.020	0.020	2	2	0.8104(88)	0.7987(48)
0.030	0.030	0.030	-1	0	0.216 66(88)	0.215 07(66)
0.030	0.030	0.030	-1	1	0.6226(34)	0.6140(24)
0.030	0.030	0.030	-1	-1	0.2442(20)	0.2462(11)
0.030	0.030	0.030	-2	0	0.8709(35)	0.8643(26)
0.030	0.030	0.030	-2	1	1.4670(77)	1.4477(54)
0.030	0.030	0.030	-2	-1	0.7087(44)	0.7108(25)
0.030	0.030	0.030	2	-2	2.502(13)	2.4663(97)
0.030	0.030	0.030	2	2	0.9830(81)	0.9901(44)

TABLE XVII. Proton and neutron masses on unitary points for QCD + QED configurations. The masses are from size 16^3 box source, point-sink correlation functions for both 16^3 and 24^3 lattices. The fit range for 16^3 lattices is 5–10. The fit range for 24^3 lattices is 6–11. The χ^2/dof is from a covariant fit.

Lattice size	m_f	m_p	χ^2/dof	m_n	χ^2/dof
16^3	0.010	0.7125(57)	0.70(85)	0.7122(57)	0.70(85)
16^3	0.020	0.7986(40)	1.8(1.3)	0.7982(40)	1.8(1.3)
16^3	0.030	0.8747(36)	2.2(1.5)	0.8742(36)	2.2(1.5)
24^3	0.005	0.6477(53)	0.85(94)	0.6474(53)	0.85(94)
24^3	0.010	0.7121(31)	0.20(46)	0.7118(32)	0.21(46)
24^3	0.020	0.8065(25)	0.82(92)	0.8060(25)	0.84(93)
24^3	0.030	0.8871(23)	0.53(72)	0.8865(23)	0.53(72)

TABLE XVIII. Proton and neutron masses on QCD configurations with nondegenerate u, d quark masses. The p - n masses are from wall source, point-sink correlation functions for 16^3 and 24^3 lattices. The fit range for 16^3 lattices is 5–10. The fit range for 24^3 lattices is 7–12. The χ^2/dof is from a covariant fit.

Lattice size	m_{sea}	m_u	m_d	m_p	χ^2/dof	m_n	χ^2/dof
16^3	0.010	0.010	0.020	0.7416(49)	0.59(78)	0.7562(43)	0.83(92)
16^3	0.010	0.010	0.030	0.7684(45)	0.77(88)	0.7981(36)	1.3(1.1)
16^3	0.010	0.020	0.030	0.8086(36)	1.7(1.2)	0.8238(33)	2.0(1.4)
16^3	0.020	0.010	0.020	0.7553(51)	0.88(95)	0.7698(46)	1.5(1.2)
16^3	0.020	0.010	0.030	0.7825(46)	1.0(1.0)	0.8120(40)	2.4(1.5)
16^3	0.020	0.020	0.030	0.8230(38)	2.2(1.4)	0.8380(36)	2.9(1.7)
16^3	0.030	0.010	0.020	0.7721(60)	1.6(1.2)	0.7839(51)	1.3(1.1)
16^3	0.030	0.010	0.030	0.7988(55)	1.6(1.3)	0.8241(42)	1.2(1.1)
16^3	0.030	0.020	0.030	0.8361(41)	1.7(1.3)	0.8496(38)	1.7(1.3)
24^3	0.005	0.005	0.010	0.6676(85)	1.3(1.1)	0.6747(73)	1.0(1.0)
24^3	0.005	0.005	0.020	0.6992(68)	1.5(1.2)	0.7225(51)	1.0(1.0)
24^3	0.005	0.005	0.030	0.7279(59)	1.5(1.2)	0.7680(41)	1.2(1.1)
24^3	0.005	0.010	0.020	0.7225(51)	1.6(1.2)	0.7383(44)	1.4(1.2)
24^3	0.005	0.010	0.030	0.7502(44)	1.7(1.3)	0.7824(37)	1.7(1.3)
24^3	0.005	0.020	0.030	0.7928(33)	2.4(1.5)	0.8090(32)	2.5(1.6)
24^3	0.010	0.010	0.020	0.7304(77)	0.70(96)	0.7461(61)	0.9(1.1)
24^3	0.010	0.010	0.030	0.7575(71)	0.63(94)	0.7895(48)	1.3(1.2)
24^3	0.010	0.020	0.030	0.7980(46)	1.0(1.2)	0.8146(40)	1.8(1.5)

APPENDIX B: PARTIALLY QUENCHED CHIRAL PERTURBATION THEORY FRAMEWORK

The aim of this appendix is twofold: (1) to obtain all possible terms in the chiral Lagrangian relevant to the kaon mass squared at order $O(e^2)$ and $O(e^2 p^2)$ for the partially quenched $SU(2) +$ kaon system, and (2) to derive the expression for the EM correction to the kaon mass squared to order $O(e^2 p^2)$. This appendix is compact, mainly summarizing results and defining notation. Much of the machinery, of course, has been worked out before, and we refer the interested reader to the literature. Here we follow closely the works in Refs. [10–13]. The new contributions in this work are $O(e^2)$ terms and electromagnetic one-loop chiral-logarithmic correction to the kaon mass squared. We also list the $O(e^2 p^2)$ operators relevant to the kaon-mass squared, which serves as a check of the possible dependence of $O(e^2 p^2)$ corrections on charges and masses.

We begin by reminding the reader of the important details and notation, then construct the Lagrangian density, and finally compute the corrections to the kaon mass squared to the order of our interest.

1. $SU(2)$ pion sector

In the partially quenched system composed of N_V valence quarks, N_S sea quarks and N_V ghost quarks, the field $\Pi(x)$ representing the Nambu-Goldstone multiplet is the local coordinate of the coset space G/H ($G \equiv SU(N_S + N_V|N_V)_L \times SU(N_S + N_V|N_V)_R$, $H \equiv SU(N_S + N_V|N_V)_V$) at each x

$$u[\Pi(x)] \equiv \exp\left(i \frac{\Pi(x)}{\sqrt{2}F}\right). \quad (\text{B1})$$

With the normalization of F such that $F \simeq 92$ MeV, the LO chiral Lagrangian reads

$$\mathcal{L}_{\text{QCD},2} = \frac{F^2}{4} \langle u_\mu u^\mu + \chi_+ \rangle, \quad (\text{B2})$$

where \langle, \rangle denotes the supertrace in the partially quenched light quark sector, whose flavors can be indexed as

$$\begin{aligned} I = 1, \dots, N_V: & \text{ light valence quark flavors,} \\ I = N_V + 1, \dots, N_V + N_S: & \text{ light sea quark flavors,} \\ I = N_V + N_S + 1, \dots, 2N_V \\ & + N_S: \text{ light ghost quark flavors.} \end{aligned} \quad (\text{B3})$$

The variables appearing in Eq. (B2),

$$\begin{aligned} u_\mu & \equiv i\{u^\dagger(\partial_\mu u - iR_\mu u) - u(\partial_\mu u^\dagger - iL_\mu u^\dagger)\}, \\ \chi_\pm & \equiv u^\dagger \chi u^\dagger \pm u \chi^\dagger u, \quad \chi \equiv 2B_0 \mathcal{M}, \end{aligned} \quad (\text{B4})$$

are given in terms of the spurion field \mathcal{M} in place of the ordinary quark mass matrix, and the external fields R_μ, L_μ , which transform under the local chiral rotation $(g_L(x), g_R(x)) \in G$ as

$$\begin{aligned} R_\mu & \mapsto R'_\mu = g_R R_\mu g_R^\dagger + i g_R \partial_\mu g_R, \\ L_\mu & \mapsto L'_\mu = g_L L_\mu g_L^\dagger + i g_L \partial_\mu g_L, \\ \mathcal{M} & \mapsto \mathcal{M}' = g_R \mathcal{M} g_L^\dagger. \end{aligned} \quad (\text{B5})$$

For

$$\begin{aligned} u[\Pi] & \mapsto u[\Pi'] = g_R u[\Pi] h((g_L, g_R); \Pi)^\dagger \\ & = h((g_L, g_R); \Pi) u[\Pi] g_L^\dagger, \end{aligned} \quad (\text{B6})$$

with $h((g_L, g_R); \Pi) \in H$, it turns out that u_μ and χ_\pm transform covariantly with respect to h

$$A \mapsto A' = h A h^\dagger, \quad (\text{B7})$$

and that $\mathcal{L}_{\text{QCD},2}$ is invariant under the local chiral transformation.

The high frequency modes of photons coupled to quarks also generate local interactions in the low-energy effective Lagrangian of QCD. The coupling of quarks to photons preserves chiralities;

$$A_\mu (\bar{q}_L \gamma^\mu \mathcal{Q} q_L + \bar{q}_R \gamma^\mu \mathcal{Q} q_R), \quad (\text{B8})$$

where \mathcal{Q} represents the charge matrix and takes the form

$$\mathcal{Q} = e \text{diag}(q_{uV}, q_{dV}, q_{uS}, q_{dS}, q_{uV}, q_{dV}), \quad (\text{B9})$$

for two-light flavors. The systematic dependence on these quark charges can hence be traced back once \mathcal{Q} is promoted to a set of Hermitian spurion fields, $\mathcal{Q}_{R,L}$, that transform under chiral rotations as

$$\begin{aligned} \mathcal{Q}_L & \mapsto \mathcal{Q}'_L = g_L \mathcal{Q}_L g_L^\dagger, \\ \mathcal{Q}_R & \mapsto \mathcal{Q}'_R = g_R \mathcal{Q}_R g_R^\dagger. \end{aligned} \quad (\text{B10})$$

On the other hand, to construct the effective Lagrangian, it is convenient to define quantities that transform covariantly by $h((g_L, g_R); \Pi)$, i.e., as in Eq. (B7)

$$\tilde{\mathcal{Q}}_L \equiv u \mathcal{Q}_L u^\dagger, \quad \tilde{\mathcal{Q}}_R \equiv u^\dagger \mathcal{Q}_R u. \quad (\text{B11})$$

Since we will set $\mathcal{Q}_L, \mathcal{Q}_R$ to the diagonal EM charge matrix \mathcal{Q} after constructing the effective Lagrangian, we impose the chiral-invariant condition

$$\langle \mathcal{Q}_R \rangle = \langle \mathcal{Q}_L \rangle \equiv \langle \mathcal{Q} \rangle, \quad (\text{B12})$$

which reduces just to the charge matrix in the end. The leading-order ($O(p^2) \sim O(e^2)$) Lagrangian involving Nambu-Goldstone bosons is thus given by

$$L_{\pi,2} = \frac{F^2}{4} \langle u_\mu u^\mu + \chi_+ \rangle + C \langle \tilde{\mathcal{Q}}_R \tilde{\mathcal{Q}}_L \rangle, \quad (\text{B13})$$

The QED corrections from the low frequency photons can also be included by coupling the Nambu-Goldstone bosons to the $U(1)$ -gauge potential $A_\mu(x)$ and by setting the external fields L_μ, R_μ along the direction of \mathcal{Q} in the end;

$$L_\mu = \mathcal{Q}A_\mu = R_\mu. \quad (\text{B14})$$

2. The kaon sector

In SU(2) chiral perturbation theory, the strange quark is treated as being heavy, and hence the kaons are no longer treated as Nambu-Goldstone bosons. Since the EM charge of the sea strange quark, s_S , differs from that of the valence strange quark, s_V , in our simulation, these together with the ghost strange quark, \bar{s} , are regarded as constituting the partially quenched strange sector. Nevertheless, for the purpose of the analysis of our lattice data, it suffices to write down the effective Lagrangian with respect to the kaon multiplet including the valence antistrange quark \bar{s}_V , keeping track explicitly of the dependence on the electric charges $Q_{s,V}$, $Q_{s,S}$ (including e) of s_V and s_S , respectively, with the low-energy constants having implicit dependence on the sea strange quark mass. The relativistic form of the kinetic and mass terms of the kaon multiplet K (U , D denote *constituent quarks*)

$$K \sim \begin{pmatrix} [U_V \bar{s}_V] \\ [D_V \bar{s}_V] \\ [U_S \bar{s}_V] \\ [D_S \bar{s}_V] \\ [U_G \bar{s}_V] \\ [D_G \bar{s}_V] \end{pmatrix}, \quad (\text{B15})$$

which is subject to the chiral rotation

$$K \mapsto h[\Pi(x), (g_L, g_R)]K, \quad (\text{B16})$$

is given by

$$\mathcal{L}_{K,\text{kin}} = \nabla_\mu K^\dagger \nabla^\mu K - M^2 K^\dagger K, \quad (\text{B17})$$

where M is the LO mass of the kaon and the covariant derivative $\nabla_\mu K$ is with respect to the Maurer-Cartan form Γ_μ

$$\nabla_\mu K \equiv \partial_\mu K - i\Gamma_\mu K,$$

$$\Gamma_\mu \equiv -\frac{1}{2i} \{u^\dagger (\partial_\mu u - iR_\mu u) + u (\partial_\mu u^\dagger - iL_\mu u^\dagger)\}. \quad (\text{B18})$$

As is well known [67], K is not suitable for the chiral order counting since that variable also carries the high frequency modes. The fluctuation is decomposed into the high frequency modes originating from M and the low frequency modes represented by $k \equiv k_v$

$$\mathcal{K}(x) = e^{iMv \cdot x} k(x), \quad (\text{B19})$$

where v is a lightlike four-vector. In terms of k , Eq. (B17) becomes

$$\mathcal{L}_{K,\text{kin}} = -iMv^\mu (k^\dagger \nabla_\mu k - (\nabla_\mu k^\dagger)k) + \nabla_\mu k^\dagger \nabla^\mu k. \quad (\text{B20})$$

The field k carries the momentum of the order $p \lesssim 4\pi F_\pi$, M , and the above Lagrangian is $O(p)$. In the succeeding sections the effective Lagrangian is constructed in terms of k and is converted to the relativistic form described by K .

3. $O(e^2)$ and $O(e^2 p^2)$ Lagrangian for the kaon sector

Having established the partially quenched framework and notation, we construct the electromagnetic part of the chiral Lagrangian by writing down all possible $O(e^2)$ terms possessing the symmetries of massless (QCD + QED) in the nonrelativistic theory and their relativistic counterparts, and $O(e^2 p^2)$ terms that can induce the tree-level contribution to the kaon mass squared.

To this end, Tables XIX and XX list the building blocks of chiral order $O(p^2)$ and $O(e^2)$ that transform as Eq. (B7). The definition of various variables appearing in Table XX are as follows:

$$k_{\pm,\mu} \equiv i((\nabla_\mu k)k^\dagger \pm k(\nabla_\mu k)^\dagger), \quad (\text{B21})$$

$$\begin{aligned} k_{(\mu\nu)} &\equiv \nabla_{(\mu} k \nabla_{\nu)} k^\dagger = \frac{1}{2}(\nabla_\mu k \nabla_\nu k^\dagger + \nabla_\nu k \nabla_\mu k^\dagger), \\ k_{[\mu\nu]} &\equiv \nabla_{[\mu} k \nabla_{\nu]} k^\dagger = \frac{1}{2}(\nabla_\mu k \nabla_\nu k^\dagger - \nabla_\nu k \nabla_\mu k^\dagger), \end{aligned} \quad (\text{B22})$$

$$\begin{aligned} k_{\pm,\mu\nu} &\equiv (\nabla_{\mu\nu} k)k^\dagger \pm k(\nabla_{\mu\nu} k)^\dagger, \\ \nabla_{\mu\nu} &\equiv \nabla_\mu \nabla_\nu + \nabla_\nu \nabla_\mu, \end{aligned} \quad (\text{B23})$$

$$k_\pm^{W,\tilde{Q}} \equiv W(kk^\dagger \tilde{Q}_\pm \pm \tilde{Q}_\pm kk^\dagger). \quad (\text{B24})$$

In Table XIX, u_μ , for instance, is omitted, as it will not be used hereafter. Tables XIX and XX include $O(e^2)$ terms but not $O(e)$ and $O(ep)$, because EM charges are left in pairs in the low-energy effective theory after the high frequency photon modes are integrated out.

From Tables XIX and XX, we find that there are 13 $O(e^2)$ operators bilinear in kaon fields that are invariant under chiral, P and C transformations

$$\langle kk^\dagger \mathcal{A} \rangle, \quad W \langle kk^\dagger \mathcal{B} \rangle, \quad W_1 W_2 \langle kk^\dagger \rangle, \quad (\text{B25})$$

where W is $Q_{s,V}$ or $Q_{s,S}$, and

$$\begin{aligned} \mathcal{A} &\in \{\tilde{Q}_{(+)}^2, \tilde{Q}_{RL,+}, \langle \mathcal{Q} \rangle \tilde{Q}_+, \langle \mathcal{Q}^2 \rangle, \langle \tilde{Q}_{RL,+} \rangle, (\langle \mathcal{Q} \rangle)^2\}, \\ \mathcal{B} &\in \{\tilde{Q}_+, \langle \mathcal{Q} \rangle\}, \\ (W_1, W_2) &\in \{(Q_{s,V}, Q_{s,V}), (Q_{s,V}, Q_{s,S}), (Q_{s,S}, Q_{s,S})\}. \end{aligned} \quad (\text{B26})$$

The relativistic forms of the individual operators are read from the relation (B19), and $O(e^2)$ -Lagrangian density in the kaon sector is hence given by

TABLE XIX. Parity (P) and charge conjugation (C) transformation properties for operators at chiral order $O(p^2)$, $O(e^2)$ that do not contain kaon fields and transform as $A \mapsto hAh^\dagger$. Under P , $x = (x^0, \mathbf{x})$ transforms to $\tilde{x} = (x^0, -\mathbf{x})$.

Building block	Definition	Order	P	C
χ_\pm	Equation (B4)	$O(p^2)$	$\pm \chi_\pm(\tilde{x})$	$(\chi_\pm)^T$
$\langle \mathcal{Q} \rangle \tilde{\mathcal{Q}}_\pm$	$\langle \mathcal{Q} \rangle (\tilde{\mathcal{Q}}_R \pm \tilde{\mathcal{Q}}_L)$	$O(e^2)$	$\pm \langle \mathcal{Q} \rangle \tilde{\mathcal{Q}}_\pm(\tilde{x})$	$\pm \langle \mathcal{Q} \rangle (\tilde{\mathcal{Q}}_\pm)^T$
$\tilde{\mathcal{Q}}_{(\pm)}^2$	$(\tilde{\mathcal{Q}}_R)^2 \pm (\tilde{\mathcal{Q}}_L)^2$	$O(e^2)$	$\pm \tilde{\mathcal{Q}}_{(\pm)}^2(\tilde{x})$	$\pm (\tilde{\mathcal{Q}}_{(\pm)}^2)^T$
$\tilde{\mathcal{Q}}_{RL,\pm}$	$\tilde{\mathcal{Q}}_R \tilde{\mathcal{Q}}_L \pm \tilde{\mathcal{Q}}_L \tilde{\mathcal{Q}}_R$	$O(e^2)$	$\pm \tilde{\mathcal{Q}}_{RL,\pm}(\tilde{x})$	$(\tilde{\mathcal{Q}}_{RL,\pm})^T$

TABLE XX. Parity (P) and charge conjugation (C) transformation properties of operators at chiral order $O(p^2)$, $O(e^2)$ that are bilinear in kaon fields and transform as $A \mapsto hAh^\dagger$. W is either one of $Q_{s,V}$ or $Q_{s,S}$. Under P , $x = (x^0, \mathbf{x})$ transforms to $\tilde{x} = (x^0, -\mathbf{x})$.

	Definition	Order	P	C
kk^\dagger		$O(1)$	$kk^\dagger(\tilde{x})$	$(kk^\dagger)^T$
$k_{\pm,\mu}$	Equation (B21)	$O(p)$	$k_{\pm,\mu}^\mu(\tilde{x})$	$\pm (k_{\pm,\mu})^T$
$k_{[\mu\nu]}$	Equation (B22)	$O(p^2)$	$k_{[\mu\nu]}(\tilde{x})$	$\pm (k_{[\mu\nu]})^T$
$k_{\pm}^{\mu\nu}$	Equation (23)	$O(p^2)$	$k_{\pm}^{\mu\nu}(\tilde{x})$	$\pm (k_{\pm}^{\mu\nu})^T$
$k_{\pm}^{\tilde{W},\tilde{\mathcal{Q}}_+}$	Equation (24)	$O(e^2)$	$k_{\pm}^{\tilde{W},\tilde{\mathcal{Q}}_+}(\tilde{x})$	$\pm (k_{\pm}^{\tilde{W},\tilde{\mathcal{Q}}_+})^T$
$k_{\pm}^{\tilde{W},\tilde{\mathcal{Q}}_-}$	Equation (24)	$O(e^2)$	$-k_{\pm}^{\tilde{W},\tilde{\mathcal{Q}}_-}(\tilde{x})$	$\mp (k_{\pm}^{\tilde{W},\tilde{\mathcal{Q}}_-})^T$

$$\begin{aligned}
\mathcal{L}_{K,e^2} = & -A_K^{(1,1)} K^\dagger ((\tilde{\mathcal{Q}}_R)^2 + (\tilde{\mathcal{Q}}_L)^2) K - A_K^{(1,2)} \langle (\tilde{\mathcal{Q}}_R)^2 \\
& + (\tilde{\mathcal{Q}}_L)^2 \rangle K^\dagger K - A_K^{(2,1)} K^\dagger (\tilde{\mathcal{Q}}_R \tilde{\mathcal{Q}}_L + \tilde{\mathcal{Q}}_L \tilde{\mathcal{Q}}_R) K \\
& - A_K^{(2,2)} \langle \tilde{\mathcal{Q}}_R \tilde{\mathcal{Q}}_L + \tilde{\mathcal{Q}}_L \tilde{\mathcal{Q}}_R \rangle K^\dagger K \\
& - A_K^{(3)} \langle \mathcal{Q} \rangle K^\dagger (\tilde{\mathcal{Q}}_R + \tilde{\mathcal{Q}}_L) K - A_K^{(4)} \langle \mathcal{Q} \rangle^2 K^\dagger K \\
& - A_K^{(s,1)} Q_{s,V}^2 K^\dagger K - A_K^{(s,1,2)} Q_{s,S}^2 K^\dagger K \\
& - A_K^{(s,1,3)} Q_{s,V} Q_{s,S} K^\dagger K - A_K^{(s,2)} Q_{s,V} K^\dagger (\tilde{\mathcal{Q}}_R \\
& + \tilde{\mathcal{Q}}_L) K - A_K^{(s,3)} \langle \mathcal{Q} \rangle Q_{s,V} K^\dagger K \\
& - A_K^{(s,3,2)} \langle \mathcal{Q} \rangle Q_{s,S} K^\dagger K - A_K^{(s,3,3)} Q_{s,S} K^\dagger (\tilde{\mathcal{Q}}_R \\
& + \tilde{\mathcal{Q}}_L) K.
\end{aligned} \tag{B27}$$

There are $O(e^2 p)$ terms bilinear in kaon fields that are allowed from the symmetries. All possible terms are obtained from Eq. (B26) by the replacement $kk^\dagger \rightarrow v_\mu k^\mu$. These operators generate no $O(e^2)$ contribution and chiral-logarithmic corrections to the kaon mass squared. They, however, induce $O(e^2 p^2)$ contribution to the kaon mass squared after the renormalization of the kaon field. We shall come back to this point in Appendix B 4.

Next we turn to listing $O(e^2 p^2)$ terms that induce the corrections to the kaon mass squared at the tree level. The building blocks are those in Tables XIX, XX, and XXI. The definition of the quantities in Table XXI is as follows:

$$k_{[\mu\nu],\pm}^{\tilde{W},\tilde{\mathcal{Q}}_\pm} = W(k_{[\mu\nu]}) \tilde{\mathcal{Q}}_\pm \pm \tilde{\mathcal{Q}}_\pm k_{[\mu\nu]}, \tag{B28}$$

$$k_{\pm(1),\pm(2),\mu\nu}^{\tilde{W},\tilde{\mathcal{Q}}_\pm} = W(k_{\pm(1),\mu\nu}) \tilde{\mathcal{Q}}_\pm \pm_{(2)} \tilde{\mathcal{Q}}_\pm k_{\pm(1),\mu\nu}, \tag{B29}$$

$$k_{\pm(1),\pm(2),\mu}^{\tilde{W},\nabla_\nu\tilde{\mathcal{Q}}_\pm} \equiv W(k_{\pm(1),\mu}) \nabla_\nu \tilde{\mathcal{Q}}_\pm \pm_{(2)} (\nabla_\nu \tilde{\mathcal{Q}}_\pm) k_{\pm(1),\mu}, \tag{30}$$

$$k_{\pm}^{\tilde{W},\nabla_{\mu\nu}\tilde{\mathcal{Q}}_\pm} \equiv W(kk^\dagger \nabla_{\mu\nu} \tilde{\mathcal{Q}}_\pm \pm (\nabla_{\mu\nu} \tilde{\mathcal{Q}}_\pm) kk^\dagger). \tag{31}$$

The $O(e^2 p^2)$ terms with no derivatives are

$$\begin{aligned}
& \langle kk^\dagger \{ \chi_+, C_+ \} \rangle, & \langle kk^\dagger \tilde{\mathcal{Q}}_+ \chi_+ \tilde{\mathcal{Q}}_+ \rangle, \\
& \langle kk^\dagger \tilde{\mathcal{Q}}_- \chi_+ \tilde{\mathcal{Q}}_- \rangle, & \langle kk^\dagger [\chi_-, C_-] \rangle, \\
& \langle kk^\dagger \{ \chi_-, \tilde{\mathcal{Q}}_{RL,-} \} \rangle, & \langle kk^\dagger (\tilde{\mathcal{Q}}_+ \chi_- \tilde{\mathcal{Q}}_- - \tilde{\mathcal{Q}}_- \chi_- \tilde{\mathcal{Q}}_+) \rangle, \\
& k^\dagger k \langle \chi_+ C_+ \rangle, & \langle kk^\dagger C_+ \rangle \langle \chi_+ \rangle, & \langle kk^\dagger \chi_+ \rangle \langle C_+ \rangle, \\
& k^\dagger k \langle \chi_+ \rangle \langle C_+ \rangle, & \langle kk^\dagger \tilde{\mathcal{Q}}_+ \rangle \langle \chi_+ \tilde{\mathcal{Q}}_+ \rangle, \\
& \langle kk^\dagger \tilde{\mathcal{Q}}_- \rangle \langle \chi_+ \tilde{\mathcal{Q}}_- \rangle, & \langle kk^\dagger \tilde{\mathcal{Q}}_{RL,-} \rangle \langle \chi_- \rangle, \\
& k^\dagger k \langle \chi_- \tilde{\mathcal{Q}}_{RL,-} \rangle, & W \langle kk^\dagger \{ \chi_+, \tilde{\mathcal{Q}}_+ \} \rangle, \\
& W \langle kk^\dagger [\chi_-, \tilde{\mathcal{Q}}_-] \rangle, & W k^\dagger k \langle \chi_+ \tilde{\mathcal{Q}}_+ \rangle, \\
& W \langle kk^\dagger \chi_+ \rangle \langle \mathcal{Q} \rangle, & W \langle kk^\dagger \tilde{\mathcal{Q}}_+ \rangle \langle \chi_+ \rangle, \\
& W k^\dagger k \langle \chi_+ \rangle \langle \mathcal{Q} \rangle, & W_1 W_2 \langle kk^\dagger \chi_+ \rangle, & W_1 W_2 k^\dagger k \langle \chi_+ \rangle,
\end{aligned} \tag{32}$$

where

$$\begin{aligned}
C_+ & \in \{ \langle \mathcal{Q} \rangle \tilde{\mathcal{Q}}_+, \tilde{\mathcal{Q}}_{(+)}^2, \tilde{\mathcal{Q}}_{RL,+} \}, \\
C_- & \in \{ \langle \mathcal{Q} \rangle \tilde{\mathcal{Q}}_-, \tilde{\mathcal{Q}}_{(-)}^2 \}.
\end{aligned} \tag{B33}$$

TABLE XXI. Parity (P) and charge conjugation (C) transformation properties of operators at chiral order $O(e^2 p^2)$ that are bilinear in kaon fields and transform as $A \mapsto hAh^\dagger$.

Definition	P	C
$k_{\tilde{W}, \tilde{Q}_\pm}^{W, \tilde{Q}_\pm}$	Equation (B28)	$(\pm_{(1)} 1)(\pm_{(2)} 1)(\pm 1)(k_{\tilde{W}, \tilde{Q}_\pm}^{W, \tilde{Q}_\pm})^T$
$k_{\tilde{W}, \tilde{Q}_\pm}^{W, \tilde{Q}_\pm, \mu\nu}$	Equation (B29)	$(\pm_{(1)} 1)(\pm_{(2)} 1)(k_{\tilde{W}, \tilde{Q}_\pm}^{W, \tilde{Q}_\pm, \mu\nu})^T$
$k_{\tilde{W}, \tilde{Q}_\pm}^{W, \tilde{Q}_\pm, \mu\nu}$	Equation (B29)	$-(\pm_{(1)} 1)(\pm_{(2)} 1)(k_{\tilde{W}, \tilde{Q}_\pm}^{W, \tilde{Q}_\pm, \mu\nu})^T$
$k_{\tilde{W}, \tilde{Q}_\pm}^{W, \tilde{Q}_\pm, \mu}$	Equation (30)	$(\pm_{(1)} 1)(\pm_{(2)} 1)(k_{\tilde{W}, \tilde{Q}_\pm}^{W, \tilde{Q}_\pm, \mu})^T$
$k_{\tilde{W}, \tilde{Q}_\pm}^{W, \tilde{Q}_\pm, \mu}$	Equation (30)	$-(\pm_{(1)} 1)(\pm_{(2)} 1)(k_{\tilde{W}, \tilde{Q}_\pm}^{W, \tilde{Q}_\pm, \mu})^T$
$k_{\tilde{W}, \tilde{Q}_\pm}^{W, \tilde{Q}_\pm, \mu}$	Equation (31)	$\pm(k_{\tilde{W}, \tilde{Q}_\pm}^{W, \tilde{Q}_\pm, \mu})^T$

The $O(e^2 p^2)$ terms with two derivatives that contribute to the kaon mass squared at the tree level are ($\eta^{\mu\nu}$ is the metric in Minkowski space)

$$\begin{aligned} &\langle \eta^{\mu\nu} k_{(\mu\nu)} \mathcal{A} \rangle, & \langle \eta^{\mu\nu} k_{+, \mu\nu} \mathcal{A} \rangle, & W \langle \eta^{\mu\nu} k_{(\mu\nu)} \mathcal{B} \rangle, \\ &W \langle \eta^{\mu\nu} k_{-, \mu\nu} \tilde{\mathcal{Q}}_- \rangle, & W \langle \eta^{\mu\nu} k_{+, \mu\nu} \mathcal{B} \rangle, \\ &W_1 W_2 \langle \eta^{\mu\nu} k_{(\mu\nu)} \rangle, & W_1 W_2 \langle \eta^{\mu\nu} k_{+, \mu\nu} \rangle, \end{aligned} \quad (\text{B34})$$

where \mathcal{A} , \mathcal{B} are the same as in Eq. (B26).

4. EM correction to kaon mass squared

In this subsection, the explicit expression for the $O(e^2)$ and the $O(e^2 p^2)$ chiral-logarithmic correction to the kaon mass squared is obtained by setting the charge matrices \mathcal{Q} in light flavor partially quenched system as in Eq. (B9), $\mathcal{Q}_{s,V} = e q_{sV}$ and $\mathcal{Q}_{s,S} = e q_{sS}$. The EM contribution to the K^+ mass squared at order e^2 is

$$\begin{aligned} (M_{K^+}^{e^2})^2 = & 2e^2((A_K^{(1,1)} + A_K^{(2,1)})q_{uV}^2 + e^2(2A_K^{(1,2)} + 2A_K^{(2,2)} \\ & + e^2 A_K^{(4)})(q_{uS}^2 + q_{dS}^2) + e^2 A_K^{(3)}(q_{uS} + q_{dS})q_{uV} \\ & + e^2 A_K^{(s,1)} q_{sV}^2 + e^2 A_K^{(s,1,2)} q_{sS}^2 + e^2 A_K^{(s,1,3)} q_{sV} q_{sS} \\ & + 2e^2 A_K^{(s,2)} q_{uV} q_{sV} + e^2 A_K^{(s,3)} (q_{uS} + q_{dS}) q_{sV} \\ & + e^2 A_K^{(s,3,2)} (q_{uS} + q_{dS}) q_{sS} + 2e^2 A_K^{(s,3,3)} q_{uV} q_{sS}. \end{aligned} \quad (\text{B35})$$

In quenched QED this becomes

$$\begin{aligned} (M_{K^+}^{e^2})^2 = & 2e^2(A_K^{(1,1)} + A_K^{(2,1)})q_{uV}^2 + e^2 A_K^{(s,1)} q_{sV}^2 \\ & + 2e^2 A_K^{(s,2)} q_{uV} q_{sV}. \end{aligned} \quad (\text{B36})$$

The $O(e^2)$ correction to the neutral kaon mass squared, $(M_{K^0}^{e^2})^2$, is given by substituting q_{dV} for q_{uV} in Eq. (B35).

We next consider the one-loop contribution to kaon mass squared. The scalar QED Lagrangian density (B17) gives the correction from the diagrams, in each of which a photon propagates explicitly, but these contributions are absorbed by the redefinition of the coefficients in Eq. (B27) and those of $O(e^2 p)$ operators in the infinite volume. The leading EM chiral-logarithmic correction comes only from the tadpole diagrams induced by Eq. (B27)

$$\begin{aligned} (M_{K,i}^{\log})^2 = & -\frac{e^2}{16\pi^2} \frac{A_K^{(1,1)}}{F_0^2} \sum_{n: \text{sea}} (q_{iV}^2 - q_{nS}^2) \chi_{in} \ln\left(\frac{\chi_{in}}{\mu^2}\right) \\ & -\frac{e^2}{16\pi^2} \frac{A_K^{(2,1)}}{F_0^2} \sum_{n: \text{sea}} \{2q_{iV}(q_{iV} - q_{nS}) \\ & + (q_{iV} - q_{nS})^2\} \chi_{in} \ln\left(\frac{\chi_{in}}{\mu^2}\right) - \frac{e^2}{16\pi^2} \\ & \times \frac{2A_K^{(2,2)}}{F_0^2} \sum_{n,m: \text{sea}, n \neq m} (q_{nS} - q_{mS})^2 \chi_{mn} \ln\left(\frac{\chi_{mn}}{\mu^2}\right) \\ & - \frac{e^2}{16\pi^2} \frac{A_K^{(3)} N_S \bar{\mathcal{Q}} + A_K^{(s,2)} q_{sV} + A_K^{(s,3,3)} q_{sS}}{F_0^2} \\ & \times \sum_{n: \text{sea}} (q_{iV} - q_{nS}) \chi_{in} \ln\left(\frac{\chi_{in}}{\mu^2}\right), \end{aligned} \quad (\text{B37})$$

where $i = u$ or d , μ is the renormalization scale, and

$$\begin{aligned} \chi_{mn} = & \frac{\chi_m + \chi_n}{2}, & \chi_n = & 2B_0 m_n, \\ \bar{\mathcal{Q}} = & \frac{1}{N_S} \sum_{n: \text{sea}} q_{nS}. \end{aligned} \quad (\text{B38})$$

In our simulation, all sea quarks are neutral and the two light sea quarks are degenerate in mass $m_{(S)}$. Hence, $(M_{K,i}^{\log})^2$ reduces to

$$\begin{aligned} (M_{K,i}^{\log})^2 = & -2 \frac{e^2}{16\pi^2} \frac{1}{F_0^2} \{q_{iV}^2 (A_K^{(1,1)} + 3A_K^{(2,1)}) \\ & + q_{iV} q_{sV} A_K^{(s,2)}\} \chi_{i(S)} \ln\left(\frac{\chi_{i(S)}}{\mu^2}\right), \end{aligned} \quad (\text{B39})$$

where $\chi_{i(S)} \equiv B_0(m_i + m_{(S)})$.

There are two types of finite-volume corrections induced at the one-loop level. The first type is given by the scalar QED diagrams

$$\begin{aligned} \Delta(M_{K^+})^2|_{\text{EM, photonic}}(L) = & (q_K)^2 e^2 \left\{ -3 \frac{\kappa}{4\pi} \frac{1}{L^2} + \frac{1}{(4\pi)^2} \right. \\ & \left. \times \frac{\mathcal{K}(m_K L)}{L^2} - 4 \frac{1}{(4\pi)^2} \frac{m_K}{L} \mathcal{H}(m_K L) \right\}, \end{aligned} \quad (\text{B40})$$

where κ and various functions are defined in Eqs. (14), (16), and (17). Another type is the finite-volume correction to the

terms (B37), $\Delta(M_{K,i}^{\log})^2(L)$, whose expression is obtained by making the following substitution to each logarithm in Eq. (B37):

$$m^2 \ln\left(\frac{m^2}{\mu^2}\right) \Rightarrow \frac{\mathcal{M}(mL)}{L^2}, \quad (\text{B41})$$

with $\mathcal{M}(x)$ in Eq. (13). The finite size scaling effect on the $O(e^2)$ wave function renormalization could induce $O(e^2 p^2)$ correction to kaon mass squared after the renormalization of the kaon field. The explicit calculation, however, shows that such effects do not exist.

There are as many LEC's as $O(e^2 p^2)$ operators in Eqs. (32) and (B34) participating in the $O(e^2 p^2)$ contribution to kaon mass squared, while our lattice study here can determine at best the linear combinations of LEC's of terms

with the same charge and light quark mass dependence of order $e^2 m$, from the response of the data to the variation of these parameters in the (QCD + QED) action. The dependence on those parameters can be read off from Eqs. (32) and (B34). In effect, Eq. (32) alone leads to the following form of the charge and mass dependence of the $O(e^2 m)$ correction ($i = u, d$) in quenched QED, as anticipated,

$$\begin{aligned} (M_{K,i}^{e^2 p^2}) = & e^2 m_{iV} (x_3^{(K)} (q_{iV} + q_{sV})^2 + x_4^{(K)} (q_{iV} - q_{sV})^2 \\ & + x_5^{(K)} (q_{iV}^2 - q_{sV}^2)) + e^2 m_{(S)} (x_6^{(K)} (q_{iV} + q_{sV})^2 \\ & + x_7^{(K)} (q_{iV} - q_{sV})^2 + x_8^{(K)} (q_{iV}^2 - q_{sV}^2)). \quad (\text{B42}) \end{aligned}$$

We note that m_{iV} and $m_{(S)}$ are denoted by m_1 and $m_4 = m_5$, respectively, in Eq. (23).

-
- [1] E. E. Scholz, Proc. Sci., LATTICE2009 (2009) 005 [arXiv:0911.2191].
- [2] T. Blum, T. Doi, M. Hayakawa, T. Izubuchi, and N. Yamada, Phys. Rev. D **76**, 114508 (2007).
- [3] R. F. Dashen, Phys. Rev. **183**, 1245 (1969).
- [4] C. Amsler *et al.* (Particle Data Group), Phys. Lett. B **667**, 1 (2008).
- [5] D. B. Kaplan, Phys. Lett. B **288**, 342 (1992).
- [6] Y. Shamir, Nucl. Phys. **B406**, 90 (1993).
- [7] C. Allton *et al.* (RBC-UKQCD Collaboration), Phys. Rev. D **78**, 114509 (2008).
- [8] A. Duncan, E. Eichten, and H. Thacker, Phys. Rev. Lett. **76**, 3894 (1996).
- [9] A. Duncan, E. Eichten, and H. Thacker, Phys. Lett. B **409**, 387 (1997).
- [10] M. Hayakawa and S. Uno, Prog. Theor. Phys. **120**, 413 (2008).
- [11] J. Bijnens and N. Danielsson, Phys. Rev. D **75**, 014505 (2007).
- [12] A. Roessl, Nucl. Phys. **B555**, 507 (1999).
- [13] S. M. Ouellette, arXiv:hep-ph/0101055.
- [14] D. J. Antonio *et al.* (RBC Collaboration), Phys. Rev. Lett. **100**, 032001 (2008).
- [15] C. Kelly, P. A. Boyle, and C. T. Sachrajda, Proc. Sci., LAT2009 (2009) 087 [arXiv:0911.1309].
- [16] R. Mawhinney (RBC), Proc. Sci., LAT2009 (2009) 081 [arXiv:0910.3194].
- [17] Y. Aoki *et al.* (RBC and UKQCD Collaborations) arXiv:1011.0892.
- [18] S. Aoki *et al.* (PACS-CS Collaboration), Phys. Rev. D **79**, 034503 (2009).
- [19] D. Kadoh *et al.* (PACS-CS Collaboration), Proc. Sci., LATTICE2008 (2008) 092 [arXiv:0810.0351].
- [20] R. Zhou *et al.*, Proc. Sci., LATTICE2008 (2008) 131 [arXiv:0810.1302].
- [21] R. Zhou and S. Uno, Proc. Sci., LAT2009 (2009) 182 [arXiv:0911.1541].
- [22] S. Basak *et al.* (MILC Collaboration), Proc. Sci., LATTICE2008 (2008) 127 [arXiv:0812.4486].
- [23] A. Duncan, E. Eichten, and R. Sedgewick, Phys. Rev. D **71**, 094509 (2005).
- [24] A. Hasenfratz, R. Homann, and S. Schaefer, Phys. Rev. D **78**, 014515 (2008).
- [25] C. Jung, arXiv:1001.0941.
- [26] S. Aoki *et al.* (PACS-CS Collaboration), Phys. Rev. D **81**, 074503 (2010).
- [27] T. Ishikawa, Y. Aoki, and T. Izubuchi, Proc. Sci., LAT2009 (2009) 035 [arXiv:1003.2182].
- [28] T. Izubuchi, T. Blum, T. Doi, M. Hayakawa, T. Ishikawa, S. Uno, N. Yamada, and R. Zhou, Proc. Sci., LATTICE2010 (2010) 30.
- [29] M. Abramczyk, T. Blum, G. Petropoulos, and R. Zhou, arXiv:0911.1348.
- [30] C. Allton *et al.* (RBC and UKQCD collaborations), Phys. Rev. D **76**, 014504 (2007).
- [31] V. Furman and Y. Shamir, Nucl. Phys. **B439**, 54 (1995).
- [32] T. Blum, Nucl. Phys. B, Proc. Suppl. **73**, 167 (1999).
- [33] D. J. Antonio *et al.* (RBC Collaboration), Phys. Rev. D **77**, 014509 (2008).
- [34] T. Doi, T. Blum, M. Hayakawa, T. Izubuchi, and N. Yamada, Proc. Sci., LAT2006 (2006) 174 [arXiv:hep-lat/0610095].
- [35] W. Press, S. Teukolsky, W. Vetterling, and B. Flannery, *Numerical Recipes in C* (Cambridge University Press, Cambridge, UK, 1992), 2nd ed..
- [36] L. Lellouch, Proc. Sci., LATTICE2008 (2009) 015 [arXiv:0902.4545].
- [37] S. Durr *et al.*, Science **322**, 1224 (2008).
- [38] C. Dawson, in *The 27th International Symposium on Lattice Field Theory July 25 (Saturday)– 31 (Friday), 2009 Beijing, China, 2009* (unpublished).
- [39] M. Luscher and F. Palombi, Proc. Sci., LATTICE2008 (2008) 049 [arXiv:0810.0946].
- [40] C. Sturm *et al.*, Phys. Rev. D **80**, 014501 (2009).
- [41] M. Gorbahn and S. Jager, arXiv:1004.3997.

- [42] Y. Aoki, Proc. Sci., LAT2009 (2009) 012 [arXiv:1005.2339].
- [43] L.G. Almeida and C. Sturm, Phys. Rev. D **82**, 054017 (2010).
- [44] R. Arthur and P.A. Boyle, arXiv:1006.0422.
- [45] D.B. Kaplan and A. V. Manohar, Phys. Rev. Lett. **56**, 2004 (1986).
- [46] H. Leutwyler, Phys. Lett. B **378**, 313 (1996).
- [47] D.R. Nelson, G. T. Fleming, and G. W. Kilcup, Phys. Rev. Lett. **90**, 021601 (2003).
- [48] G. 't Hooft, Phys. Rep. **142**, 357 (1986).
- [49] K. Choi, C. W. Kim, and W. K. Sze, Phys. Rev. Lett. **61**, 794 (1988).
- [50] T. Banks, Y. Nir, and N. Seiberg, arXiv:hep-ph/9403203.
- [51] H. Davoudiasl and A. Soni, Phys. Rev. D **76**, 095015 (2007).
- [52] M. Creutz, Phys. Rev. Lett. **92**, 162003 (2004).
- [53] E. Shintani *et al.* (JLQCD), Phys. Rev. Lett. **101**, 242001 (2008).
- [54] P.A. Boyle, L. Del Debbio, J. Wennekers, and J.M. Zanotti (RBC Collaboration), Phys. Rev. D **81**, 014504 (2010).
- [55] J. Gasser and H. Leutwyler, Nucl. Phys. **B250**, 465 (1985).
- [56] G. Amoros, J. Bijnens, and P. Talavera, Nucl. Phys. **B602**, 87 (2001).
- [57] C. Aubin *et al.* (MILC Collaboration), Phys. Rev. D **70**, 114501 (2004).
- [58] J. Gasser and H. Leutwyler, Nucl. Phys. **B250**, 539 (1985).
- [59] W. J. Marciano, Phys. Rev. Lett. **93**, 231803 (2004).
- [60] M. Antonelli *et al.*, arXiv:1005.2323.
- [61] V. Cirigliano and I. Rosell, J. High Energy Phys. **10** (2007) 005.
- [62] S.R. Beane, K. Orginos, and M.J. Savage, Nucl. Phys. **B768**, 38 (2007).
- [63] S. Sasaki, T. Blum, and S. Ohta, Phys. Rev. D **65**, 074503 (2002).
- [64] W.N. Cottingham, Ann. Phys. (N.Y.) **25**, 424 (1963).
- [65] J. J. Kelly, Phys. Rev. C **70**, 068202 (2004).
- [66] D. Renfrew, T. Blum, N. Christ, R. Mawhinney, and P. Vranas, Proc. Sci., LATTICE2008 (2008) 048 [arXiv:0902.2587].
- [67] E. E. Jenkins and A. V. Manohar, Phys. Lett. B **255**, 558 (1991).